ISAS - INTERNATIONAL SCHOOL FOR ADVANCED STUDIES

First Principles Molecular Dynamics Study of Liquid and Amorphous Silicon

Thesis submitted for the degree of

"Doctor Philosophiæ"

CANDIDATE

Ivan Štich

SUPERVISOR

Prof. R. Car

Prof. M. Parrinello

October 1989

TRIESTE

SISSA - SCUOLA INTERNAZIONALE SUPERIORE DI STUDI AVANZATI

TRIESTE

Strada Costiera 11

Scuola Internazionale Superiore di Studi Avanzati

International School for Advanced Studies

First Principles Molecular Dynamics Study of Liquid and Amorphous Silicon

Thesis submitted for the degree of

"Doctor Philosophiæ"

CANDIDATE

Ivan Štich

SUPERVISOR

Prof. R. Car

Prof. M. Parrinello

October 1989

Table of Contents

I. Introduction

In this work we report our results achieved during the PhD. study in Trieste. The main objective of this work was understanding the physics of the disordered silicon phases, i.e. liquid (l-Si) and amorphous (a-Si) silicon at the microscopic level using ab-initio methods.

The reason for studying this subject is twofold. Silicon is the most studied prototype of elemental semiconductor. Its crystalline phases, including the high pressure metallic phases, have been extensively studied (Yin and Cohen 1982b, Chang and Cohen 1985). The metallic liquid phase, however, was relatively little explored, both experimentally (Gabathuler and Steeb 1979, Waseda and Suzuki 1975, Hague et al 1980) and theoretically (Stillinger and Weber 1985, Car and Parrinello 1987, Hafner and Kahl 1984, Allan and Broughton 1987). The crystal to liquid transition occurs at the unusually high temperature of $\sim 1700K$, which makes experiments difficult to make. Nevertheless, l-Si is physically interesting. The atomic structure is dissimilar to that of most other liquid metals. The coordination number of ~ 6.4 is intermediate between that characteristic of open tetrahedral systems and the highly coordinated closed packed systems, raising the question of the nature of chemical bonding. The reason for the metallic character of the melt and its electrical conductivity have been only poorly understood. The dynamical properties of l-Si are essentially unknown.

Much more work has been devoted to a-Si in the past twenty years. There is a vast number of physically interesting properties of a-Si. They include structural, dynamic, electronic, and defect-controlled properties (Elliot 1984, Zallen 1983). Until recently, the modeling of a-Si at the microscopic level was a highly empirical procedure. As a further step in this old but never fully understood field one would like to have a nonempirical scheme to study these properties.

The other motivation for this work is that the disordered Si phases besides being physically interesting are also technologically important. Single crystals are grown from the liquid phase. Novel dopant profiles are generated by zone refining at advancing liquid interfaces in laser-melted Si surfaces. The metallic nature of the melt is used to determine the thickness of the laser-melted region and an alternating magnetic field is used to improve the quality of crystal growth. While crystalline Si (c-Si) is of overwhelming importance in electronic industry and in special photovoltaic applications, it is too expensive for use in large-scale solar energy applications. On the other hand, large-area films of a-Si to be used in solar energy application can be prepared at a significantly lower cost than c-Si.

The properties we intend to study range from structural to dynamical and electronic properties in a wide range of temperatures. A first principles approach that allows to treat all these properties on the same footing was pioneered by Car and Parrinello (1985). This method is a first-principles molecular dynamics scheme where the interatomic forces are calculated from the potentials that are derived from the instantaneous electronic ground-state calculated within density functional theory in the local density approximation. Thus no arbitrary assumptions are made on the form of the many-body potentials.

We applied this technique to study the properties of l- and a-Si. For both systems the resulting atomic structure compares very favorably with the experimental data. The knowledge of atomic coordinates enables to study other correlation functions, like, e.g., the triplet correlations, that are difficult to obtain experimentally. A vibrational spectrum for l-Si was obtained which is quite dissimilar to that of most simple liquids. The calculated diffusion coefficients are in good agreement with indirect experimental estimates. The calculated electronic density of states and electrical conductivity show metallic behavior in agreement with experiments. A significant portion of covalent chemical bonds was found in the metallic l-Si. The prevalence of broken bonds, however, leads to a high value of the diffusion coefficient and to the metallic nature of the melt. Both vibrational and electronic densities of states of a-Si agree well with available experimental data. Our MD simulation has revealed the existence of interesting mechanisms of defect dynamics that correlate well with proposed theoretical models.

The thesis is organized as follows. The method is described in chapter 2. Chapter 3 contains a detailed study of l-Si including structural, dynamical, bonding and electronic properties. The results on a-Si as well as the structural changes occurring upon cooling are presented in chapter 4. Finally, we present our conclusions in chapter 5.

II. Interatomic Potentials and First-Principles Molecular Dynamics

II.1 Interatomic Potentials Within Density Functional Theory

As stated in the introduction, we intend to study structural, dynamical, and electronic properties of condensed systems in a wide range of temperatures. Numerical simulations based on *molecular dynamics* (MD) have proven to be a powerful tool in this respect (Rahman 1978, Binder 1979,1984, Hoover 1986, Heermann 1986). MD generates the ionic trajectories which allow to calculate both equilibrium and nonequilibrium statistical averages. A considerable insight into microscopic details of atomic dynamics, which often is not easily available in (real) experiments, is accessible to numerical simulations.

MD is based on the assumption that atomic dynamics obeys the equations of classical mechanics, i.e. Newton's equations. It means that (i) the electronic and ionic degrees of freedom are separable (*Born-Oppenheimer* BO *approximation*) and (ii) the quantum effects on the atomic dynamics are negligible. Assumption (ii) requires validity of (i) and is satisfied for most systems of interest, provided the temperature is not too low. Let us consider N atoms with coordinates $\{\vec{R}_1, \vec{R}_2, ..., \vec{R}_N\}$. The BO approximation assumes that the atomic forces are derived from the potential $\Phi\left[\{\vec{R}_I\}\right]$ that is calculated from the electronic ground-state ψ_0 as

$$\Phi\left[\{\vec{R}_I\}\right] = \langle\psi_0|H_{eI} + \tfrac{1}{2}\sum_{I\neq J}\frac{Z_I Z_J}{|\vec{R}_I - \vec{R}_J|}|\psi_0\rangle, \qquad (II.1.1)$$

where H_{eI} is the operator of the electron-ion interaction and Z_I are the ionic charges. Then the main ingredient of MD is the calculation of the atomic forces

$$\vec{F}_I = -\frac{\partial\Phi\left[\{\vec{R}_I\}\right]}{\partial\vec{R}_I}. \qquad (II.1.2)$$

The BO many-body energy surface $\Phi\left[\{\vec{R}_I\}\right]$ may be obtained either from first principles by explicitly finding the electronic ground-state ψ_0 for any ionic configuration $\{\vec{R}_I\}$ or by a suitable empirical parametrization. The discussion of the empirical interatomic potential is left to Appendix 1.

A more fundamental and satisfactory approach treats explicitly also the electronic degrees of freedom and finds directly the potential $\Phi\left[\{\vec{R}_I\}\right]$ defined in equa-

tion II.1.1. This difficult electronic quantum many-body problem is formally equivalent to a simpler self-consistent single-particle problem, that can be solved by making certain approximations. This is the standard approach used in most electronic structure calculations. According to *density functional theory* (DFT) the total ground-state energy of a system of interacting electrons and ions is a unique functional of the electronic density $n(\vec{r})$ (Hohenberg and Kohn 1964). If $n(\vec{r})$ is expressed in terms of N_e doubly occupied single-particle orbitals $\psi_i(\vec{r})$

$$n(\vec{r}) = 2\sum_{i}^{occ} |\psi_i(\vec{r})|^2, \qquad (II.1.3)$$

then the ground-state energy surface can be found by minimizing the functional $E\left[\{\psi_i\},\{\vec{R}_I\}\right]$ with respect to the "electronic degrees of freedom" $\{\psi_i\}$, i.e.

$$\Phi\left[\{\vec{R}_I\}\right] = \min_{\{\psi_i\}} E\left[\{\psi_i\},\{\vec{R}_I\}\right]. \qquad (II.1.4)$$

The functional $E\left[\{\psi_i\},\{\vec{R}_I\}\right]$ is given by:

$$E\left[\{\psi_i\},\{\vec{R}_I\}\right] = 2\sum_{i}^{occ}\int \mathrm{d}\vec{r}\psi_i^*(\vec{r})\left(-\tfrac{1}{2}\nabla^2\right)\psi_i(\vec{r}) + \int \mathrm{d}\vec{r}\; V^{ext}(\vec{r})\; n(\vec{r}) +$$

$$\tfrac{1}{2}\int \mathrm{d}\vec{r}\mathrm{d}\vec{r}\,'\frac{n(\vec{r})\; n(\vec{r}\,')}{|\vec{r}-\vec{r}\,'|} + E^{xc}[n] + \tfrac{1}{2}\sum_{I\neq J}\frac{Z_I Z_J}{|\vec{R}_I-\vec{R}_J|}. \qquad (II.1.5)$$

Atomic units $e = \hbar = m_e = 1$ are used throughout the thesis. $E^{xc}[n]$ is the exchange-correlation energy (see e.g. Lundqvist and March 1983), $V^{ext}(\vec{r})$ is the total external potential felt by electrons, and Z_I are the ionic charges. $E^{xc}[n]$ is a universal functional of n and represents all corrections to the independent-electron model (nonclassical many-body effects of xc), but remains unknown. This difficulty is circumvented by making approximations, such as *local density approximation* (LDA) (Kohn and Sham 1965, Lundqvist and March 1983) or the more general *local spin density approximation* (LSD) (Gunnarson and Lundqvist 1976). In the LDA scheme one assumes that the real inhomogeneous electron system behaves locally as the uniform electron gas of the same density:

$$E^{xc}[n] \simeq \int \mathrm{d}\vec{r} n(\vec{r})\varepsilon^{xc}[n(\vec{r})], \qquad (II.1.6)$$

where $\varepsilon^{xc}[n(\vec{r})]$ is the xc energy per electron of a uniform gas of density n (see e.g. Lundqvist and March 1983). A number of prescriptions for ε^{xc} are available: Kohn-Sham (1965) (pure exchange), Wigner (1937), Gunnarsson and Ludqvist (1976), Ceperley and Alder (1980), and X_α (Slater 1974). The quantum Monte-Carlo scheme of Ceperley and Alder, however, is considered to be the most accurate among the approximate prescriptions available. Since the other terms in equation

II.1.5 may be (in principle) evaluated with arbitrary accuracy, approximations to $E^{xc}[n]$ play a central role in this theory. The single-particle orbitals $\{\psi_i\}$ are subject to the orthonormality constraints

$$\int \mathrm{d}\vec{r}\ \psi_i^*(\vec{r})\ \psi_j(\vec{r}) = \delta_{ij}. \qquad (II.1.7)$$

Chemical bonding is mediated by outer electrons. Core electrons are little affected by bonding but represent additional complications. The orthonormality constraints force the wave functions to have rapid oscillations in the core region and also the external potential must be very strong in order to bind them. The core states may be projected out by replacing the core electrons plus the nuclei by pseudoions (Cohen et al 1970). This approach will be adopted here. Then in equation II.1.5 first-principles norm-conserving *pseudopotentials* (Hamann et al 1979) will be used for $V^{ext}(\vec{r})$, and Z_I are the charges of the ionic cores. The first-principles norm-conserving pseudopotentials have been constructed so as to (i) reproduce the all electron eigenvalues ε_i for a chosen atomic configuration, (ii) reproduce the atomic wave functions beyond some core radius r_c, (iii) reproduce the integrals of the charge densities for $r > r_c$ for the valence states, (iv) make the logarithmic derivatives of the real and pseudo wave function and their first energy derivative to agree for $r > r_c$. Properties (iii) and (iv) are crucial for the pseudopotential in order to have optimal *transferability* in different chemical environments. Calculations have shown that norm-conserving pseudopotentials give structural and vibrational properties of similar quality to all-electron calculations for a variety of systems.

Clearly, the first-principles approach outlined here is able to describe fine details of the potential $\Phi\left[\{\vec{R}_I\}\right]$ but is much more computationally demanding than the approach based on empirical potentials. Thus the size of the tractable systems is limited.

II.2 Minimization of the Energy Functional

In this section we describe methods of solving equation II.1.4 subject to the constraints of equation II.1.7. This subject has been discussed at length elsewhere (Štich 1987, Štich 1989, Štich et al 1989a), so only a brief sketch of the main ideas and methods is given here.

In the following we shall assume that $E\left[\{\psi_i\},\{\vec{R}_I\}\right]$ as a functional of $\{\psi_i\}$ for fixed atomic positions $\{\vec{R}_I\}$ has a single minimum. Experience has shown the validity of this assumption. The standard approach to this problem consists in solving the associated Euler-Lagrange equations, i.e.

$$\frac{\delta}{\delta\psi_i(\vec{r})}\left(E-\sum_j \varepsilon_j \int \mathrm{d}\vec{r}\,'|\psi_j(\vec{r}\,')|^2\right)=0, \qquad (II.2.1)$$

which leads to

$$H\psi_i(\vec{r})=\varepsilon_i\psi_i(\vec{r}) \qquad (II.2.2)$$

where

$$H=-\tfrac{1}{2}\nabla^2+V^{ext}(\vec{r})+V^H(\vec{r})+\mu^{xc}(\vec{r}). \qquad (II.2.3)$$

Here $V^H(\vec{r})=\int \mathrm{d}\vec{r}\,'\frac{n(\vec{r}\,')}{|\vec{r}-\vec{r}\,'|}$ is the Hartree potential and $\mu^{xc}(\vec{r})=\frac{\delta E^{xc}[n]}{\delta n(\vec{r})}$ is the exchange-correlation potential. The Schrödinger-type equations II.2.2 are called *Kohn-Sham* (K-S) *equations* (Kohn and Sham 1965). By expanding the $\{\psi_i\}$ in a basis set the K-S equations are converted into a self-consistent matrix eigenvalue problem. In the following we adopt the plane-wave pseudopotential formalism (Yin and Cohen 1982b), i.e.

$$\psi_i(\vec{r})=\psi_{n\vec{k}}(\vec{r})=\sum_{\vec{G}} c_{\vec{G}}^{n\vec{k}}e^{i(\vec{k}+\vec{G}).\vec{r}}. \qquad (II.2.4)$$

The use of plane waves assumes periodic boundary conditions. This is also the usual way of terminating free surfaces in MD simulations. The sum over $\vec{G}$ is usually truncated to include only M plane waves up to a cutoff G_{max}, which in turn determines the accuracy of the calculation. We assume here that the unit cell is so large that the band dispersion in the Brillouin zone (BZ) can be neglected. In this case it is sufficient to consider the $\vec{k}=(0,0,0)$ point only. If the band dispersion is nonegligible, a more accurate BZ sampling is obtained by using the special points (Baldereschi 1973, Chadi and Cohen 1973). The Hamiltonian matrix is given by

$$H_{\vec{G}\vec{G}'}=\tfrac{1}{2}|\vec{G}|^2\delta_{\vec{G},\vec{G}'}+V^H_{\vec{G}-\vec{G}'}+\mu^{xc}_{\vec{G}-\vec{G}'}+V^{ext}_{\vec{G}-\vec{G}'}. \qquad (II.2.5)$$

In equation II.2.5 the index $\vec{k}$ has been dropped and V^{ext} is treated as local. We leave the discussion of nonlocal pseudopotentials to Appendix 2.

The standard approach is rather costly in large-scale problems, since it requires $O(M^3)$ floating-point operations for each diagonalization, which must be repeated I_{sc} times to achieve self-consistency. This approach becomes prohibitively inconvenient as the system size is increased. To find the ground-state energy within DFT, only the lowest N_e occupied K-S orbitals are necessary. In plane-wave schemes, N_e is normally much smaller than M and a more convenient formulation is provided by iterative methods such as e.g. the Davidson method (see e.g. Davidson 1983) or the direct minimization of the energy functional II.1.5 without using the K-S equations (Štich et al 1989a). Here we concentrate on the latter approach. That can be conveniently done by introducing an appropriate fictitious dynamics in the space of the electronic degrees of freedom.

Conceptually the simplest way of finding a minimum of a function with many variables is provided by the *steepest descent* (SD) *method* (Press et al 1986). It is natural to use this idea also for the electronic structure problem (Car et al 1987). In the present case SD can be formulated in terms of the equations:

$$\begin{aligned} \dot{\psi}_i(\vec{r},t) &= -\frac{\delta E}{\delta \psi_i^*(\vec{r},t)} + OC \\ &= -H\psi_i(\vec{r},t) + OC, \end{aligned} \qquad (II.2.6)$$

where the dot indicates the derivative with respect to a fictitious time variable t, and OC stands for the orthogonality constraint of equation II.1.7. When a minimum is attained, $\{\dot{\psi}_i = 0\}$ and equations II.2.6 are equivalent, within a unitary transformation, to the K-S equations. The SD may be seen as an alternative way of solving the K-S equations without treating them as a self-consistent eigenvalue problem.

In practice, equations II.2.6 are discretized and a SD step can be written as

$$\psi_i(\vec{r},t+\Delta t) = \psi_i(\vec{r},t) - \Delta t H\psi_i(\vec{r},t) + OC. \qquad (II.2.7)$$

The elementary time step Δt in equation II.2.7 fixes the time scale and therefore is the parameter controlling the convergence rate of the SD scheme (i.e. the number of "time steps" I_{SD}). The initial trial guess $\{\psi_i(\vec{r},t=0)\}$ must be nonorthogonal to the ground-state in order for the SD procedure to work correctly. Since E is invariant with respect to unitary transformations among occupied states, the orthonormalization scheme chosen is in this context largely arbitrary. The simple Gram-Schmidt procedure is one of the possible choices.

There are two basic ingredients of a single SD step: action on the $\{\psi_i\}$ with the Hamiltonian H and orthonormalization of $\{\psi_i\}$. In a plane-wave formulation the latter operation requires $O(N_e^2 M)$ floating-point operations. The former operation can be made efficient by making use of fast Fourier transform (FFT) techniques (Car and Parrinello 1985) and carrying out operations always in the "easy" space. Some relevant details are presented in Appendix 3. The kinetic energy term is diagonal in reciprocal space, requiring $O(N_e M)$ operations. The action of the local potential

is conveniently calculated in real space requiring $O(N_e M \log M)$ operations. In conclusion, the big dimension M enters only linearly or via $M \log M$ in the count of the operations. Thus a single SD step represents a significant improvement over standard diagonalization where M enters as M^3. This is partially counterbalanced by a larger number of steps I_{SD} necessary to achieve convergence ($I_{SD} > I_{sc}$).

The straightforward SD method is known not to be the most efficient minimization algorithm, and may be improved in several ways (Press et al 1986). In order to increase the maximum time integration step Δt in equation II.2.7 and so accelerate convergence, one can use some properties of the minimization problem, such as the diagonal dominance of the Hamiltonian matrix for sufficiently large G. If we assume it to be diagonally dominated for all G's then we can separate in equation II.2.7 the action on the wave functions of the diagonal part of H from that of the off-diagonal part. The result is

$$\begin{aligned} \dot{c}^i_{\vec{G}} &= -\left[\tfrac{1}{2}|\vec{k}+\vec{G}|^2 + V_{\vec{G}-\vec{G}} - \varepsilon^i_p\right] c^i_{\vec{G}} - \sum_{\vec{G}' \neq \vec{G}} V_{\vec{G}-\vec{G}'}\, c^i_{\vec{G}'} + OC \\ &= -\omega_{\vec{G}} c^i_{\vec{G}} - R + OC. \end{aligned} \qquad (II.2.8)$$

In equation II.2.8 a constant $\varepsilon^i_p = \langle \psi_i(t)|H(t)|\psi_i(t)\rangle$ has been subtracted from the diagonal part of H. By explicitly integrating the diagonal term and treating the off-diagonal one as a perturbation we obtain:

$$c^i_{\vec{G}}(t+\Delta t) = \exp(-\omega_{\vec{G}}\Delta t)\left\{ c^i_{\vec{G}}(t) + \frac{R}{\omega_{\vec{G}}}\left[1 - \exp(\omega_{\vec{G}}\Delta t)\right]\right\} + OC. \qquad (II.2.9)$$

Equation II.2.9 replaces the ordinary SD equations II.2.7 and we call this scheme the *modified steepest descent* (MSD). MSD represents an adaptation to SD of the idea introduced by Payne et al (1986) for MD equations. In some cases MSD constitutes a definite improvement over SD by allowing a larger time integration step Δt and consistently increasing the convergence rate. However, in many important cases and particularly in low symmetry situations the MSD algorithm does not improve over SD (Štich et al 1989a). We found this method useful if employed in nonself-consistent calculations, i.e. with fixed potential.

We have developed a very robust method for minimization of the energy functional (Štich et al 1989a, Štich 1989) based on the well-known method of conjugate gradient (CG) minimization (Press et al 1986, Hageman and Young 1981). An important advantage of CG methods over other approaches is that they take full advantage of the matrix of second derivatives without explicitly calculating it. Convergence tests of the CG method are given elsewhere (Štich et al 1989a). Details of the CG method are summarized in Appendix 4. Further distinct advantage is the absence in the CG method of any convergence controlling parameter, such as the time integration step Δt. The conclusion is that the CG approach is significantly superior to any SD-based method. A heavy use of the electronic CG minimization has been made in computations presented in sections III and IV.

II.3 First Principles Molecular Dynamics

Since the ab-initio * MD method recently introduced by Car and Parrinello (1985) (CP) is the main methodological aspect of this thesis we briefly introduce this technique. More details are given elsewhere (Car and Parrinello 1988b).

One conceivable way of an ab-initio MD would consist in calculating the Hellman-Feynman (HF) forces

$$\vec{F}_I = -\frac{\partial \Phi[\{\vec{R}_I\}]}{\partial \vec{R}_I} = \langle \psi_0 | - \frac{\partial}{\partial \vec{R}_I}\left(H_{eI} + \tfrac{1}{2}\sum_{I\neq J} \frac{Z_I Z_J}{|\vec{R}_I - \vec{R}_J|}\right)|\psi_0\rangle \qquad (II.3.1)$$

needed in an MD scheme for the ions by finding explicitly the electronic ground-state. This naive straightforward approach has been found significantly less convenient (Štich 1987) than the generalized Lagrange formulation (Car and Parrinello 1985). This point is more fully discussed in Appendix 5. Generally, besides the HF forces also the Pulay (1969) forces must be taken into account. With plane-waves these forces do not arise.

The CP technique consists in considering the parameters $\{\psi_i\}$ and $\{\vec{R}_I\}$ in the energy functional to be time dependent and writing the Lagrangian (Car and Parrinello 1985)

$$L = \tfrac{1}{2}\mu \sum_i \int_\Omega d\vec{r}|\dot{\psi}_i(\vec{r})|^2 + \tfrac{1}{2}\sum_I M_I \dot{\vec{R}}_I^2 - E[\{\psi_i\},\{\vec{R}_I\}] + \sum_{ij}\Lambda_{ij}\int_\Omega d\vec{r}(\psi_i^*\psi_j - \delta_{ij}) \qquad (II.3.2)$$

where Ω is the unit cell volume, M_I are physical masses of the ions, and μ is an arbitrary parameter of appropriate units which serves to define the fictitious kinetic energy of the K-S orbitals. In equation II.3.2 the first two terms are classical kinetic energies associated with electronic and ionic degrees of freedom and the energy functional E plays the role of potential energy. The Lagrange multipliers Λ_{ij} impose the orthonormality constraints of equation II.1.7.

The Lagrangian II.3.2 generates a dynamics in the coupled electron-ion parameter space through equations of motion

$$\mu\ddot{\psi}_i(\vec{r},t) = -\frac{\delta E}{\delta \psi_i^*(\vec{r},t)} + \sum_j \Lambda_{ij}\psi_j(\vec{r},t) \qquad (II.3.3a)$$

$$M_I\ddot{\vec{R}}_I = -\frac{\partial E}{\partial \vec{R}_I}. \qquad (II.3.3b)$$

Equation II.3.3b generates the correct classical dynamics of the ions if at each time step also equation II.1.4 is satisfied. This is approximately the case if the time

* A method is ab-initio if it doesn't contain any empirical relationship or adjustable parameter, i.e. the potential is calculated from first principles.

scale for the motion of the electronic degrees of freedom is much shorter than that for the ions. To set up such a regime requires $\mu << M_I$ and $\{\psi_i\}$ to be initially in the ground-state. In these conditions, the electronic degrees of freedom acquire only a very small classical kinetic energy to follow adiabatically the ions, and the ionic trajectories, initially lying on the BO surface, deviate from it very slowly on the time scale of the MD simulation. Thus very few or no separate electronic minimizations are necessary to keep the system on the BO surface during an MD run. The electronic minimizations, when necessary, can be efficiently carried out by employing methods described in section II.2. Equation II.3.3b, thus describes a true atomic dynamics. Equation II.3.3a instead, describes a fictitious dynamics and must be viewed only as a tool of finding the ground-state potential $\Phi\big[\{\vec{R}_I\}\big]$. A distinct feature of the ab-initio MD is that it generates simultaneously atomic trajectories and the corresponding ground-state charge densities and potentials. These make possible to follow directly the evolution of the chemical bonds resulting from atomic motion or to compute electronic properties, like densities of states and conductivities.

For an ergodic system one can identify temporal averages with ensemble averages. In particular, the equilibrium value of the classical kinetic energy of ions can be related to the temperature T of the system through the equipartition theorem

$$\langle \sum_I \tfrac{1}{2} M_I \dot{\vec{R}}_I^2 \rangle = \tfrac{3}{2} N k_B T. \qquad (II.3.4)$$

By variation of the ionic velocities $\{\dot{\vec{R}}_I\}$, one can control the temperature of the system and let it vary. In this way thermal treatments, such as *annealing* and *quenching*, are possible with the ionic subsystem. Also the concept of *simulated annealing* recently introduced by Kirkpatrick, Gelat, and Vecchi (1983) can be applied.

In practice, equations II.3.3 are integrated numerically. If the integration time step Δt is short, low-order formulae, such as the Verlet (1967) algorithm, are convenient. This leads to

$$\psi_i(\vec{r}, t+\Delta t) = -\psi_i(\vec{r}, t-\Delta t) + 2\psi_i(\vec{r}, t) + \frac{\Delta t^2}{\mu}\Big(-\frac{\delta E}{\delta \psi_i^*(\vec{r}, t)} + \sum_j \Lambda_{ij}\psi_j(\vec{r}, t)\Big) \qquad (II.3.5a)$$

$$\vec{R}_I(t+\Delta t) = -\vec{R}_I(t-\Delta t) + 2\vec{R}_I(t) - \frac{\Delta t^2}{M_I}\frac{\partial E}{\partial \vec{R}_I}. \qquad (II.3.5b)$$

The method of finding the Lagrange multipliers in equation II.3.3a has been described elsewhere (Car and Parrinello 1988b) and is not elaborated further here. The operations to calculate the unconstrained electronic forces (first term on RHS of equation II.3.3a) are identical as for the SD equations (II.2.6). Srivastava and Weaire (1987) give a detailed account of evaluation of ionic forces within plane-wave

pseudopotential formalism (RHS of equation II.3.3b). The operations required to solve these equations scale essentially as described in section II.2.

A small μ requires a small maximal integration time step Δt. It turns out that Δt in the CP scheme can sometimes be as large as $\sim \frac{1}{2}\ \Delta t$ used with empirical potentials. This makes the CP method efficient. In practice, in the case of insulators and semiconductors the ionic trajectories show no deviation from the BO surface on the time scale given by the MD observation time in a wide range of temperatures. As explained in Appendix 5, this can be checked by monitoring the constant of motion in the microcanonical ensemble

$$\sum_I \tfrac{1}{2} M_I \dot{\vec{R}}_I^2 + E\big[\{\psi_i\},\{\vec{R}_I\}\big] = const. \qquad (II.3.6)$$

Now we turn to the application of the CP method to metallic systems. In this case we have observed a tendency to thermal equilibration between electronic and ionic subsystems related to the existence of empty electronic states degenerate or nearly degenerate with the occupied states (Štich et al 1989b). It means that there is some energy transfer from the ionic to the electronic subsystem. This process can not be fully eliminated but may be controlled by the difference in the time scales of electronic and ionic processes, i.e. by μ. These effects have two consequences: (i) the electronic wave functions deviate from ground-state, (ii) the ionic subsystem spontaneously decreases its temperature due to the energy transfer between the electronic and ionic subsystems. As for (i), it turns out that the electronic subsystem and hence also the forces acting on ions are relatively weakly perturbed by the effects of equilibration and the perturbation can be remedied by systematic electronic minimizations. Hence as long as the deviation of the wave functions from the ground-state is "small enough" and does not substantially change the character of the wave functions, the resulting noise in the ionic forces is not critical. As for (ii) we have tested several solutions and in order to stabilize the ionic temperature we found most useful to couple the ionic subsystem to a Nosé thermostat (Nosé 1984 a,b). The resulting modified equations II.3.3 read

$$\mu \frac{d^2}{dt}\psi_i(\vec{r},t) = -\frac{\delta E}{\delta \psi_i^*(\vec{r},t)} + \sum_j \Lambda_{ij}\psi_j(\vec{r},t) \qquad (II.3.7a)$$

$$M_I \frac{d^2}{dt}\vec{R}_I = -\frac{\partial E}{\partial \vec{R}_I} - \frac{M_I}{s}\frac{d\vec{R}_I}{dt}\frac{ds}{dt} \qquad (II.3.7b)$$

$$Q\frac{d^2}{dt}s = s\sum_I M_I\Big(\frac{d\vec{R}_I}{dt}\Big)^2 - sgk_BT + \frac{Q}{s}\Big(\frac{ds}{dt}\Big)^2. \qquad (II.3.7c)$$

Note that the equations II.3.7a-c are written in *real variables* (Nosé 1984 a,b). In equations II.3.7b,c the extra degree of freedom s, having the dynamical "mass" Q, couples the ionic subsystem, with $g = 3N$ degrees of freedom, to a heat bath at a temperature T. Note that the ionic degrees of freedom move both under the

action of the interparticle forces and of the coupling to the heat bath. It is this coupling that continuously rescales the particle velocities $\{\frac{d\vec{R}_I}{dt}\}$ and supplies to the ions kinetic energy necessary to maintain T constant. As demonstrated by Nosé (1984a,b), equations II.3.7b,c lead to a *canonical distribution* in the ionic phase space.

The constant of motion in the canonical ensemble is the sum of kinetic plus potential energies of the ions and of the extra particle s

$$\sum_I \tfrac{1}{2} M_I \dot{\vec{R}}_I^{\,2} + E[\{\psi_i\},\{R_I\}] + \tfrac{1}{2} Q(\dot{s}s)^2 + gkTlns = const \qquad (II.3.8)$$

and the average temperature

$$\langle T \rangle = const. \qquad (II.3.9)$$

We have also tested the Gaussian isothermal method (Hoover 1986) which constraints the total kinetic energy term of the ions

$$\sum_I \tfrac{1}{2} M_I \dot{\vec{R}}_I^{\,2} = \tfrac{1}{2} g k_B T \qquad (II.3.10)$$

and thus suppresses the total kinetic energy fluctuations. This method, however, turned out to be much less stable in combination with CP than sampling in the true canonical ensemble.

By supplying energy to the ions from an external heat bath the temperature of the ions is stabilized in the above scheme. Nevertheless, the deviation of the single-particle orbitals from ground-state will continue (equations II.3.3a and II.3.7a are identical) and must be accounted for by reoptimization of the electronic structure when some preset toleration is exceeded. By setting appropriately the time scales of the fast electronic and the slow ionic degrees of freedom, the rate of equilibration between the two subsystem can be made so slow that only few electronic minimizations are necessary during an MD run. This guarantees the usefulness of our method even for metals.

In the case of metals the validity of the BO approximation may be questioned. In practice, however, this does not pose serious problems as demonstrated numerically by the sucess of the phonon calculations or theoretically by the Migdal's theorem. Generally, one should use the quantum dynamics, what constitutes a difficult problem. An intermediate approach might consist in treating the ions still classically and considering the finite temperature effects on the electrons; i.e. substituting the K-S functional by the Mermin (1965) functional. However, the blurring of the Fermi surface at the temperatures of interest here is still relatively small. Hence it is reasonable to consider a perfectly sharp Fermi surface as at $T = 0K$. Moreover, the generalization of the CP method to the Mermin functional is not trivial.

III. Liquid Silicon

III.1 Principal Properties of Liquid Silicon

The prototype elemental semiconductor Si (similarly to Ge) has in its liquid state several intriguing and poorly understood properties. Some of them, which are related to the properties we study in the following, are listed below.

l-Si has an unusually high melting point occurring at the temperature $T_m = 1683K$ (Glazov at al 1969). Upon melting the density of Si increases by $\sim 10\%$ (Waseda 1980) (Tab.III.1.1 and Fig.III.1.1) and its structure goes from an open structure with a coordination number 4 to a more compact liquid structure characterized by a coordination number exceeding 6 (Waseda and Suzuki 1975, Gabathuler and Steeb 1979). It is fairly unusual for a liquid metal to have a coordination number between 6 and 7, because most liquid metals are more closely packed with a coordination ~ 12 (Faber 1972, Croxton 1974). This indicates a partial collapse of the tetrahedral network.

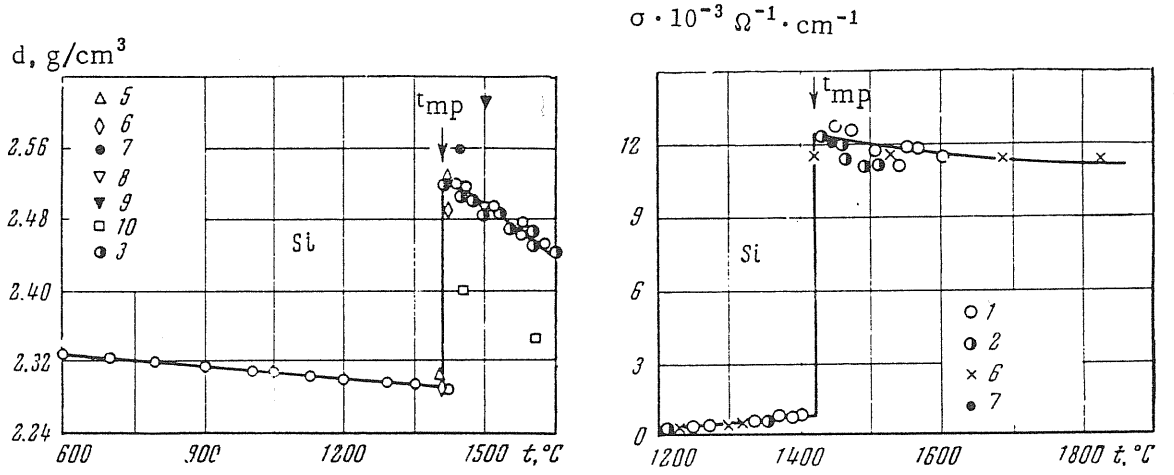

Fig.III.1.1. Left panel: Temperature dependence of the density of Si. Right panel: Temperature dependence of the electrical conductivity of Si.

Table III.1.1. *Density ρ and electrical conductivity σ of Si and Ge in the solid state and near the melting point (Glazov et al 1969)*

	ρ_s gcm^{-3}	ρ_l gcm^{-3}	$\frac{(\rho_l-\rho_s)}{\rho_s}$ %	σ_s $\Omega^{-1}cm^{-1}$	σ_l $\Omega^{-1}cm^{-1}$	$\frac{\sigma_l}{\sigma_s}$
Si	2.30	2.53 2.59†	~10	~580	~12000	~20
Ge	5.26	5.51	~4.75	~1250	~14000	~11

†Waseda 1980

Liquid silicon (l-Si) undergoes on melting a semiconductor to metal phase transition as evidenced by the jump in conductivity by a factor of 20 (11 for Ge) (Glazov et al 1969) (Fig.III.1.1 and Tab.III.1.1). The a.c. electrical conductivity has also been studied (Shvarev et al 1975) and the results indicate a Drude-like behavior, even though the electronic mean free path is short (Shvarev et al 1975). The electronic structure was only partially explored and only the $3p$ band was measured (Hague et al 1980).

The low coordination of l-Si indicates a persistence of some covalent bonds in the liquid. However, no quantitative description of such effects has so far been provided.

This unusual properties of l-Si are a challenge for the theory. An analysis of these properties of the melt based on a first principles MD will be given in the following.

III.2 MD Simulation of Liquid Silicon

In order to study the structural, dynamical, and electronic properties of l-Si outlined in section III.1 we employed the CP method suitably modified as explained in section II.3 (equations II.3.7a-c).

We have performed a Nosé-type constant temperature, constant volume MD simulation at the experimental density $\rho = 2.59 gcm^{-3}$ ($0.0555 \mathring{A}^{-3}$) (Waseda 1980). The MD cell contained 64 atoms with periodic boundary conditions of the simple cubic type. The average temperature was kept at $T = 1800K$, close to the experimental melting point $T_m = 1680K$.We used nonlocal norm-conserving pseudopotentials of the Bachelet-Hamann-Schlüter (1982) type with s-nonlocality only. Kleinman and Bylander's (1982) factorized form was adopted to speed up the calculation. Exchange and correlation effects were treated within LDA in the parametrized form (Perdew and Zunger 1981). The electronic orbitals were expanded in plane-waves. The Γ point, $\vec{k} = (0,0,0)$, only was used to sample the Brillouin zone of the MD supercell. To ascertain the validity of this approximation with a relatively small cell size, we have tested it against the variations of the total energy vs. atomic volume for both semiconducting and metallic Si phases. A satisfactory agreement with a more elaborate calculation (Yin and Cohen 1982b) has been found. The occupation numbers of the K-S orbitals were kept fixed during the simulation. A tiny integration time step of $5.5 a.u.$ ($1.3 \times 10^{-16} s$) was chosen, while the fictitious "mass" μ was taken to be $300 a.u.$ This choice is very close to that made in the previous study of the disordered Si phases (Car and Parrinello 1988a) and guarantees a slow rate of thermal equilibration between electronic and ionic degrees of freedom. Some attention must be paid to the choice of the dynamical "mass" Q in order to guarantee an efficient sampling of the phase space. As suggested by Nosé (1984b) the most efficient sampling will be achieved by choosing the same order of time scales for both the physical system and the variable s. If only small fluctuations of s around the average value $\langle s \rangle$ are considered, the frequency of this motion can be found to be

$$\omega^2 = \frac{2 g k_B T}{Q \langle s \rangle}. \qquad (III.2.1)$$

We set $Q = 2.5 \times 10^5 a.u.$, what makes ω comparable to the optical phonon frequency in the c-Si.

The initial configuration was generated by starting from atoms in diamond lattice positions with small random displacements. Then the system was heated up to $\sim 6000K$ by rescaling the particle's velocities. After melting has occurred the temperature was reduced to $T = 1800K$ and the Nosé thermostat switched on. After equilibration we have followed the system for a total time of $1.2 ps$. This observation time is much larger than the typical relaxation times.

We have checked the convergence of the calculation with respect to periodic

boundary conditions, cell size, inclusion of p-nonlocality in the pseudopotential, and energy cutoff in the plane-wave expansion of the electronic wave functions. We present the results of the convergence study in Appendix 6.

We end this section by showing how equations II.3.8, II.3.9 are satisfied in our simulation. Fig.III.2.1 shows the variation of the canonical constant of motion vs. time step at the temperature $T = 1800K$.

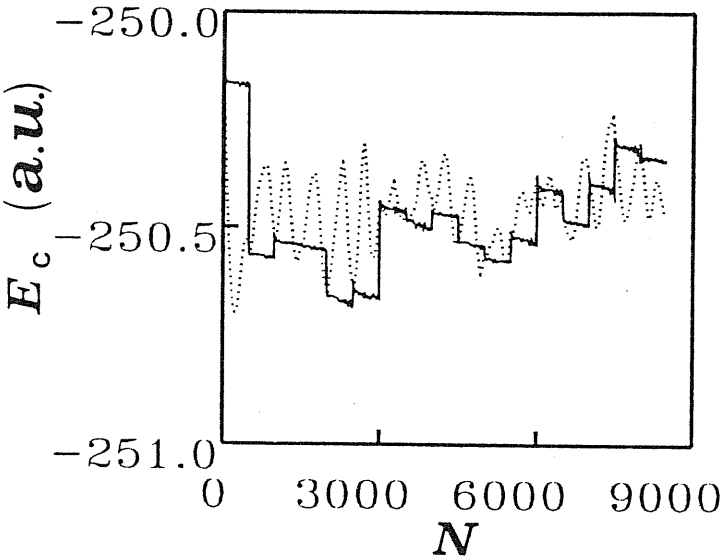

Fig.III.2.1. Constant of motion in canonical ensemble as a function of MD step N (full line). Dotted line shows the variation of kinetic plus potential energy of ions. The discontinuities correspond to periodic quenches of electrons and resetting of initial conditions of the Nosé thermostat.

A periodic discontinuity in this curve appears every 500 time steps ($\sim$ optical phonon period in c-Si), where a quench of the electrons to the instantaneous ground-state was performed and the initial conditions of the Nosé thermostat reset. We note that this choice ensures that the maximal deviation of the electrons from the BO surface is $<\sim 1.3 \times 10^{-2} eV/atom$ and the electrons remain very close to the BO surface in the course of the whole simulation. Fig.III.2.2 shows the variation of the instantaneous temperature during the simulation. The rather large temperature fluctuations are consistent with the canonical ensemble where

$$\langle (\delta T)^2 \rangle = \frac{2}{g} T^2 \qquad (III.2.2)$$

and are larger than in the microcanonical ensemble (Nosé 1984a). This constitutes an indirect check that the system is well equilibrated.

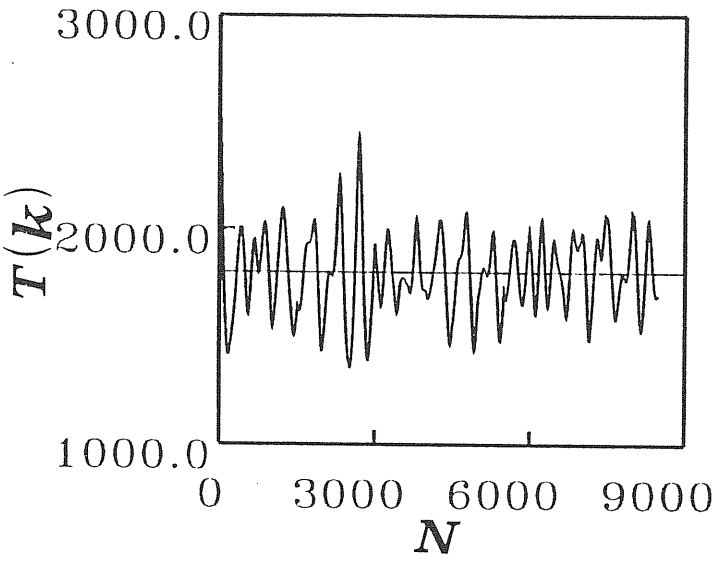

Fig.III.2.2. Instantaneous temperature of the ions as a function of MD step N. The horizontal line indicates the externally set temperature $T = 1800K$.

III.3 Short Range Order in Liquid Silicon

In this section we study the short range order (SRO) in l-Si and compare our MD results with available experimental data. In connection with our model we discuss the plausibility of existing empirical and microscopic structural models of l-Si.

It is known that the structural correlations in liquids fall off rapidly and only the SRO up to $5-6\mathring{A}$ persists. SRO is conveniently characterized by *equilibrium distribution functions*. Let us assume canonical ensemble (Ω, T, N) and a configuration of the system $\{\vec{R}_1, \vec{R}_2, ..., \vec{R}_N\}$. Then the probability of simultaneously finding particle 1 in a volume $d\vec{R}_1$ around $\vec{R}_1$, particle 2 in $d\vec{R}_2$ around $\vec{R}_2$,..., particle n in $d\vec{R}_n$ around $\vec{R}_n$ is

$$P_N^{(n)}(\vec{R}_1, \vec{R}_2, ..., \vec{R}_n) = \langle \delta(\vec{R}_1 - \vec{R}_1')\delta(\vec{R}_2 - \vec{R}_2'), ..., \delta(\vec{R}_n - \vec{R}_n')\rangle. \qquad (III.3.1)$$

In the limit

$$|\vec{R}_I - \vec{R}_J| \to \infty \qquad 1 \leq I, J \leq n \qquad (III.3.2)$$

$$P_N^{(n)}(\vec{R}_1, \vec{R}_2, ..., \vec{R}_n) = P_N^{(1)}(\vec{R}_1).P_N^{(1)}(\vec{R}_2)...P_N^{(1)}(\vec{R}_n). \qquad (III.3.3)$$

From equations III.3.1, III.3.3 the *n-particle distribution function* can be defined as

$$g_N^{(n)}(\vec{R}_1, \vec{R}_2, ..., \vec{R}_n) = \frac{P_N^{(n)}(\vec{R}_1, \vec{R}_2, ..., \vec{R}_n)}{\prod_{I=1}^{n} P_N^{(1)}(\vec{R}_I)}. \qquad (III.3.4)$$

In the limit III.3.2

$$g_N^{(n)}(\{\vec{R}_I\}) \to 1. \qquad (III.3.5)$$

For a homogeneous system

$$P_N^{(1)}(\{\vec{R}_I\}) = \frac{1}{\Omega} \qquad (III.3.6)$$

and the definition III.3.4 can be written as

$$g_N^{(n)}(\{\vec{R}_I\}) = \Omega^n P_N^{(n)}(\{\vec{R}_n\}). \qquad (III.3.7)$$

We find important besides the *pair correlation function* which in an isotropic system is given as

$$g_N^{(2)}(\vec{R}_1, \vec{R}_2) = g(|\vec{R}_1 - \vec{R}_2|) = g(r) \qquad (III.3.8)$$

also the higher-order distribution functions, especially the *triplet correlation function* $g_N^{(3)}(\vec{R}_1, \vec{R}_2, \vec{R}_3)$. The $g_N^{(3)}$ is important in our case, since we want to describe systems that retain some covalent bonds and have directional forces.

In principle, information on these two functions can be obtained experimentally. The scattering intensity $I(k)$ measured in a scattering experiment (X-rays,

neutrons) is proportional to the *static structure factor* which in turn is related to $g(r)$ via

$$S(k) = \frac{1}{N}\sum_{m,n}\langle e^{i\vec{k}.(\vec{R}_m - \vec{R}_n)}\rangle$$
$$= 1 + 4\pi\rho\int r^2 \frac{\sin kr}{kr}[g(r)-1]\mathrm{d}r. \qquad (III.3.9)$$

Information on g^3 might be obtained from an X-ray absorption spectroscopy (XAS) measurement (Filipponi 1989). However, no such experiment has been done for l-Si as yet. Thus presence of disorder precludes an experimental determination of the individual atomic coordinates since only incomplete and averaged information can be obtained experimentally.

Only very few experimental data are available on $g(r)$ and $S(k)$ in l-Si. Waseda and Suzuki (1975) have carried out an X-ray study of l-Si at a temperature of $1730K$ for k from the interval $0.5\mathring{A}^{-1} < k < 12\mathring{A}^{-1}$. Gabathuler and Steeb (1979) have studied l-Si at $1700K$ by neutron diffraction for angles corresponding to $0.2\mathring{A}^{-1} < k < 10\mathring{A}^{-1}$. The X-ray scattering data are summarized in Fig.III.3.1 and Tabs.III.3.1, III.3.2; the neutron diffraction data are given in Fig.III.3.2 and Tabs.III.3.1,III.3.2.

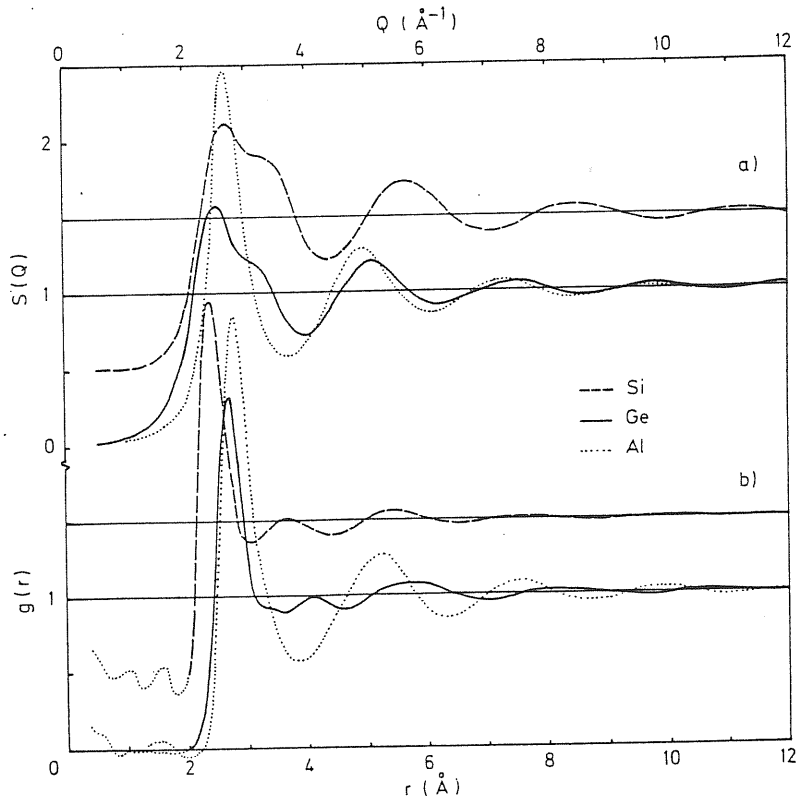

Fig.III.3.1. X-ray scattering data of Waseda and Suzuki (1975).

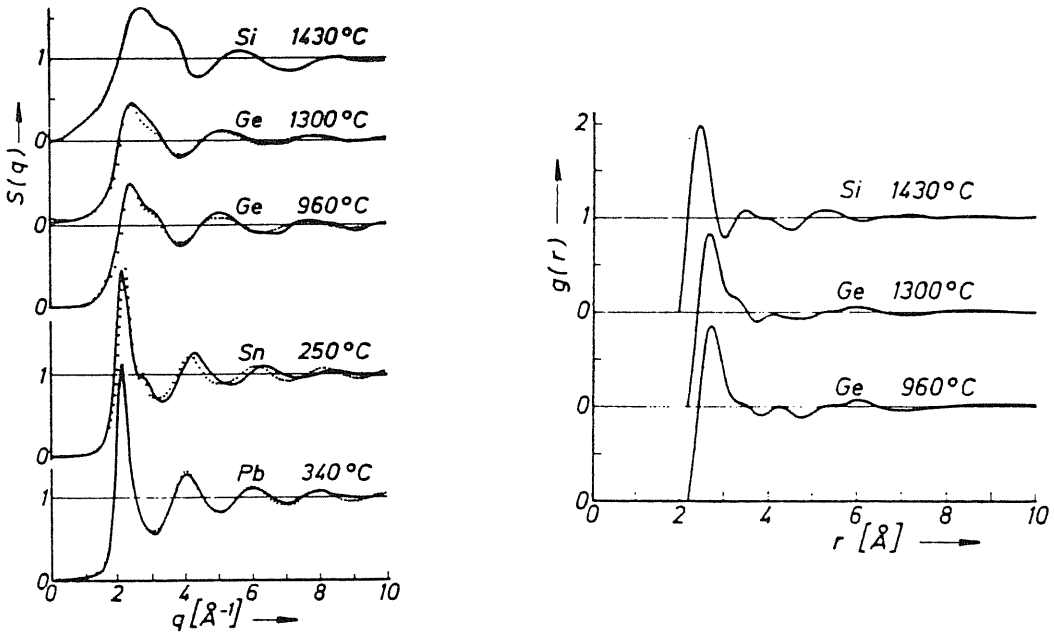

Fig.III.3.2. Neutron diffraction data of Gabathuler and Steeb (1975).

Table III.3.1. *g(r) from X-ray (Waseda and Suzuki 1975) and neutron (Gabathuler and Steeb 1979) scattering data*

Technique	T K	R^I Å	R^{II} Å	R^{III} Å	$\frac{R^{II}}{R^I}$	$\frac{R^{III}}{R^I}$	$g(r)$	N^I
X-rays	1730	2.40	3.70	5.50	1.54	2.29	2.46	6.4
neutrons	1700	2.50		5.33		2.14	2.23	6.4

Table III.3.2 *S(k) from X-ray (Waseda and Suzuki 1975) and neutron (Gabathuler and Steeb 1979) scattering data*

Technique	T K	K^I $Å^{-1}$	K^{II} $Å^{-1}$	$\frac{K^{II}}{K^I}$	$S(K^I)$
X-rays	1730	2.70	5.60	2.07	1.62
neutrons	1700	2.78	5.70	2.05	1.68

It is evident from these data that the first peak of $S(k)$ is highly asymmetric with a well pronounced shoulder on the high k side. Also the $g(r)$ is unusual, unlike simple liquids that have a symmetric first peak and oscillate regularly around one. Especially the second peak appears in an anomalous position with respect to simple liquids. The low coordination number $N^I = 6.4$ indicates an open structure and presence of directional covalent bonds, while most simple liquids are closely packed with coordination ~ 12 (Faber 1972, Croxton 1974).

A closer inspection reveals marked differences between the two experimental data sets. In principle, one should expect some differences, because neutrons are sensitive to the distribution of nuclei, whereas X-rays measure the distribution of electrons. Moreover, to obtain $g(r)$, eq. III.3.9 must be inverted. Thus $\tilde{g}(r)$ with

$$4\pi\rho r[\tilde{g}(r)-1]=\frac{2}{\pi}\int_{k_{min}}^{k_{max}}k[S(k)-1]\sin krdk, \qquad (III.3.10)$$

rather the true $g(r)$ is obtained, corresponding to different experimental resolution and data processing.

The structural characteristics of liquids may be taken from a wider perspective. It is well known that the structure of simple liquids can be qualitatively described by hard-spheres model (Hansen and McDonald 1976), i.e. once the volume is fixed the most important effect is the excluded volume. For nonsimple liquids the interparticle interactions are more complex and the structure deviates accordingly from that given by hard-spheres. Roughly one can classify structure of liquids into three classes (Hafner and Kahl 1984):

-*Simple structures* (Mg,Al,Pb) with $S(k)$ similar to that of hard-spheres with symmetric first peaks of $g(r)$ and $S(k)$ and peak ratios

$$\frac{K^{II}}{K^{I}}\sim 1.86 \qquad \frac{R^{II}}{R^{I}}\sim 1.91.$$

The coordination number is

$$N^{I}\sim 9-11.$$

-*Distorted structures* (Zn,Cd,Hg) with asymmetric first peaks of $g(r)$, $S(k)$ and peaks ratios slightly different from that of simple liquids and

$$N^{I}\sim 10-11.$$

-*Open structures* (Si,Ge,Sn) with highly asymmetric first peak of $S(k)$, with a shoulder on high-k side. There is a secondary maximum of $g(r)$ that appears at the position where simple liquids have the first minimum. The ratio of peak positions is anomalous with *

$$\frac{K^{II}}{K^{I}}\sim 1.96-2.1 \qquad \frac{R^{II}}{R^{I}}\sim 2.0-2.3.$$

and

$$N^{I}\sim 6.4-7.$$

* Actually, in these structures R^{II} is the third peak of $g(r)$ but corresponds to the second peak in other structures.

Clearly, l-Si is a particular case where the detailed microscopic nature of the interparticle many-body potential plays an extremely important role. In l-Si the structural departure from the hard-sphere behaviour is most pronounced as evidenced by the failure to fit a hard-sphere $S(k)$ to l-Si (Fig.III.3.3).

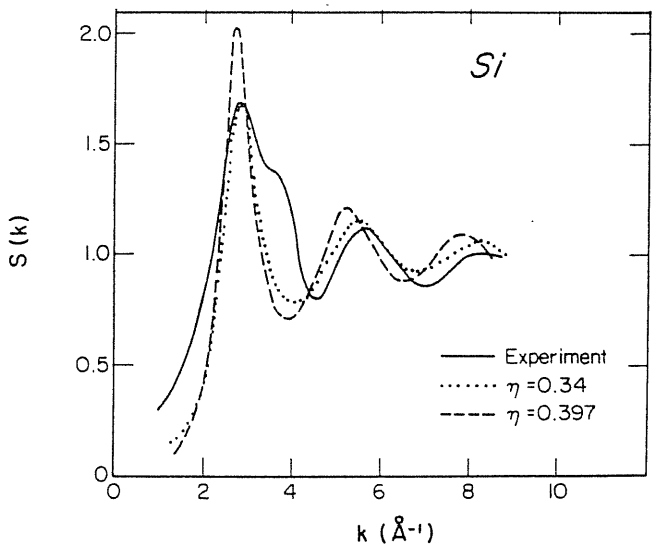

Fig.III.3.3. Percus-Yevick hard-sphere fit of S(k) to l-Si (Shih and Stroud 1984). Full line indicates the experimental data of Gabathuler and Steeb (1979). Dotted line corresponds to the packing fraction that fits the height of the first peak and the dashed line to the packing fraction that yields the best overall fit.

It is an indirect indication of the importance in l-Si of the attractive interactions and probably their directionality relative to the repulsive forces that take care of excluded volume effects. This is a situation where the ab-initio MD is particularly suitable, because no arbitrary assumption is made on the interaction potential which is obtained as discussed in section II from an accurate LDA calculation. Since the atomic correlations fall off rapidly in liquids, the effect of a relatively small size of the unit cell does not pose serious limitations on our model.

In Fig.III.3.4 we show the results obtained for $S(k)$ and $g(r)$ (Štich et al 1989b, Štich 1989). Comparison with X-ray and neutron scattering experiments is very favorable, especially if one considers the differences between the two sets of experimental data and the absence of any fitting parameter in the theory. The theory correctly predicts the shoulder on the first peak of $S(k)$, the anomalous secondary peak of $g(r)$ and the first peak position at $R^I = 4.65a.u.$ appreciable larger than the value $4.44a.u.$ in c-Si. The coordination number, as obtained by integrating $g(r)$ up to the first minimum $r_m = 5.85a.u.$

$$N^I = 4\pi\rho \int_0^{r_m} t^2 g(t)\mathrm{d}t \qquad (III.3.11)$$

is ~ 6.5 in close agreement with the experimental value of ~ 6.4 * (Gabathuler and Steeb 1979, Waseda and Suzuki 1975).

* The experimentally determined coordination numbers may be subject to large

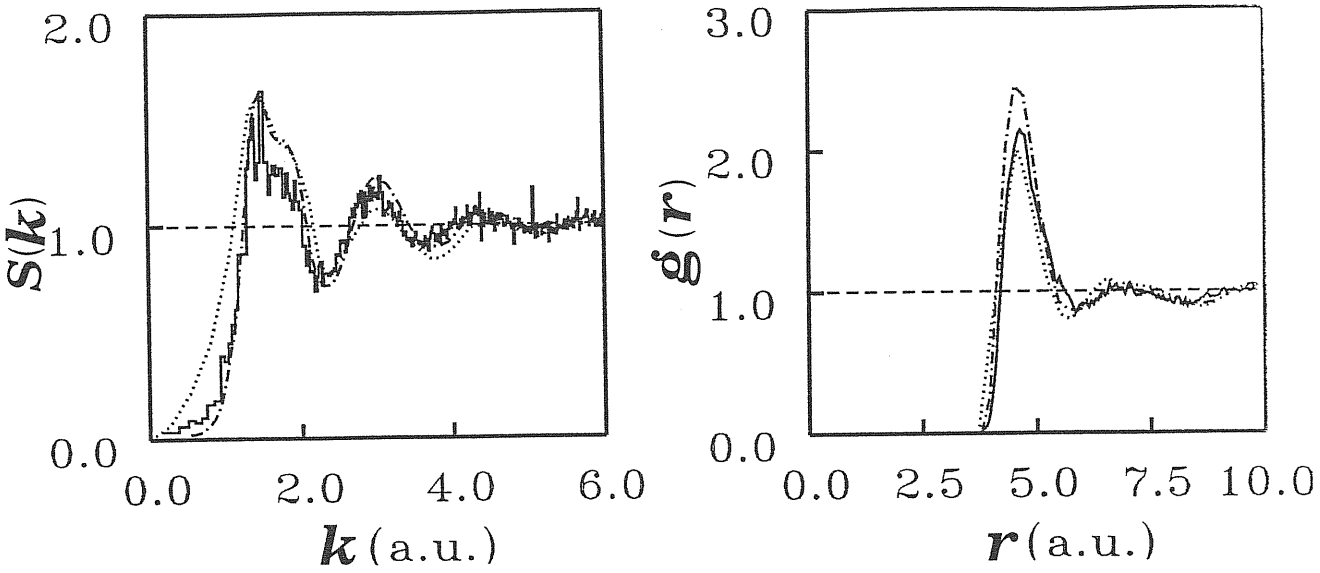

Fig.III.3.4. $S(k)$ and $g(r)$ of l-Si. Full line: MD simulation, dotted line: neutron diffraction experiment (Gabathuler and Steeb 1979), dash-dotted line: X-ray diffraction experiment (Waseda and Suzuki 1975).

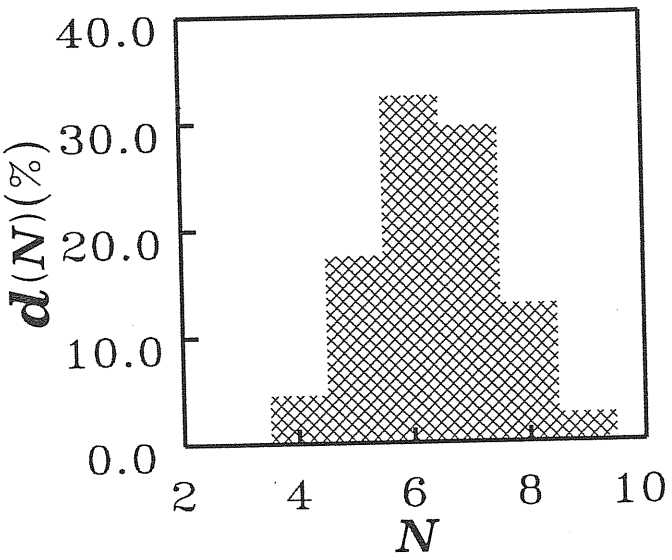

Fig.III.3.5. Distribution $d(N)$ of local coordinations in l-Si. The neighbour is defined by r_m, the first minimum of $g(r)$.

As shown in Fig.III.3.5, our results indicate presence of a broad distribution of local coordinations.

Triplet correlations in the melt are conveniently measured by *bond angle dis-*

uncertainty. They depend besides the experimental real space resolution also on the way in which they are determined (Waseda 1980)

tribution function $g_3(\theta, r_m)$. Here θ is the angle between the two vectors that join a central particle with two neighbours at a distance less than r_m. Our $g_3(\theta, r_m)$ shown in Fig.III.3.6 is rather broad with maxima centered at $\theta \sim 60°$ and $\theta \sim 90°$. In section III.4 we shall argue that covalent bonds persist in the melt and almost always form between pairs of atoms separated by a distance $\lesssim 4.7 a.u.$. For larger separations the great majority of the bonds are broken. We can therefore define $r_c = 4.7 a.u.$ as the cutoff distance for covalent bonds. The triplet correlation function $g_3(\theta, r_c)$ corresponding to these atoms is shown in Fig.III.3.6. $g_3(\theta, r_c)$ is peaked around an angle close to tetrahedral ($\theta \sim 109.5°$). A similar, albeit considerably narrower bond-angle distribution, is found in a-Si (c.f. sect.IV.4).

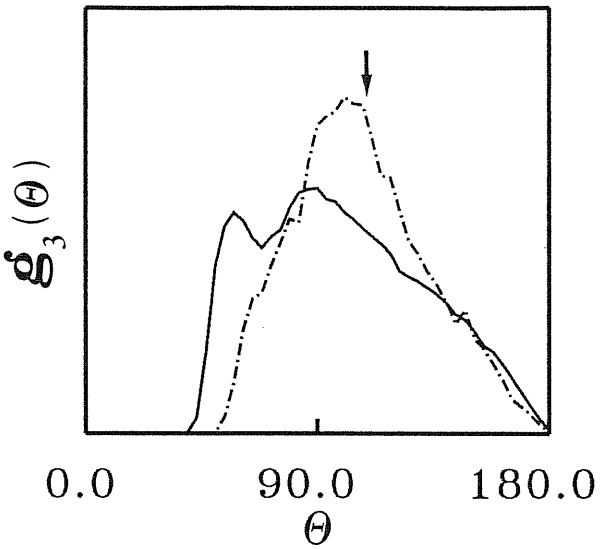

Fig.III.3.6. Bond angle distribution functions $g_3(\theta, r)$. The cutoff distance r is equal (a) to r_m, the first minimum of $g(r)$ (full line) and (b) to covalent cutoff r_c defined in text (dash-dotted line). The arrow indicates the position of the tetrahedral angle.

In the past various empirical models have been proposed to describe SRO in l-Si. They either assume presence of two kinds of atom differing either in size (Orton 1975, Gabathuler and Steeb 1979) or coordination (Waseda and Suzuki 1975) (either fourfold covalent or twelvefold metallic type) or suggest that SRO in l-Si is close to $\beta-$tin or Simple cubic (SC) structures (Gaspard et al 1984) which both are sixfold coordinated and metallic. Our results do not support these models. They indicate presence of a broad distribution of local coordinations and bond-angle distribution distinctly different from that of SC or $\beta-$ tin.

We now consider two microscopic models for l-Si based on few-body potentials. Hafner and Kahl (1984) consider an effective two-body pseudopotential of the empty-core type screened by the Ichimaru-Utsumi (1981) dielectric function. The potential has a repulsive part, a first minimum followed by damped Friedel oscillations. The form of the potential is controlled by two parameters: the electronic density ρ_e and the pseudopotential core radius R_c. They use the O.R.P.A (optimized random phase approximation) technique to describe the structure of l-

Si. The agreement with experiment is qualitatively correct; the $S(k)$ deviates from the experimental curve at large k resulting in less satisfactory $g(r)$ near the first peak. This may be the consequence of considering only the two-body interactions and neglecting three- and higher- order terms which are supposed to be important when covalent bonds are effective.

Stillinger and Weber (SW) (1985) constructed a potential that includes also the three-body terms (c.f. Appendix 1) and used it in an MD study of l-Si. Again agreement with experiments is qualitatively correct. The model, however, yields a too high coordination of ~ 8 and $S(k)$ and $g(r)$ slightly out of phase with respect to experiments (Fig.III.3.7).

Even though these methods may yield $S(k)$ and $g(r)$ that are in reasonable agreement with experiments, they may represent liquids whose structure is qualitatively different form ours. This can be seen e.g. by comparing the SW $g_3(\theta, r_m)$ (Luedtke and Landman 1988) with our result (Fig.III.3.8). As can be seen from this figure, the SW liquid overestimates the tendency to tetrahedrality (built in in the potential). On the other hand, the $g_3(\theta, r_m)$ of Hafner and Kahl (1984) (calculated by MD for l-Ge) is very similar to ours.

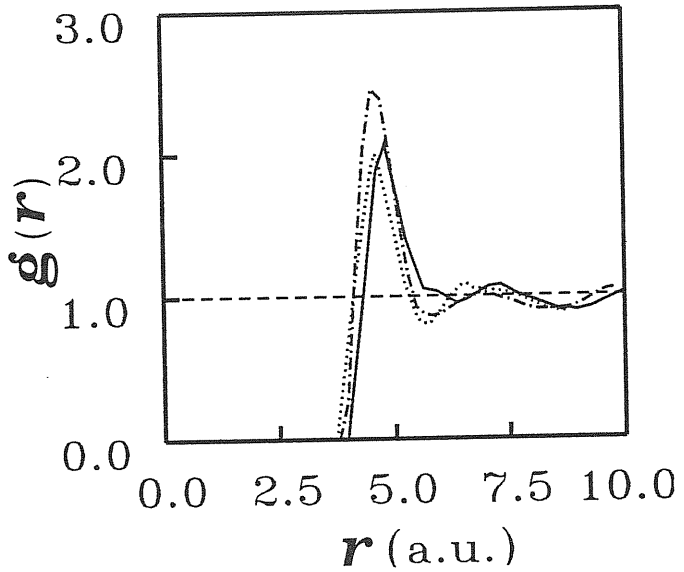

Fig.III.3.7. g(r) of the Stillinger-Weber (1985) l-Si (full line) compared with the X-ray scattering data of Waseda and Suzuki (1975) (dash-dotted line) and the neutron scattering data of Gabathuler and Steeb (1979) (dotted line).

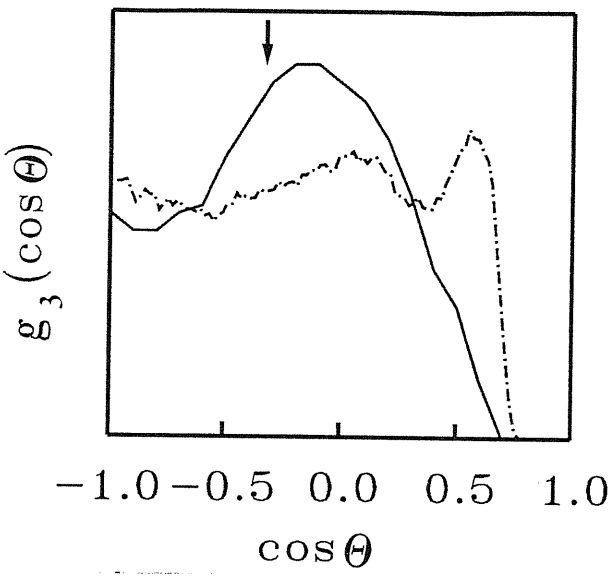

Fig.III.3.8. Bond angle distribution function $g_3(\theta, r)$ of the Stillinger-Weber (1985) (full line) and our (dash-dotted line) l-Si. The arrow indicates the position of the tetrahedral angle.

The structural characteristics of our model compare well with other existing microscopic models. Moreover, electronic, ionic, and vibrational properties are all treated on the same footing in our model.

We have carried out an extensive convergence study of our calculation with respect to parameters quoted in section III.2. These results are presented in Appendix 6.

In conclusion, the calculated $g(r)$ and $S(k)$ agree well with experiments. A converged calculation is necessary to produce a correct coordination number.

III.4 Bonding Properties of Liquid Silicon

In this section we study the valence electronic charge density and the related bonding properties of l-Si.

Si in its semiconducting phases has strong covalent directional bonds. A covalent bond can be conveniently represented by the *Bond-Charge* (BC) *model* (Phillips 1973). In this model the covalent bond is schematized by a point charge (BC) midway between neighboring atoms. Here we study how this picture is changed on melting.

A plot of the valence charge density

$$\rho_e(\vec{r}) = \sum_{i}^{occ} |\psi_{i,\vec{k}=0}(\vec{r})|^2 \qquad (III.4.1)$$

in a plane defined by three neighboring atoms in the liquid is shown in Fig.III.4.1 where for comparison we also report $\rho_e(\vec{r})$ in the (110) plane of c-Si. In Fig.III.4.1b,c the bonding distances between the two pairs of atoms in l-Si are very close to those in c-Si (Fig.III.4.1a) and consequently the two $\rho_e(\vec{r})$ have several common characteristics. In both cases the charge density is strongly nonuniform and there is an accumulation of charge density (BC) between pairs of adjacent atoms. Fig.III.4.1 provides striking evidence for the persistence of covalent bonds in the liquid. Fig.III.4.1b shows a snapshot of an instantaneous local configuration which changes in time with the typical time scale of the diffusive motion of the atoms. Its subsequent evolution at intervals of time of $\sim 5.5 \times 10^{-3} ps$ is shown in Fig.III.4.1c-i. We notice that in Fig.III.4.1e one of the two bonds starts to break, while the other is substantially weakened. Finally, in Fig.III.4.1i both bonds have disappeared, while in the upper left corner one can see the formation of a new bond with an incoming atom not shown in the picture. Another striking feature one can recognize in Fig.III.4.1 is the tendency towards creating tetrahedral order between covalently bonded atoms. The pile up of the electronic charge density in the covalent bonds is formed upon bonding. This can be seen by taking the difference between the self-consistent charge density $\rho_e^{SCF}(\vec{r})$ and the superposition of the free atom valence pseudocharge densities $\rho_e^{at}(|\vec{r} - \vec{R}_I|)$

$$\Delta\rho_e(\vec{r}) = \rho_e^{SCF}(\vec{r}) - \sum_{I} \rho_e^{at}(|\vec{r} - \vec{R}_I|). \qquad (III.4.2)$$

$\Delta\rho_e(\vec{r})$ for the configurations from Fig.III.4.1 are shown in Fig.III.4.2. This figure provides an evidence that the covalent chemical bonds are relatively weakly influenced by subtraction of the free atom densities and hence are formed upon bonding. A spatial view of these processes is shown by means of a ball-stick model in Fig.III.4.3. The rebonding from one zig-zag chain to another is clearly visible.

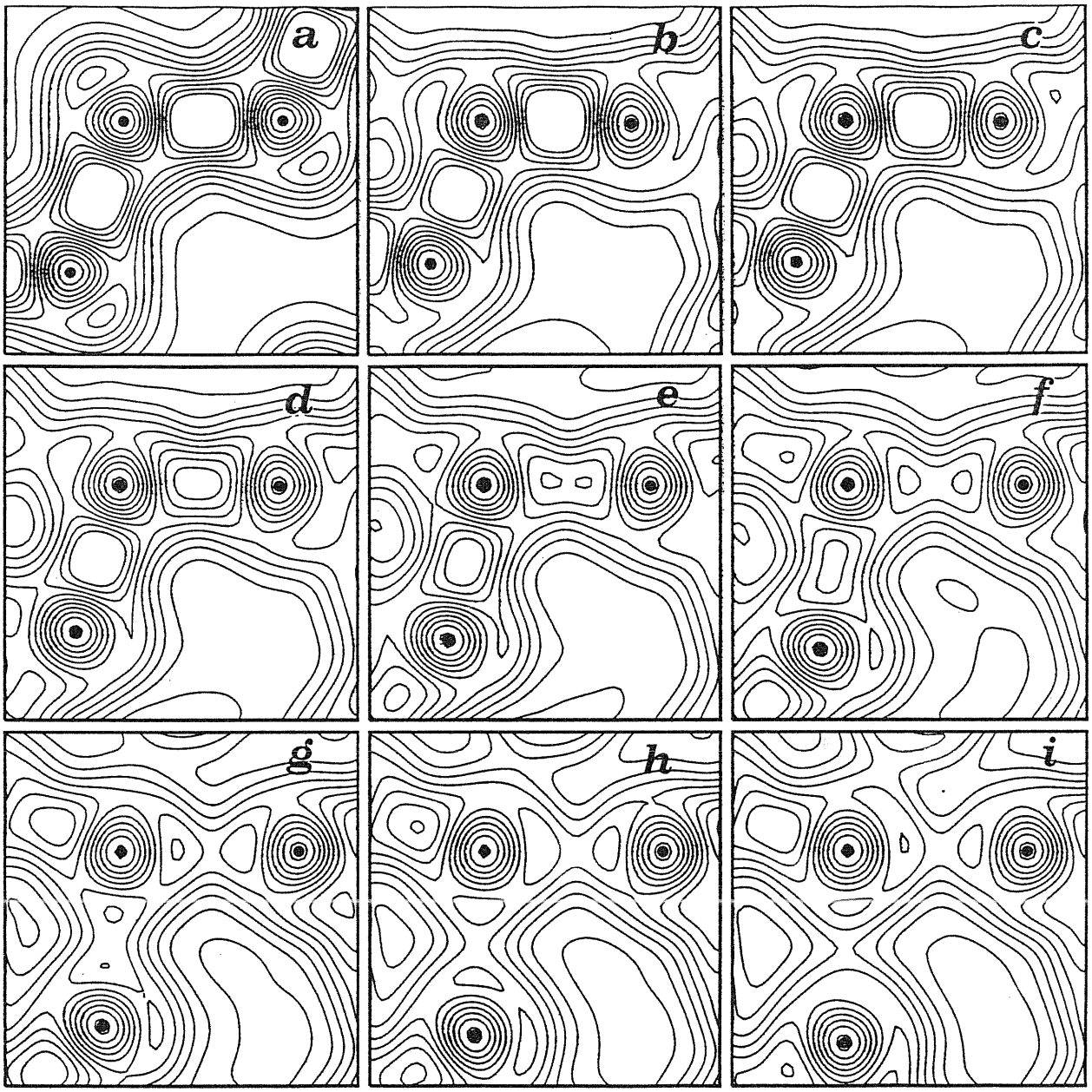

Fig.III.4.1. Contour plots of the valence electronic charge density $\rho_e(\vec{r})$. (a) c-Si in the (110) plane. (b)-(i) evolution of $\rho_e(\vec{r})$ in l-Si at time intervals of $\sim 5.5 \times 10^{-3} ps$. The dots indicate the positions of ions.

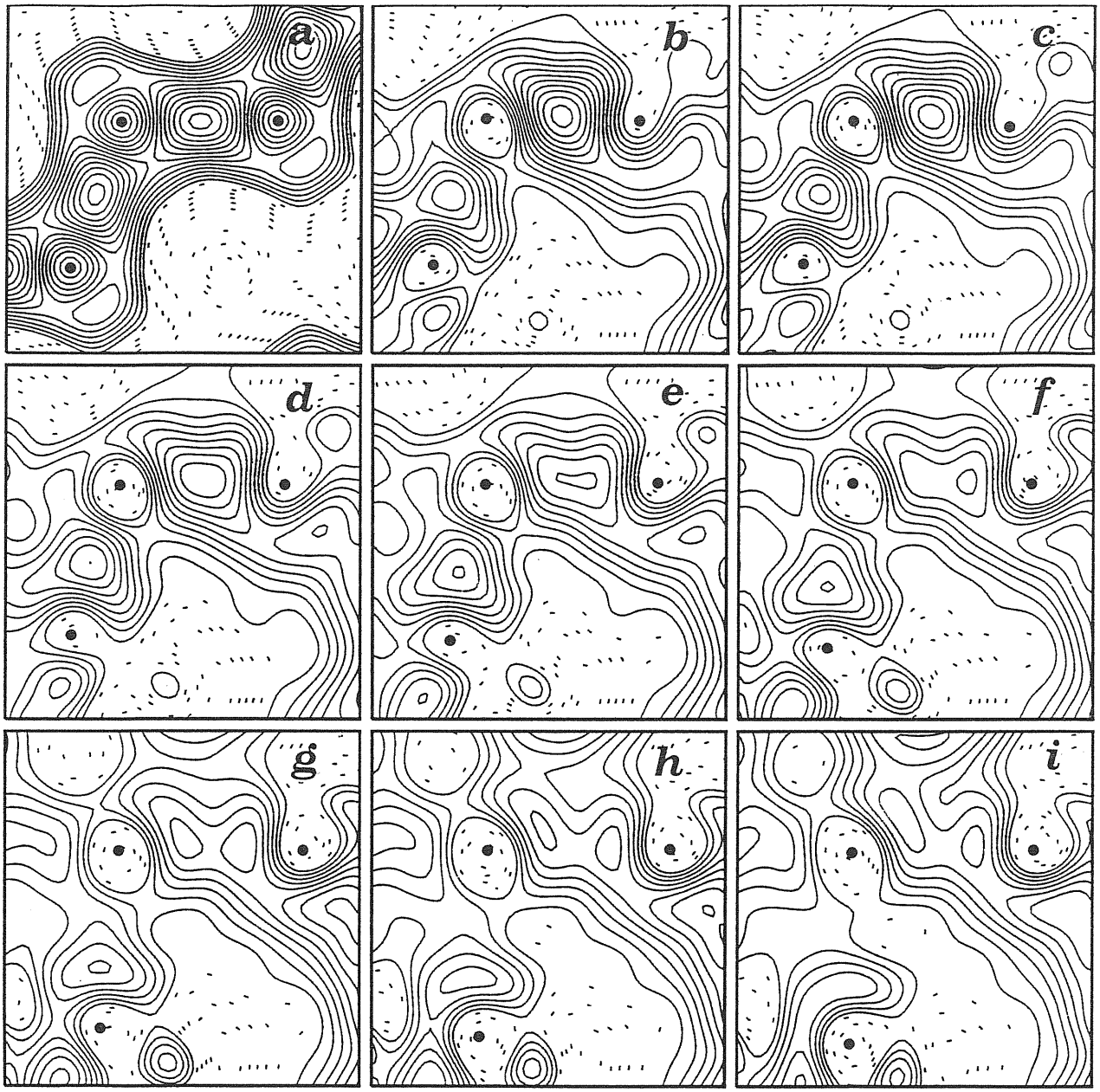

Fig.III.4.2. Difference charge densities $\Delta\rho_e(\vec{r})$ between the self-consistent and the superposition of free atom densities for the configurations from Fig.III.4.1. Positive densities are plotted by full lines and negative densities by dashed lines. The dots indicate the position of atoms.

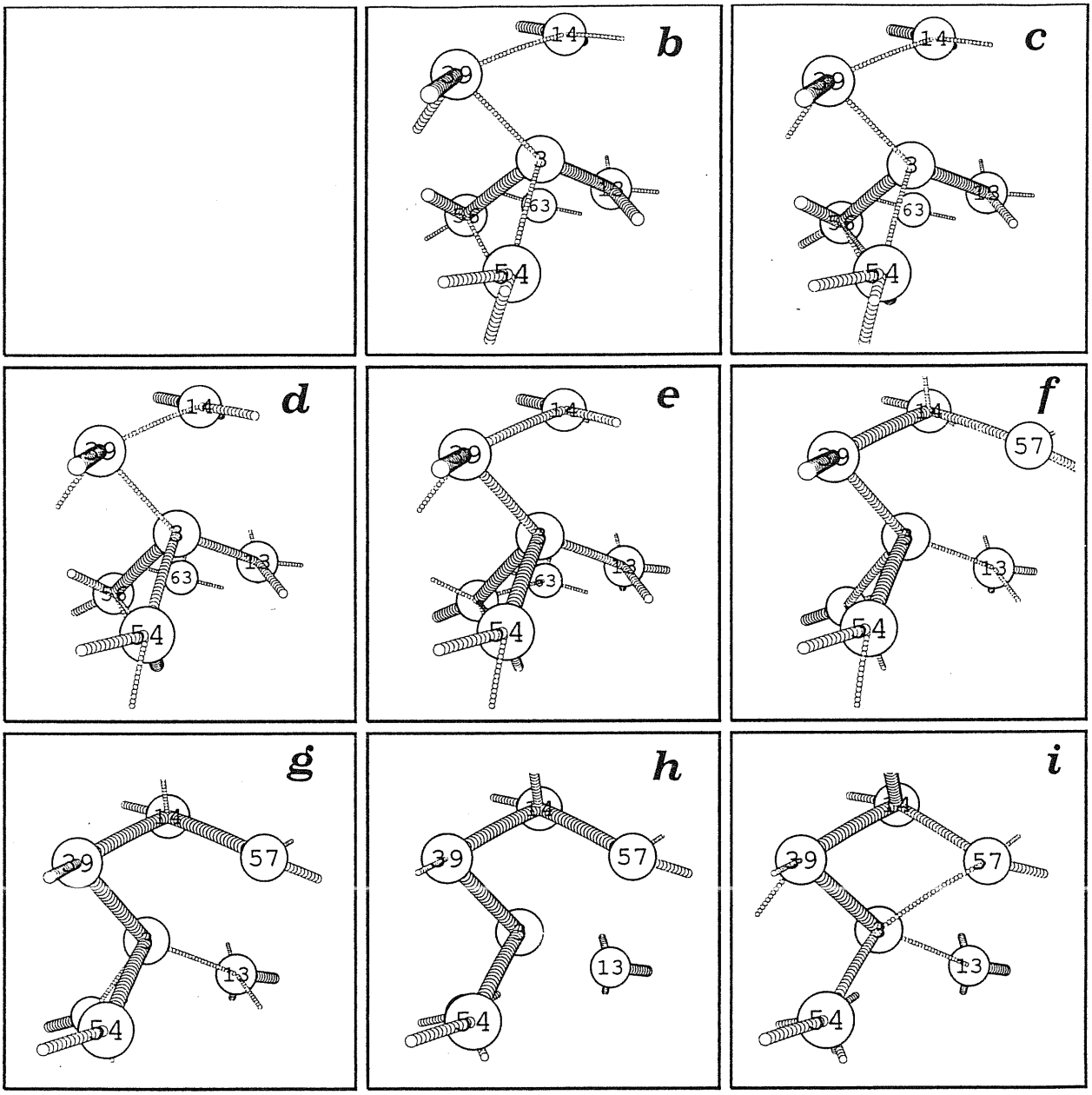

Fig.III.4.3. Ball-stick model of the local atomic configurations (b)-(i) in l-Si. The triplet of atoms from Fig.III.4.1 corresponds to atoms No. 3, 13, 56. All the atoms shown are in the first coordination shell of atom No. 3. The different bond-lengths indicated correspond to cutoffs of $4.4, 4.7, 5.0 a.u.$ for strong bonds, weak bonds, and atoms without covalent bonds, respectively.

The presence in l-Si of such strongly covalently bonded chains may play an important role in explaining why Si is able to reconstruct easily a tetrahedral network upon cooling. An extensive analysis shows that covalent bonds almost always form between pairs separated by a distance less than $\sim 4.7 a.u.$ For larger separation distances the great majority of bonds are broken. We can therefore define $r_c = 4.7 a.u.$ as the cutoff distance for covalent bonds. This is slightly larger than the equilibrium bond length of $4.44 a.u.$ of c-Si. Only a fraction of $\sim 30\%$ of the atoms in the first peak of $g(r)$ are at distances less than r_c. In section III.3 we gave the bond-angle distribution function $g_3(\theta, r_c)$ corresponding to these atoms. This function is peaked around an angle close to tetrahedral, thus making the above conjecture of fluctuations toward local tetrahedral order more quantitative. We have calculated the time decay of these fluctuations. We define the time dependent normalized covalency $c(t)$ as

$$c(t) = \frac{\langle N_c(t+s)\rangle_s}{\langle N_c(s)\rangle_s}, \qquad (III.4.3)$$

where $N_c(t)$ is the number of atoms retaining the covalent bonds at time t. $\langle ... \rangle_s$ implies the time-averaged value taken over a set of initial conditions at times expressed by s. As can be seen from Fig.III.4.4 the life time of these fluctuations is $t \sim 0.04 ps$, i.e. comparable to the falloff of the velocity autocorrelation function (c.f. Fig.III.5.2) and to the optical phonon period in c-Si.

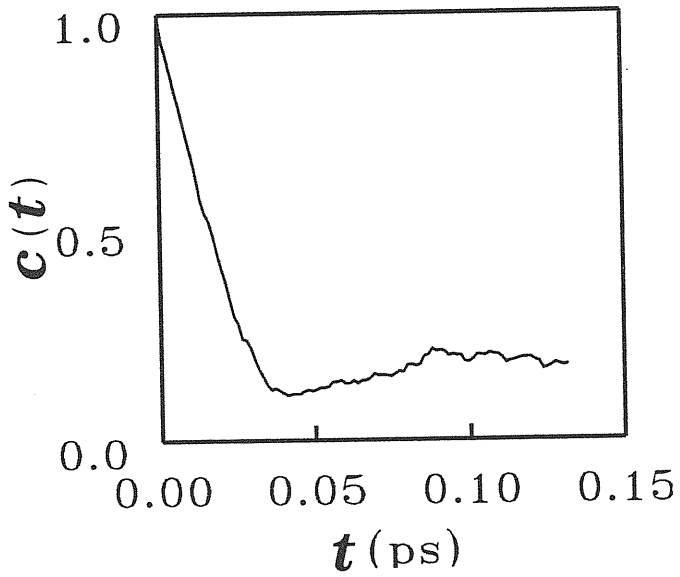

Fig.III.4.4 Time decay $c(t)$ of the covalent bonds in l-Si.

Now we want to make the above concept of covalent bonding effects in l-Si more quantitative. In accordance with the BC model the BC's may be viewed as a sort of extra particles and can be characterized by distribution functions similar to those for real particles (equations III.3.1-III.3.8). Since the valence electronic density $\rho_e(\vec{r})$ is a multimaximum function it is convenient to use statistical methods to locate its maxima. We used the combination of simulated annealing (Kirkpatrick et al 1983) with Monte-Carlo (MC) (Metropolis et al 1953) methods. The $\rho_e(\vec{r})$ generated in our MD simulation are defined on a mesh of spatial points. The MC search was

started from a randomly chosen point on the mesh. A sequence of MC moves was generated according to the Metropolis (1953) algorithm with the acceptance probability for a given move defined as

$$p = \min\{1, \exp(-\frac{\Delta\rho_e}{T})\}, \qquad (III.4.4)$$

with $\Delta\rho_e$ being the difference between charge densities at two neighboring mesh sites and T an effective "temperature". Starting at high T, the temperature was then reduced thus forcing the search to freeze in a maximum of $\rho_e(\vec{r})$.

In Fig.III.4.5 we show the pair-correlation functions $g_{BC-BC}(r)$ (bond charge-bond charge), $g_{I-BC}(r)$ (ion-bond charge), and once again $g_{I-I}(r)$ (ion-ion) calculated as described above. The correlation functions were averaged over 34 configurations well separated in time. The bond-breaking, bond-forming processes give rise in the $g(r)$'s to well pronounced features. The $g_{I-BC}(r)$ is peaked at $\sim 1.7a.u.$ which does not correspond to a BC midway between ions and has a characteristic shoulder at $\sim 3.0a.u.$ The average value between the peak and shoulder positions is exactly at the half distance of the first peak position of $g_{I-I}(r)$. This provides an evidence for bond-breaking (-forming) processes, since a broken bond is characterized by two maxima (see Fig. III.4.1). The first peak of $g_{I-BC}(r)$ is much stronger than the shoulder because it includes besides genuine (unbroken) covalent bonds also the weak residual maxima almost always present when the bond begins to disappear completely (c.f. Fig.III.4.1i). The broken bonds give also rise in $g_{BC-BC}(r)$ to peaks at $\sim 1a.u.$, which correspond to the double maxima of a broken bond.

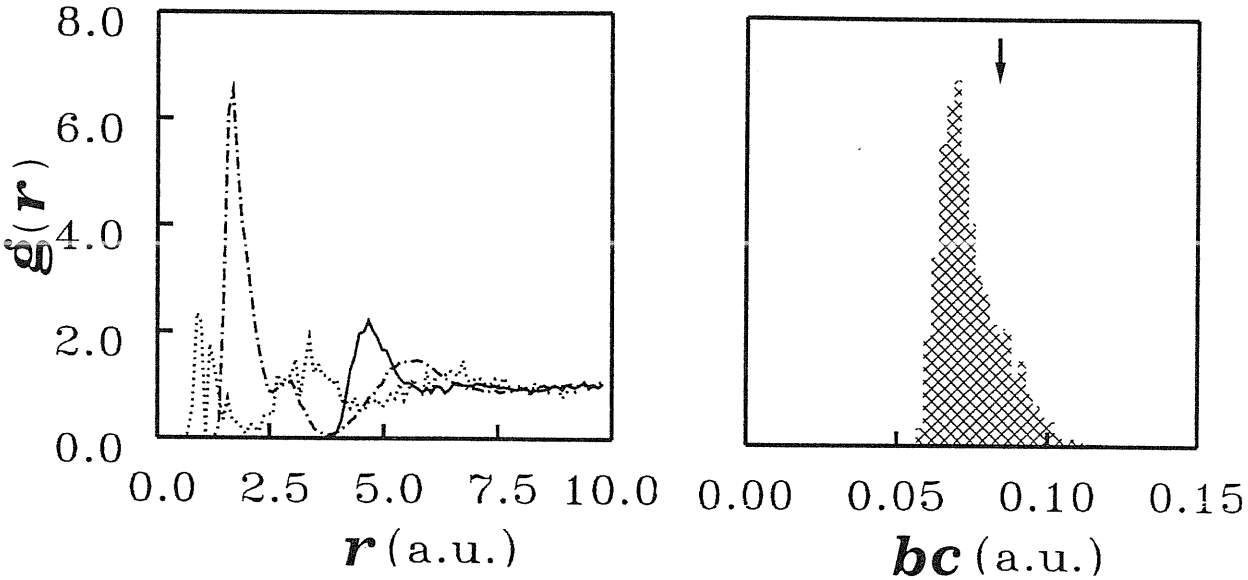

Fig.III.4.5 Characterization of bonding properties of l-Si by pair correlation functions. Left panel: Correlation functions $g_{BC-BC}(r)$, $g_{I-BC}(r)$, and $g_{I-I}(r)$ defined in text. Right panel: distribution of BC density. The arrow indicates the value of BC in c-Si.

The distribution of BC density is shown in Fig.III.4.5. A significant part of the maxima is appreciably weaker than in c-Si. The compressed bonds such as those in

Fig.III.4.1b give rise to the tail on the high BC density side of the distribution.

The knowledge of the BC locations can be used to characterize the tendency to maintain tetrahedral order between covalently bonded atoms. The BC-I-BC angle distribution $d(\theta)$ shown in Fig.III.4.6 is peaked at the tetrahedral angle. Our MC procedure finds for a broken bond two maxima which correspond to a very small BC-I-BC angle. Thus the peak in Fig.III.4.6 at small angles provides once more the evidence for the presence of broken bonds in l-Si.

The partial loss of the strong directional character of the chemical bond in the liquid with respect to c-Si can also be seen as follows. In c-Si the wave functions around the atoms are sp^3 hybrids. Hence using the projector $\hat{P}_{l,m}$ and projecting out the (l,m) component from the wave function $\psi_i(\vec{r})$

$$\hat{P}_{l,m}\psi_i(\vec{r}) = \phi_{i,(l,m)}(r)Y_{l,m}(\hat{r}) \qquad (III.4.4)$$

allows to define the state- and atom-averaged ratio

$$H_{s/p}(R) = \frac{\sum_i \sum_I \int_0^R r^2 \phi^2_{i,s}(|\vec{r} - \vec{R}_I|)\mathrm{d}r}{\sum_i \sum_I \int_0^R r^2 \left(\phi^2_{i,p_x}(|\vec{r} - \vec{R}_I|) + \phi^2_{i,p_y}(|\vec{r} - \vec{R}_I|) + \phi^2_{i,p_z}(|\vec{r} - \vec{R}_I|)\right)\mathrm{d}r} \qquad (III.4.5)$$

which for a suitable R is a measure of the hybridization. Taking R equal to the c-Si bond length (R=4.44 a.u.) yields $H_{s/p} \sim 0.38$ in c-Si and $H_{s/p} \sim 0.48$ in the melt, pointing toward a partial dehybridization.

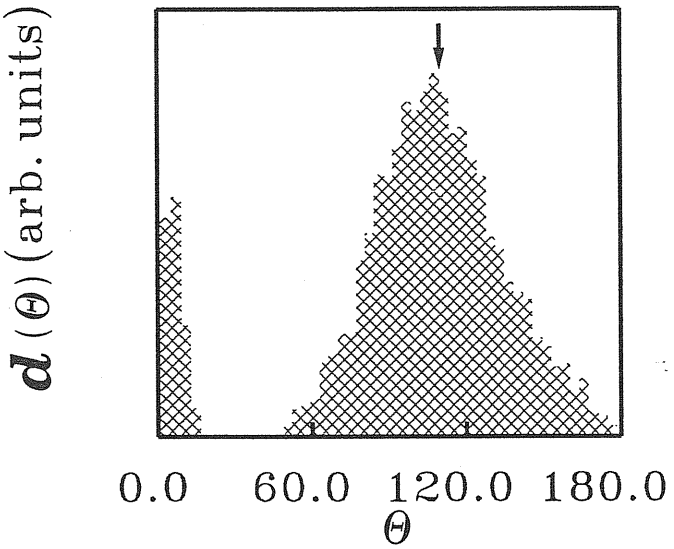

Fig.III.4.6 Distribution $d(\theta)$ of BC-I-BC angles in l-Si. The arrow indicates the position of the tetrahedral angle.

Above we have identified the presence of covalent bonds in metallic l-Si. In simple metals the valence charge density is almost uniform, whereas in c-Si the charge piles up in covalent bonds leaving large empty spaces (c.f. Fig.III.4.1a). The low density regions in c-Si have the structure of infinite pipes. The l-Si retains to

some extent the covalent bonding effects and has, as in the c-Si case, regions of very low density (Fig.III.4.1b). We have studied the structure of low density regions in l-Si, in particular whether or not they are interconnected as in c-Si. The method used was based on random walks in low density regions. First a simulated annealing- MC search for low charge density regions similar to that described above was carried out. Starting from that point a random walk on the mesh was done with high density regions acting as hard walls. The travelled distance d was monitored. Clearly, if the low density regions are closed bubbles the travelled distance as a function of step number $d(N)$ must saturate. The $d(N)$ for three such random walks started from different low density regions are shown in Fig.III.4.7. The quasi linear behaviour of the travelled distance indicates that, at least within limits given by a relatively small size of our cell, the low density regions in l-Si are interconnected.

We have shown the presence in l-Si of covalent bonds and bond breaking- (forming-) processes. In principle, in this situation the system can develop local spin fluctuations and they in turn could drive the system to explore other parts of phase space than those normally explored within LDA. To account properly for these effects one has to generalize the K-S scheme to the SD formalism. The study of this interesting aspect is now underway.

In summary, the persistence of some covalent bonding effects in metallic l-Si has been identified. These effects are accompanied by fluctuations toward local tetrahedral order. The bond-breaking (-forming) processes were studied in detail. These features together with the highly nonuniform valence charge density distinguish l-Si from simple metals.

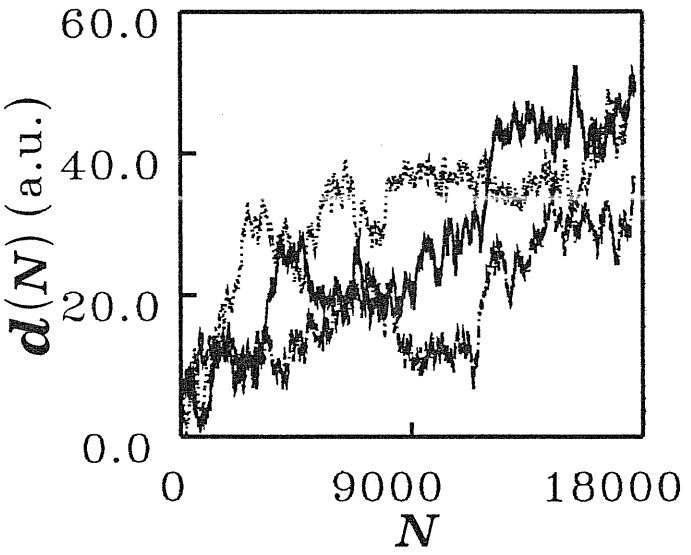

Fig.III.4.7 Travelled distance $d(N)$ for random walks in low density regions of l-Si. Three representative walks started from different low density regions are shown.

III.5 Atomic Motion in Liquid Silicon

In this section we study phenomena related to atomic motion in l-Si with a particular emphasis on the diffusion constant and vibrational density of states.

Besides static correlation functions, such as $g(r)$ or $S(k)$ also dynamic properties and their description in terms of time correlation functions are important. In this respect the MD method has the great advantage of allowing the study of time-dependent phenomena and transport coefficients.

The generalized flux $\vec{J}_i = \frac{d\vec{a}_i}{dt}$ is in linear response theory proportional to the applied forces $\vec{X}_j$

$$\vec{J}_i = \sum_j L_{ij}\vec{X}_j \qquad (III.5.1)$$

where L_{ij} are transport coefficients. The transport coefficients are expressible in molecular terms (Hansen and McDonald 1976) as

$$L_{ij} = \int_0^\infty \langle \dot{\vec{a}}_i(t)\dot{\vec{a}}_j(0)\rangle \mathrm{d}t. \qquad (III.5.2)$$

The transport coefficients thus appear as the time integrals over the correlation functions of the appropriate fluxes. Thus, for example, the diffusion constant D in an isotropic system is given (Faber 1972, Croxton 1974, Hansen and McDonald 1976) as

$$\begin{aligned} D &= \int_0^\infty \frac{1}{N}\langle \sum_{I=1}^{N} v_{xI}(t+s)v_{xI}(s)\rangle_s \mathrm{d}t \\ &= \int_0^\infty \frac{\langle \vec{v}(t+s).\vec{v}(s)\rangle_s}{3}\mathrm{d}t = \frac{3k_BT}{M}\int_0^\infty \frac{\langle \vec{v}(t+s).\vec{v}(s)\rangle_s}{3\langle \vec{v}(s).\vec{v}(s)\rangle_s}\mathrm{d}t \\ &= \frac{k_BT}{M}\int_0^\infty Z(t)\mathrm{d}t, \end{aligned} \qquad (III.5.3)$$

where $Z(t)$ is normalized *velocity autocorrelation function* (VACF). The notation $\langle ... \rangle_s$ implies the time-averaged value taken over a set of initial conditions at times expressed by s.

We shall limit our discussion here and in the following analysis of our data to the diffusion constant D and the corresponding $Z(t)$. Generally, to describe the evolution of $Z(t)$ is a restatement of the general N-body problem which can be conveniently studied by MD techniques.

If the displacement of a particle I in the time interval t is $\vec{R}_I(t)$, then

$$\vec{R}_I(t).\vec{R}_I(t) = \int_{t_0}^{t_0+t} \vec{v}_I(t_1)\mathrm{d}t_1 . \int_{t_0}^{t_0+t} \vec{v}_I(t_2)\mathrm{d}t_2 \qquad (III.5.4)$$

and the *mean square displacement* (MSD) $\langle R^2(t)\rangle$ is given (Faber 1972, Croxton 1974, Hansen and McDonald 1976) as

$$\begin{aligned}\langle R^2(t)\rangle &= \langle \frac{1}{N}\sum_{I=1}^{N}[\vec{R}_I(t+s)-\vec{R}_I(s)]^2\rangle_s \\ &= 2\langle v(0).v(0)\rangle_s \int_0^t (t-s)Z(s)\mathrm{d}s \\ &= \frac{6k_BT}{M}\int_0^t (t-s)Z(s)\mathrm{d}s,\end{aligned} \qquad (III.5.5)$$

from which for very short times

$$\langle R^2(t)\rangle = \frac{3k_BT}{M}t^2 \qquad (III.5.6)$$

characteristic of a ballistic regime. For very long times

$$\begin{aligned}\langle R^2(t)\rangle &= \frac{6k_BT}{M}t\int_0^\infty Z(s)\mathrm{d}s - \frac{6k_BT}{M}\int_0^\infty sZ(s)\mathrm{d}s \\ &= 6Dt + const;\end{aligned} \qquad (III.5.7)$$

the linear t dependence being characteristic of diffusive liquid behaviour. Equation III.5.7 is equivalent to the well-known Einstein formula

$$D = \lim_{t\to\infty}\frac{\langle R^2(t)\rangle}{6t}. \qquad (III.5.8)$$

For a Markovian system the constant in equation III.5.7 is zero, whilst for the non-Markovian evolution is non zero and contains information on the initial history of the diffusing centers. The sign of this constant tells whether the diffusion is ahead or behind the corresponding Markovian process. Thus if the constant is positive (as e.g. in l-Ar) the diffusion is impeded relative to a Markovian evolution. Moreover, in that case $Z(t)$ must somewhere reverse in sign. This is described as the backscatter effect of the diffusing particle within its cage of nearest neighbours and amounts to reduction of D as is evident from equation III.5.3.

Let us now apply the above arguments to l-Si and evaluate the diffusion constant from the MSD (equation III.5.8) and from VACF (equation III.5.3). The two relations can be proved identical. However, it is useful to see whether or not these two different procedures in a computer give the same results.

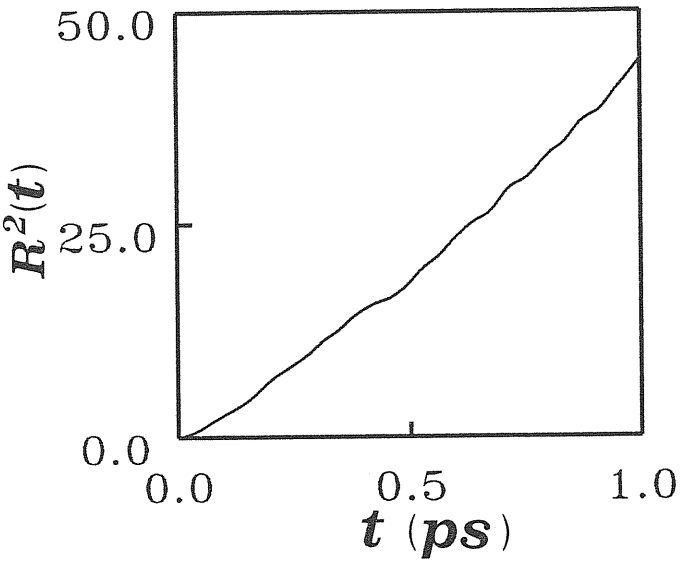

Fig.III.5.1. Time dependence of the mean square displacement $R^2(t)$ in l-Si.

The time dependence of the MSD is shown in Fig.III.5.1. For very short times the MSD has a characteristic $\sim t^2$ dependence, whereas for long times it shows a quasi linear behaviour. The constant in equation III.5.7 is found to be negative (unlike l-Ar) and we can infer that $Z(t)$ must be everywhere positive leading to a high value of D. Using the formula III.5.8 we extract $D \sim 2.20 \times 10^{-4} cm^2 s^{-1}$. This value of D implies a mean distance travelled in our simulation of $\sim 7 a.u.$ (3.7Å). It means that a substantial part of the phase space has been sampled.

MD suggests that we can determine not just the area under the $Z(t)$ curve (D) but also its shape or else its *frequency spectrum* $Z(\omega)$ defined by

$$Z(\omega) = \frac{2}{\pi} \int_0^\infty Z(t) \cos(\omega t) \mathrm{d}t \qquad (III.5.9)$$

and we might see significant differences between one liquid and another associated with differences in the interparticle potential. Thus the task of calculating reliable atomic correlations for a real liquid is obviously one of a great complexity.

There have been several attempts to describe $Z(t)$ by simple models (Faber 1972, Croxton 1974). For a sufficiently dilute system one can expect a purely Gaussian behaviour. Otherwise one can expect an initially quasi-Brownian motion with a Gaussian decay of $Z(t)$ followed by some momentum exchange of the particle with the surrounding ones, evidenced by the departure of $Z(t)$ from a Gaussian behaviour. The subsequent quasi-Brownian motion completely decorrelates the particle's velocity with its initial value. Essentially one can distinguish the low frequency *diffusive modes* from the distinct high frequency *vibratory modes* (Croxton 1974). In the simplest model the liquid can be pictured as a system of diffusing Einstein oscillators.

The vibrational behaviour is also evident from the VACF (equation III.5.3) shown in Fig.III.5.2. $Z(t)$ is always positive and has an oscillatory decay to zero after $\sim 0.15ps$. This has to be contrasted with close packed liquids like l-Ar where as a result of the caging effect of the neighboring atoms a negative oscillation in $Z(t)$ is observed. l-Si has a much more open structure and exhibits no caging but only a milder effect due to the occasional formation of covalent bonds between pairs of atoms giving rise to the vibrational motion.

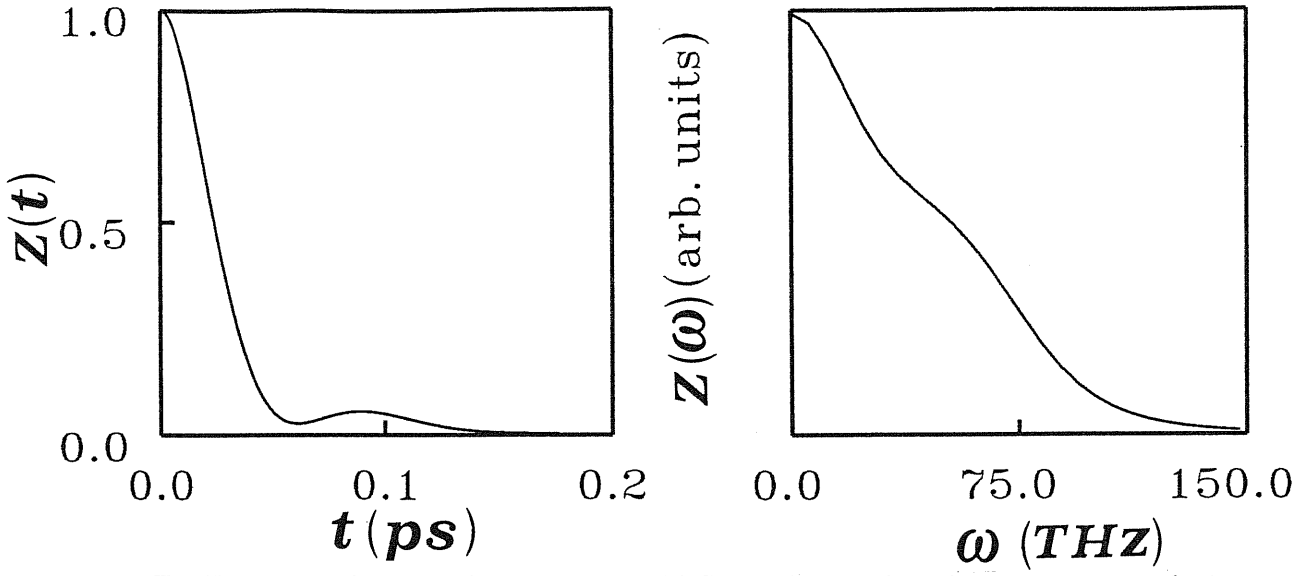

Fig.III.5.2. Vibrational properties of l-Si. Left panel: velocity autocorrelation function $Z(t)$. Right panel: the corresponding power spectrum $Z(\omega)$.

Tab.III.5.1 *Comparison of measured diffusion coefficients of some impurities in l-Si (compiled from Landolt-Börnstein 1982: different entries correspond to different experiments). The calculated values of self diffusion coefficient of l-Si are* $2.20 \times 10^{-4} cm^2 s^{-1}$ *(MSD) and* $2.02 \times 10^{-4} cm^2 s^{-1}$ *(VACF).*

Impurity	Al	P	Ga	As
D $\times 10^4$	0.23	2.3	0.66	2.4
$cm^2 s^{-1}$	5.3	2.7	3.6	2.5
		3.9		

We have determined the diffusion coefficient D also from $Z(t)$ based on equation III.5.3. This yields the value $D \sim 2.02 \times 10^{-4} cm^2 s^{-1}$ in remarkably good agreement with the value estimated from MSD. Although we are not aware of any direct experimental measurement of D for l-Si, our finding is consistent with indirect estimates. In Tab.III.5.1 we compare the calculated value of D with the diffusivity of some substitutional impurities in l-Si (Landolt-Börnstein 1982). The calculated value of D of l-Si is significantly larger than that found e.g. in l-Ar (Croxton 1974). The large value of D is a consequence of the more open structure in l-Si combined with the prevalence of broken chemical bonds (c.f. section III.4). We

note that the empirical Stillinger-Weber (SW) (1985) potential yields a value of $D \sim 6.94 \times 10^{-5} cm^2 s^{-1}$ (Broughton and Li 1987) which is significantly smaller than our estimate.

The $Z(\omega)$ (equation III.5.9) of our l-Si is shown in Fig.III.5.2. Here the bonding effects are reflected in the shoulder at the frequency of $\sim 60THz$ which is very close to the optical vibrational frequency of c-Si just below the melting point (Wang et al 1989). Our $Z(\omega)$ is again markedly different from that of the SW liquid (Fig.III.5.3), which bears some resemblance of the crystalline $Z(\omega)$ (Luedtke and Landman 1988). This is not surprising since the tetrahedrality is built in in the SW potential.

We have studied in more detail the effects of formation of chemical bonds on the atomic motion and vibrational spectra. For this purpose we define the *filtered VACF*

$$Z_{\hat{f}}(t) = \frac{\langle (\hat{f}\vec{v}(t+s)).(\hat{f}\vec{v}(s))\rangle_s}{\langle (\hat{f}\vec{v}(s)).(\hat{f}\vec{v}(s))\rangle_s}, \qquad (III.5.10)$$

where $\hat{f}$ is an operator choosing only atoms with a particular bonding characteristics. As explained in section III.4 on average only ~ 2 atoms out of 6.5 nearest neighbours are covalently bonded. Hence it is useful to distinguish atoms with $n_b = 0, 1, 2, ...$ covalent bonds. The spectra corresponding to $n_b = 0$ and $n_b = 2$ are shown in Fig.III.5.4 and Fig.III.5.5, respectively. Clearly, the vibratory modes originate from covalently bonded atoms.

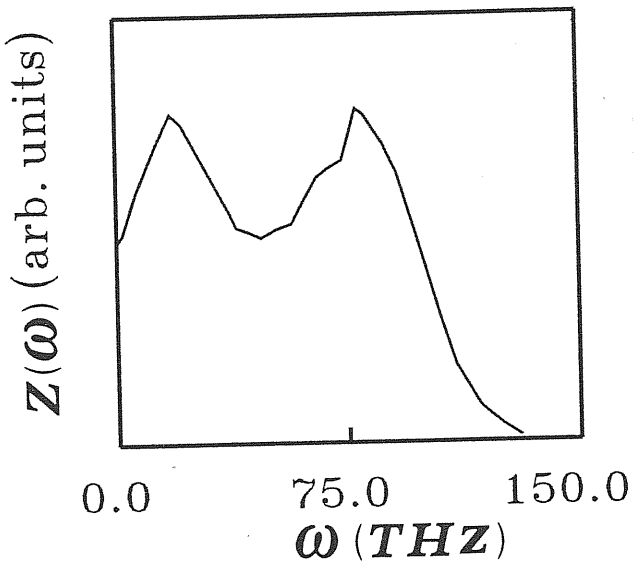

Fig.III.5.3. Vibrational density of states $Z(\omega)$ of the SW liquid (Luedtke and Landman 1988).

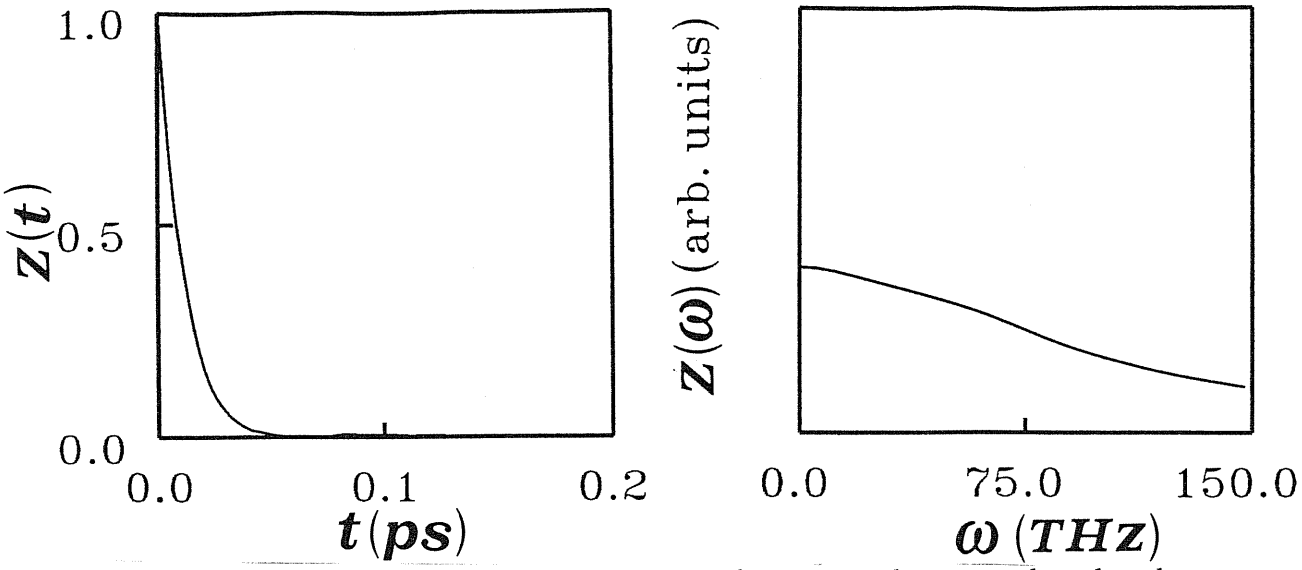

Fig.III.5.4. Vibrational characteristics of atoms without covalent bonds, $n_b = 0$. Left panel: velocity autocorrelation function $Z(t)$. Right panel: the corresponding power spectrum $Z(\omega)$.

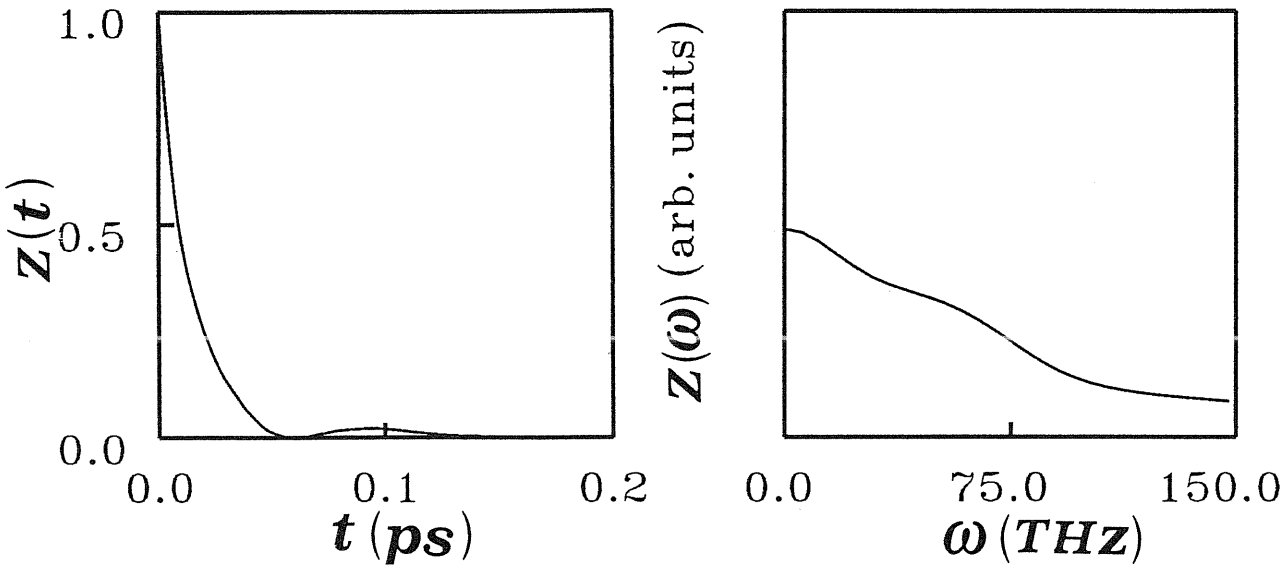

Fig.III.5.5. Vibrational characteristics of atoms with two covalent bonds, $n_b = 2$. Left panel: velocity autocorrelation function $Z(t)$. Right panel: the corresponding power spectrum $Z(\omega)$.

III.6 Electronic Properties and Conductivity of Liquid Silicon

In this section we deal with the *electronic structure* and *electrical conductivity* of l-Si. Our approach is based on finding (within DFT) instantaneous adiabatic eigenstates $\{|i\rangle\}$ and eigenvalues $\{\varepsilon_i\}$ which are functions of the atomic coordinates $\{\vec{R}_I\}$ at some time t. Strictly speaking the DFT applies only to ground-state properties and the $\{\varepsilon_i\}$ are only Lagrange multipliers (see e.g. Lundqvist and March 1983). In many cases, however, the $\{\varepsilon_i\}$ are a rather realistic approximation of the excitations energies and the formalism can be extended also to excited states. In this spirit we use the $\{|i\rangle\}$ and $\{\varepsilon_i\}$ and calculate the electronic structure and conductivity by averaging over a set of representative configurations.

To our knowledge there is very little information on electronic structure and properties of l-Si both theoretically and experimentally. Only a partial information on the $3p$ electronic structure is available since only the $3p \rightarrow 1s$ $(k\beta)$ emission band has been recorded by soft X-ray spectroscopy (SXS) (Hague et al 1980). There are several experimental results for the d.c. conductivity (Glazov et al 1969). The a.c. conductivity, however, has been much less explored. The only experimental data are those based on measurement of the complex refractive index (Shvarev et al 1975). On the theoretical side the only calculations of the electronic structure of molten Si are due to Gaspard et al (1984) and Allen and Broughton (1987). The former assumed the geometric structure to be dominated by sixfold-coordinated Si atoms which are modelled by SC and β-Sn forms, the latter have followed an approach similar to ours by generating a SW-liquid and applying a simple tight-binding model to it. In section III.3 we argued that it is not very useful to interpret the local order of l-Si in terms of crystalline phases, like SC or β-Sn. The drawback of the tight-binding model of Allen and Broughton is a serious underestimate of the conductivity by a factor of 3. In this situation our approach treating structural and electronic properties on equal footing may be useful.

Our model for the conductivity of a liquid metal is to assume that current is carried by electrons and the charged ionic cores are elastic scattering sites for mobile electrons. The contribution of positive atom cores to currents can be evaluated from the Einstein relation

$$\sigma = \frac{(Ze)^2 \rho D}{k_B T}, \qquad (III.6.1)$$

where the charge Z is taken to be 4, ρ is the number density, and D is the diffusion constant estimated from our MD simulation as $\sim 2 \times 10^{-4} cm^2 s^{-1}$. At the temperature $T = 1800K$ equation III.6.1 gives a conductivity of $4 \times 10^{-3} a.u.$ $(1.8 \times 10^{-4} (\mu\Omega cm)^{-1})$. Published values of σ for l-Si are $(1.0 - 1.3) \times 10^{-2} (\mu\Omega cm)^{-1}$ (Glazov et al 1969) which is typical of highly resistive metals but is about two orders of magnitude larger than the above estimate. Hence, the ionic contribution is negligible.

As mentioned above we generate eigenvectors and energies for given ionic con-

figurations and used them in the *Kubo-Greenwood* (K-G) *formula* for the conductivity (Economou 1983)

$$\sigma(\omega) = \frac{2\pi e^2}{\Omega m^2} \langle \sum_i^{occ} \sum_j^{unocc} \frac{|M_{ij}|^2}{\omega_{ji}} \delta(\epsilon_j - \epsilon_i - \hbar\omega) \rangle, \qquad (III.6.2)$$

where M_{ij} is the momentum matrix between states $|i\rangle$, $|j\rangle$. We remark that this is the only consistent way of calculating σ in the present case. The alternative *Ziman theory* (Faber 1982) has also been used in the past to calculate σ (Waseda and Suzuki 1975). The Ziman's theory, however, applies only to the case where the electron-atom scattering cross section is small and consequently the mean free path $l >> a$ (where a is an interatomic separation). In l-Si, taking free electron Fermi gas parameters, a mean free path $l \sim 4.5\text{Å}$ follows from the measured conductivity (Shvarev et al 1975). This is not large compared with $a \sim 2.5\text{Å}$. Hence, the Ziman theory should not be applied to l-Si.

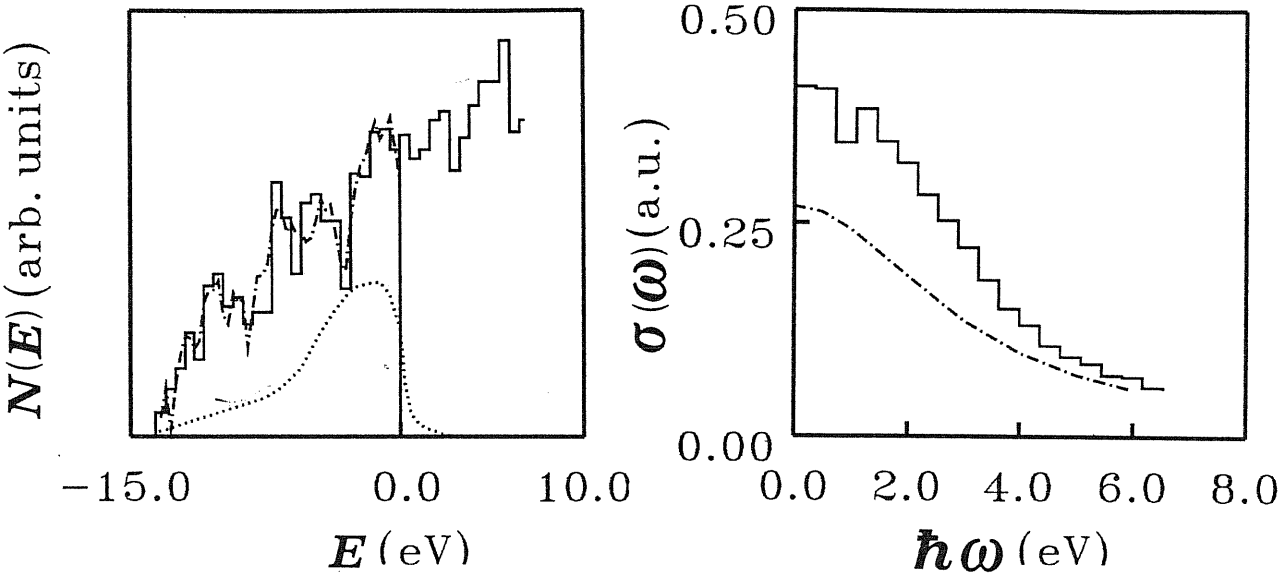

Fig.III.6.1. Electronic properties of l-Si. Left panel: Density of Kohn-Sham eigenvalues $N(E)$ calculated by (a) averaging over 12 configurations (full line), (b) averaging over the entire MD trajectory (dash-dotted line). The vertical line indicates the Fermi level. The p-band measured by SXS spectroscopy (Hague et al (1980) is indicated by dotted line. Right panel: Electrical conductivity $\sigma(\omega)$ calculated from Kubo-Greenwood formula (full line), and the Drude fit to the measured data (Shvarev et al (1975) (dash-dotted line). The atomic unit of conductivity used here is $\frac{e^2}{\hbar a_B} = 4.6 \times 10^6 (\Omega m)^{-1}$.

To implement the K-G formula we need, besides the occupied states already generated in the course of the MD run, also the unoccupied states. We took 12 self-consistent potentials from the MD run, well separated in time to generate the K-S eigenstates and eigenvalues (both occupied and unoccupied). In the present case we found convenient to use the iterative MSD algorithm. In Fig.III.6.1 we

report the density of K-S states (Štich et al 1989b)

$$N(E) = \sum_i \delta(E - \varepsilon_i). \qquad (III.6.3)$$

Because of finite sample size we broadened the δ-functions into a histogram with a finite bin width. For comparison we show in the same figure also the $N(E)$ for occupied states averaged over the entire MD trajectory. The comparison shows that, at least for the occupied states, the 12 configurations provide a sufficiently representative sample. $N(E)$ displays metallic behaviour as evidenced by the absence of a gap at the Fermi level E_F. The $\vec{k}$-point sampling may be more stringent for calculation of density of states than for the ionic forces. A more careful sampling might lead to a smoother $N(E)$ but would not have changed the metallic character of the system. The metallicity of the system can be understood qualitatively as follows. l-Si has a coordination number exceeding six. Only a fraction of $\sim 30\%$ of these atoms are covalently bonded. The least bonded atoms can be imagined as a sort of interstitial atoms that introduce gap states and fill up the gap. The comparison with the experimental $3p \rightarrow 1s$ emission band (Hague et al 1980) indicates that the states immediately below E_F are dominated by p-states. On the whole the calculated $N(E)$ relatively closely resembles that expected for a simple metal, a conclusion supported also by the SXS data. Our density of states is less structured but qualitatively similar to that obtained by Allen and Broughton (1987) with a tight-binding model.

The calculated $\sigma(\omega)$ is shown in Fig.III.6.1 (Štich et al 1989b). By extrapolating the $\sigma(\omega)$ to $\omega \rightarrow 0$, we obtain $\sigma_{d.c.} = 0.38 a.u.(0.0175(\mu\Omega cm)^{-1})$ in fairly good agreement with the experimental value of $0.27 a.u.(0.0124(\mu\Omega cm)^{-1})$ (Glazov et al 1969). In our calculation the d.c. limit has the largest uncertainty. The reason is that the number of energy pairs $(\varepsilon_i, \varepsilon_j)$ with $\varepsilon_i < E_F$ and $\varepsilon_j > E_F$ diminishes rapidly as $\omega \rightarrow 0$. We have also dropped the usual Fermi occupation numbers from the K-G formula (Economou 1983) in order to keep it consistent with the potentials that have been generated by assuming a sharp Fermi surface. The behaviour of the calculated $\sigma(\omega)$ in Fig.III.6.1 looks quite like classical Drude $(1 + \omega^2\tau^2)^{-1}$ falloff and has also been found experimentally (Sharev et al 1975). The origin of this behaviour in a strong-scattering liquid with a short mean free path l is not entirely clear. The overall good agreement with the experimental data indicates once more a realistic description of the electronic properties of l-Si by our model. We note that the tight-binding approach of Allen and Broughton (1987), in spirit similar to ours, gave qualitatively similar $N(E)$ but is off by a factor of 3 in description of the $\sigma(\omega)$.

An alternative simple estimate of $\sigma_{d.c}$ can be obtained from the approximate expression (Mott and Davies 1979)

$$\sigma_{d.c.} = \frac{S_F e^2 l g^2}{12\pi^3\hbar}, \qquad (III.6.4)$$

with S_F being the Fermi surface, l the mean free path, and $g = \frac{N(E_F)}{N(E_F)_{free}}$. Equation III.6.4 is the usual result from the Boltzmann treatment corrected for the deviations of $N(E)$ from the free-electron value. The final formula follows by assuming the scattering to be so strong that $l \sim a$ (an average nearest neighbour distance). This gives $\sigma_{d.c.} = 0.18 a.u.$ $(0.0083(\mu\Omega cm)^{-1})$ in reasonable agreement with both the K-G expression and with experimental data.

In summary, we have presented the electronic properties of l-Si resulting from our model. The single-particle electronic density of states shows metallic behaviour. We used the Kubo-Greenwood formula for the a.c. conductivity in the strong-scattering environment of l-Si. In accordance with experimental data a Drude-like behaviour has been found. An independent approach to the d.c. conductivity based on the simple Mott's formula was also considered and found in reasonable agreement with the Kubo-Greenwood result.

IV. Amorphous Silicon

IV.1 Principal Properties and Methods of Preparation of Amorphous Silicon

The vast number of interesting properties of amorphous silicon (a-Si) cannot be enumerated here. We only briefly summarize some of the important properties with emphasis on those that can be addressed by our approach. We mention also the preparation techniques since they determine crucially some of the properties.

a-Si is a metastable phase. The amorphous state in Si could also be termed glassy state because it can be prepared by very rapid quench from the melt (laser glazing) (Thompson et al 1983, Galvin et al 1983) and experimental findings (Spaepen and Turnbull 1978) led to the proposal that the phase transition it undergoes on melting is of *first order.*

The average density of a-Si is usually lower than that of the crystal because of presence of voids (Elliot 1984). The characteristics of the voids are strongly dependent on the growth conditions and subsequent thermal treatment. Radii of gyration of the voids ranging from $5\mathring{A}$ to $270\mathring{A}$ (Postol et al 1980) have been estimated experimentally leading typically to $5-15\%$ decrease in density (Mott and Davies 1979).

The diffraction experiments (Fortner and Lannin 1988,1989) revealed that the pair-correlation function of a-Si is not simply a broadened version of that of c-Si. The most striking feature being the absence in a-Si of the third, prominent, peak of the crystalline $g(r)$. Thus modeling the structure of a-Si presents an intriguing problem in space filling.

The absence of long-range order (LRO) has profound consequences also on electronic and dynamical properties of a-Si. Both electronic (Ley et al 1972) and phonon (Kamitakahara et al 1984,1987) densities of states have been studied experimentally. The results indicate that, besides the broadening effect of disorder with respect to the crystalline counterparts there are also new and more subtle effects present in these spectra. We will elaborate more on these new features in sections IV.5 and IV.7.

Many properties of a-Si, similarly to the crystalline case, are defect controlled. In the amorphous environment the natural defect can be identified as a departure from the perfect 4-fold coordination, i.e. under- and over-coordination. It has been

suggested that the coordination defects have a state in the gap that would contain a single electron when the defect is neutral (Pantelides 1988). Hence, the electron spin resonance (ESR) should provide a characteristic signature for the coordination defects (called D-centers) with large observed spin densities $\sim 10^{19} - 10^{20} cm^{-3}$ (luminiscence, absorption, DLTS, etc. also yield signals from defect states) (Elliot 1984). The D-centers can be easily created by prolonged exposure to light (Staebler-Wronski effect). The gap states exhibit a certain degree of localization. In real materials which may contain a high concentration of defects and consequently a high density of gap-states, electron transport can take place via hopping conductivity in localized states. Until recently only rigid, frozen in dangling bonds resulting from undercoordination have been considered. In section IV.6 we will study in detail the coordination defects and their dynamics.

Besides the density and coordination defects there may be also topological distortions (disclinations) (Rivier 1979) present in a-Si. Unlike the c-Si that consists only of six-membered rings in the structure, the amorphous form may contain a large variety of ring sizes, both odd and even. They influence the elastic energy of the amorphous form. Indirect conjectures correlate the presence of topological defects with some characteristic features experimentally observed in the atomic (Temkin 1978) and electronic (Joannopoulos and Cohen 1973, Singh 1981) structures of the amorphous form. We study the topological defects in section IV.6.

The properties of a-Si may depend sensitively on preparation technique. There are at least a dozen different techniques that can be used to prepare materials in an amorphous state. Here we introduce those that are relevant to a-Si (Elliot 1984) and that we shall refer to in comparing the calculated properties with experiments. Those are:

- thermal evaporation

-sputtering

-glow discharge decomposition

-laser glazing (LG) (Thompson et al 1983, Galvin et al 1983)

In the first technique the material is vaporized from the solid by bombardment with high-energy electrons and deposited in vacuo on a cold substrate. In the sputtering an r.f. field is applied to a target causing the striking of a plasma (usually Ar) and creating a negative bias on the target. The ions attracted from the plasma by the bias potential eject material from the target that is than collected on a cold substrate. The glow discharge is similar to sputtering, but the amorphous film is directly deposited from the plasma produced by applying an r.f. field. The essential common feature of all these techniques is that atomic surface mobility is greatly diminished because of the cold substrate, causing the adatoms to be frozen in the random positions at which they arrive.

A different strategy is followed in LG. By applying very short (ns) laser pulses thin surface layers can be melted. By energy conduction into the substrate ex-

tremely high quench rates of $\sim 10^{12} K/s$ are achievable that allow amorphisation from the melt. Because of these high quench rates, our numerical model of a-Si should be more closely related to a-Si produced by LG. The available experimental data, however, refer mainly to the former three methods of preparation.

IV.2 MD Simulation of Amorphous Silicon

In this section we describe the details of preparation of a-Si by using the CP method (Štich et al 1989c). The general strategy is close to that followed in real preparation of a-Si by LG, i.e. a rapid cooling of the melt.

During thermal treatment complicated processes must take place. The coordination number $\sim$ 6.4 (Waseda and Suzuki 1975, Gabathuler and Steeb 1979) characteristic of a liquid must reduce to $\sim$ 4 (Filipponi et al 1989) in the amorphous. Besides changes in SRO, the medium-range order (MRO) is also expected to develop (Elliot 1984). These changes are accompanied by a metal to semiconductor phase transition. In our approach all these changes must be entirely driven by the changes in the potential.

The present simulation was started from the l-Si data described in chapter III at the temperature $T = 1800K$. Similarly to the l-Si simulation we used the constant temperature MD (equations II.3.7a-c). The presence of the Nosé thermostat allows to control accurately both the temperature and the cooling rate. In order to describe well all the processes mentioned above we fixed a linear cooling with the rate of $10^{14}K/s$ in the region of temperatures from 1600 to $600K$. This is presently the slowest cooling rate attained within the CP. We chose the cooling rate 4 times faster in the region $600 - 300K$ and 8 times faster in the $1800 - 1600K$ region. The faster cooling rates in those temperature regions have little effect because in the high T region the structure has not yet started to change appreciably and at low T the structure has already essentially been captured in a representative minimum of the potential energy surface. The total thermal treatment took $\sim 11ps$.

To make such a long run possible we used a time step $\Delta t = 20a.u.$ ($4.82 \times 10^{-16}s$) and scaled accordingly the electronic "mass" μ to $3200a.u.$ Another saving was achieved by using a smaller cutoff for the plane-wave expansion of the potential than formally required for a given energy cutoff imposed on the wave functions. The discussion of this point is left to Appendix 3. To keep the same efficiency of phase space sampling the dynamical "mass" of the Nosé thermostat Q was reset at each temperature using equation III.2.1. All the other parameters, like number of atoms in the simulation, shape of the supercell, pseudopotential, number of plane waves, use of the Γ-point only in the BZ sampling, were the same as in the l-Si simulation. In the course of the cooling we performed periodic quenches of the electrons to the instantaneous ground-state every 250 time steps. This choice ensures that the maximal deviation of the electrons from the BO surface is $<\sim 6 \times 10^{-2}eV/atom$. This value is larger than that we tolerated in the l-Si simulation (c.f. section III.2). To test whether or not the new choice of parameters and approximations is adequate we have run the system for $\sim 0.5ps$ at the temperature $T = 1800K$. The structural characteristics of this new liquid were virtually identical to those of a more carefully prepared liquid described in chapter III. This confirms once more that the noise introduced into ionic forces by "reasonably" small deviations from the BO surface

is not critical. We remark that at lower temperatures where the system starts developing a band gap the nonadiabatic effects in the fictitious classical dynamics diminish.

The density of the melt is $\sim 10\%$ above the density of the crystal. To account for the density change, the volume of the cell was linearly changed in the temperature range $1600-600K$ from the volume $\Omega = 7781.225a.u.$ in the liquid to the value $\Omega = 8640.365a.u.$ characteristic of the crystal. In real a-Si the density is usually lower (c.f. section IV.1). The volume changes were accompanied by corresponding changes in the energy cutoff in order to keep the number of plane waves (i.e. the precision) constant. Thus the final cutoff for the a-Si was of $\sim 11.2Ry$.

At the final temperature $T = 300K$ the Nosé (1984a,b) thermostat was switched off and the system was run in the microcanonical ensemble using equations II.3.3a,b. In order to enable a long run without any drift in the microcanonical constant of motion (equation II.3.6), the integration of the MD equations II.3.3a,b was performed with the Verlet (1967) algorithm and a time step of $10a.u.$ $(2.42\times10^{-16}s)$, while the "mass" parameter μ was set equal to $612a.u.$ Tests with this new set of parameters have shown that the system remains on the BO surface for very long observation times. At the final temperature we have followed the system for a total time of $\sim 3.2ps$, much larger than the typical relaxation times.

Compared to the original simulation by Car and Parrinello (1988a) this new amorphous structure was obtained with a more careful treatment. The calculation was started from a better liquid structure with a converged value of the energy cutoff. 64 atoms in a cubic cell have been used instead of an FCC cell with 54 atoms. Also the cooling rate used in the present study was substantially (almost an order of magnitude) slower than that in the work by Car and Parrinello (1988a). This newly generated amorphous structure, however, exhibited presence of some relaxation processes in the final structure at $T \sim 300K$. Further annealing of the data presented here would be necessary to better equilibrate the structure. However, the effect of such processes on average properties, like $g(r)$ or the electronic properties, appears to be negligible.

The structural relaxations can be seen from the mean square displacement and the variation of the instantaneous temperature shown in Figs.IV.2.1, IV.2.2, respectively. As can be seen in Fig.IV.2.1 the system underwent two marked structural relaxations during which few atoms moved substantially, driving the system toward a state of lower energy, leaving the pair-correlation and bond-angle distribution functions little changed but reducing the number of coordination defects. This structural relaxation were accompanied by a slight increase in the temperature (Fig.IV.2.2).

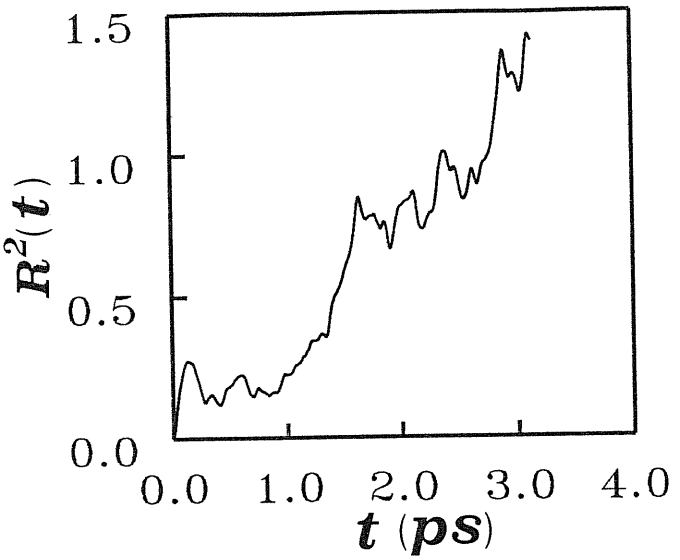

Fig.IV.2.1. Temporal evolution of the mean square displacement $R^2(t)$.

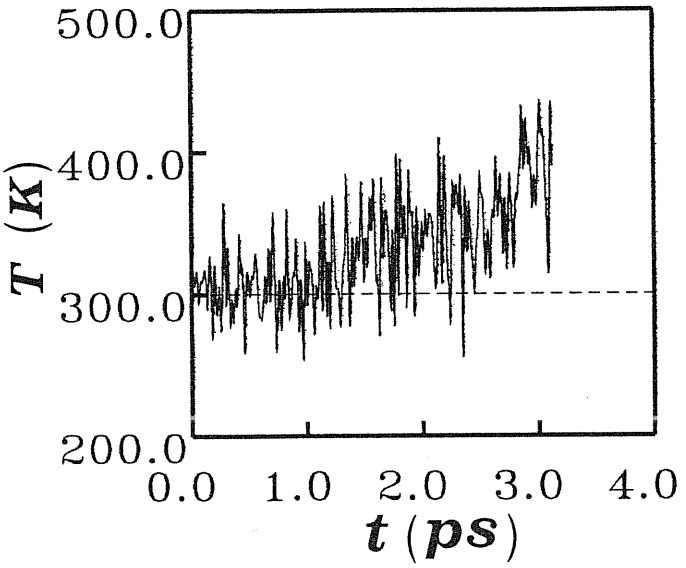

Fig.IV.2.2. Variation of the instantaneous system temperature. The horizontal line indicates the temperature $T = 300K$. Note the correlation of the increase in temperature with the variation of the MSD shown in Fig.IV.2.1.

IV.3 "Glass" Transition

The system prepared as described in the previous section is a glass where the crystallization at the melting temperature is precluded by a rapid cooling rate. Our data do not allow us to make general conclusions about the glass transition based on considerations of entropy, thermodynamics or relaxation processes. Instead, we can monitor how SRO and MRO are incorporated in the system upon cooling as the system goes through the structural changes from the liquid to the amorphous structure.

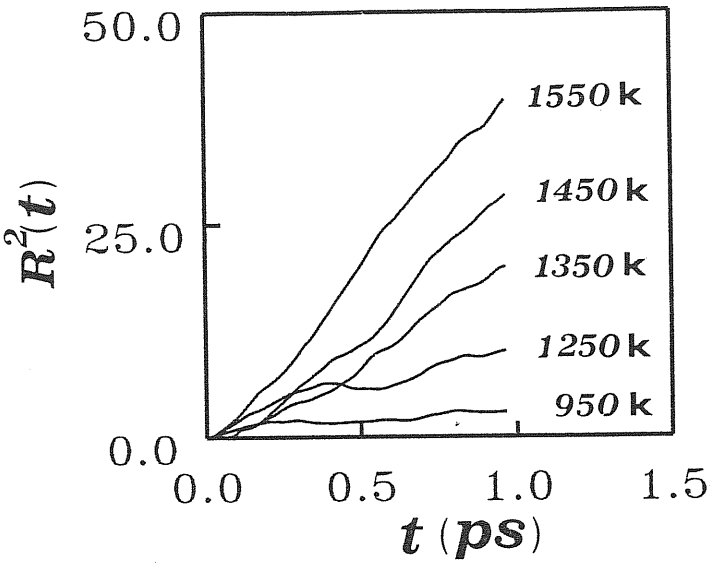

Fig.IV.3.1. Temperature dependence of the mean square displacement $R^2(t)$.

In Fig.IV.3.1 we show the decrease in MSD (proportional to the diffusion constant) with temperature. The diffusion is essentially zero at the temperature $\sim 950K$. The cease of diffusion manifests also in the static structure factor $S(k)$ shown for three different temperatures in Fig.IV.3.2. The $S(k)$ at the temperature $\sim 950K$ is practically indistinguishable from the measured $S(k)$ at the room temperature. The transition from a liquid-like to a solid-like structure factor, characterized by the splitting of the broad first peak in the liquid is well visible.

As will be seen in the next section, an idealized structural model of an amorphous solid in which directional covalent bonding is predominant can be based on the *continuous random network* (CRN) model (Elliot 1984). The CRN model put forward by Zachariasen, assumes that the atomic structure of the crystalline and amorphous phases must be similar in certain regards. If the Si atom with its four bonds is schematized by a tetrahedra, the only difference is the variable orientation of the tetrahedra in a glass, giving rise to a nonperiodic structure. An important aspect of this approach is that a nonperiodic arrangement of atoms can be attained solely as a result of the incorporation of variations in *bond-angles* and *dihedral-angles*. The dihedral angle determines the relative angle of twist between

neighboring tetrahedral units and hence the MRO.

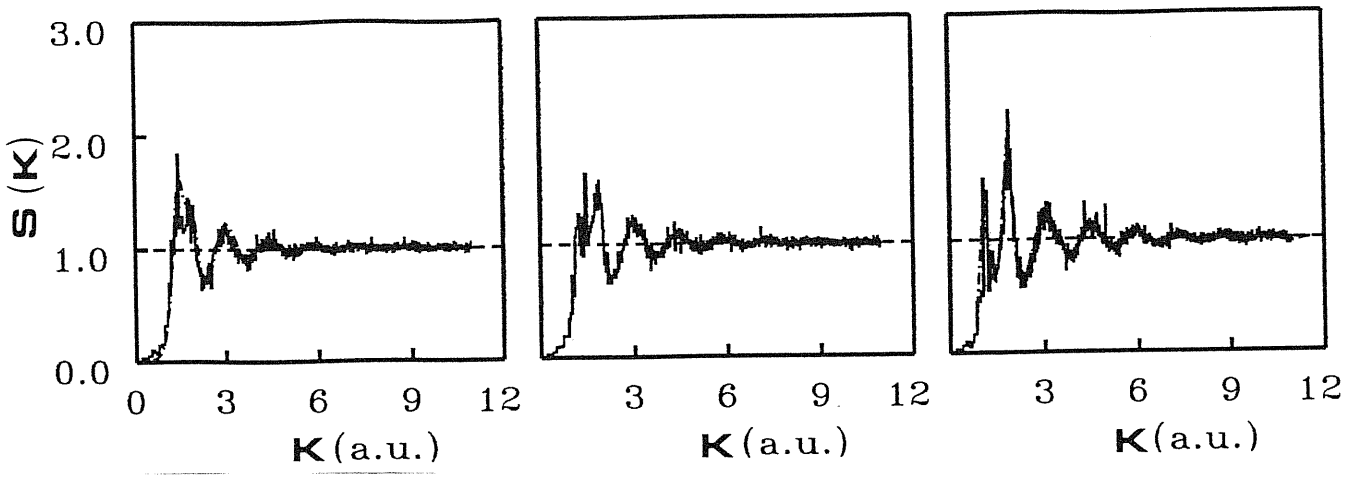

Fig.IV.3.2. Temperature dependence of the static structure factor $S(k)$. The temperatures are (from the left) $1550K$, $1250K$, and $950K$. The dash-dotted line in the left panel is the X-ray data of Waseda and Suzuki (1975) and in the right panel the neutron scattering data of Fortner and Lannin (1988,1989).

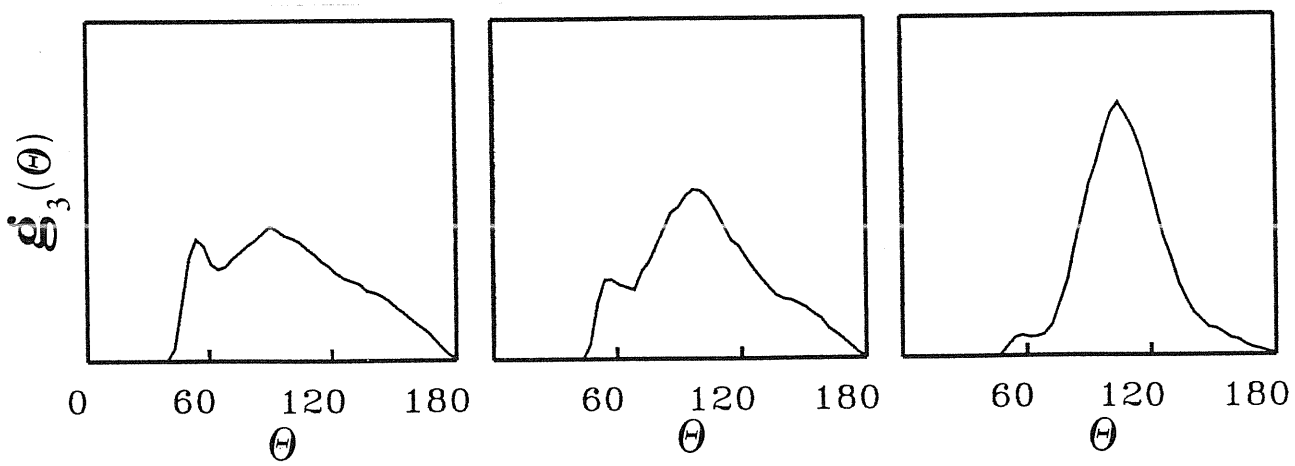

Fig.IV.3.3. Temperature dependence of triplet correlation function $g_3(\theta)$ measured by the bond-angle distribution. The temperatures are (from the left) $1550K$, $1250K$, and $950K$.

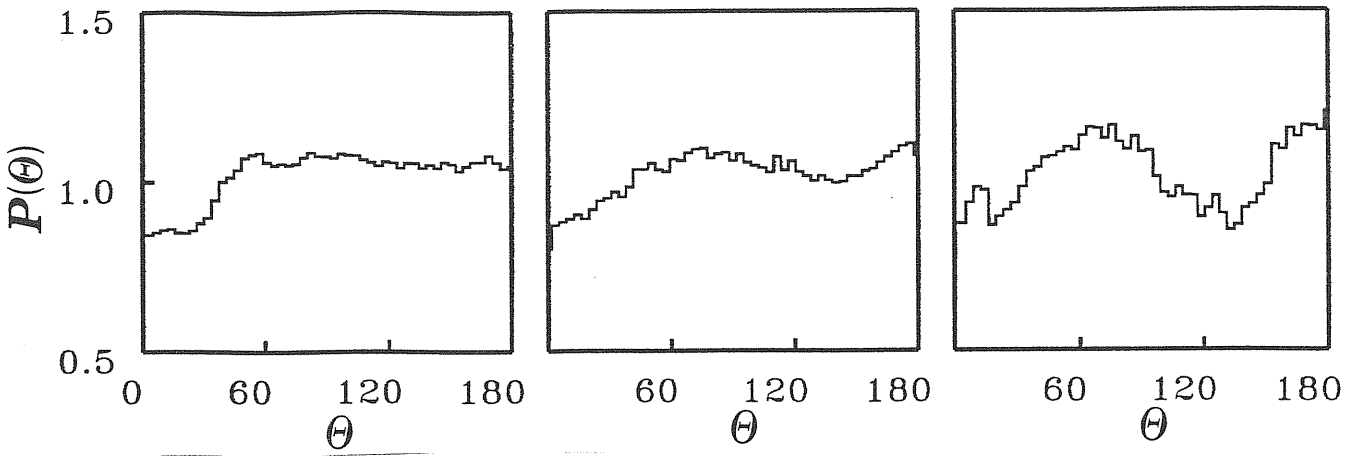

Fig.IV.3.4. Temperature dependence of the dihedral angle distribution function $P(\theta)$. The temperatures are (from the left) $1550K$, $1250K$, and $950K$.

The rearrangement in the SRO toward local tetrahedral order upon cooling can be monitored by the bond-angle distribution function $g_3(\theta)$ shown in Fig.IV.3.3. At $\sim 950K$ the system has already developed the tetrahedral order. The effect of temperature is a larger variation of bond-angles σ_θ. The normalized dihedral-angle distribution $P(\theta)$

$$\frac{1}{\pi}\int_0^\pi P(\theta)\mathrm{d}\theta = 1 \qquad (IV.3.1)$$

for three temperatures is compared in Fig.IV.3.4. Our definition of dihedral angle gives for the crystal the $2:1$ ratio of $60°:180°$ angles. The distribution is not flat at lower temperatures with maxima near $60°$ and $180°$ indicating the development of MRO.

All the structural changes on cooling we described above are driven by the changes in the potential. This changes must have consequences also on the electronic properties. In fact, the system must undergo a metal to semiconductor transition. To monitor this changes we have calculated the density of K-S states $N(E)$ and the conductivity $\sigma(\omega)$ at $T \sim 1050K$. The method used was that described in section III.6. The results are averages over 5 configurations and are reported in Fig.IV.3.5. The system has developed a minimum at the Fermi level accompanied by a deviation from a Drude-behaviour and a decrease of $\sigma(\omega)$ at small energies.

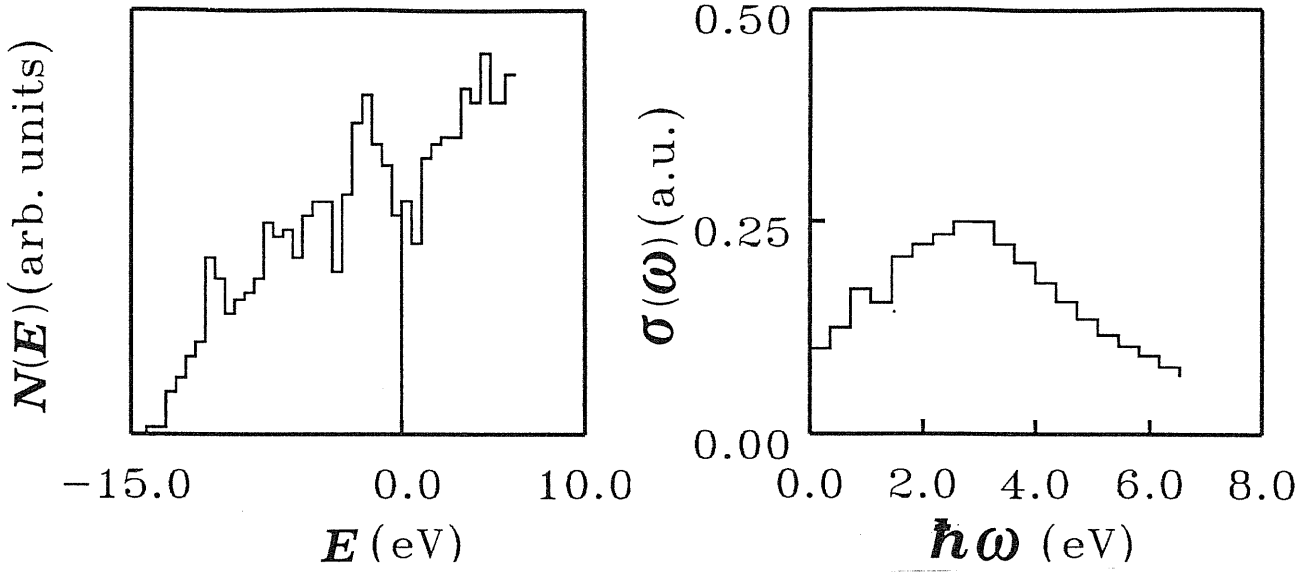

Fig.IV.3.5. Electronic properties of undercooled l-Si at $T \sim 1050K$. Left panel: Density of Kohn-Sham eigenvalues $N(E)$. The vertical line indicates the position of the Fermi energy. Right panel: Electrical conductivity $\sigma(\omega)$ calculated from Kubo-Greenwood formula (equation III.6.2).

IV.4 Structural Properties of Amorphous Silicon

This section deals with the atomic structure of a-Si. Our MD results are compared with experimental data and with other existing theoretical models.

Because of the small size of our cell only the microscopic structure up to $\sim 5.5\AA$ can be studied, i.e. SRO and some aspects of MRO, such as dihedral-angle distribution. Experimentally, also other elements of MRO have been observed, such as regions having linear dimensions up to $\sim 15\AA$ yielding coherent diffraction (Elliot 1984). In a real a-Si also the macroscopic structure plays an important role. The electron microscopy and small-angle scattering (SAS) (Postol et al 1980) of radiation give direct evidence of density fluctuations - voids - in a-Si.

The experimental information on the atomic structure of a-Si is rather limited. There were experimental structural studies made on a-Si using electron (Barna et al 1977) and X-ray diffractions. However, the elastic neutron scattering technique was applied only recently. Apart from an earlier study in a limited range of k ($< 8.75\AA^{-1}$) providing an evidence for SAS from voids (Postol et al 1980) there are only two other very recent experiments. Fortner and Lannin (1989) carried out a measurement on a-Si prepared by r.f. sputtering for $k < 22\AA^{-1}$. Kugler et al (1989) studied evaporated a-Si in the momentum transfer range $0.5 < k < 16\AA^{-1}$. The structure factors of the two experiments are compared in Fig.IV.4.1. The differences between this two data sets may be a result of different preparation techniques of a-Si used in these experiments.

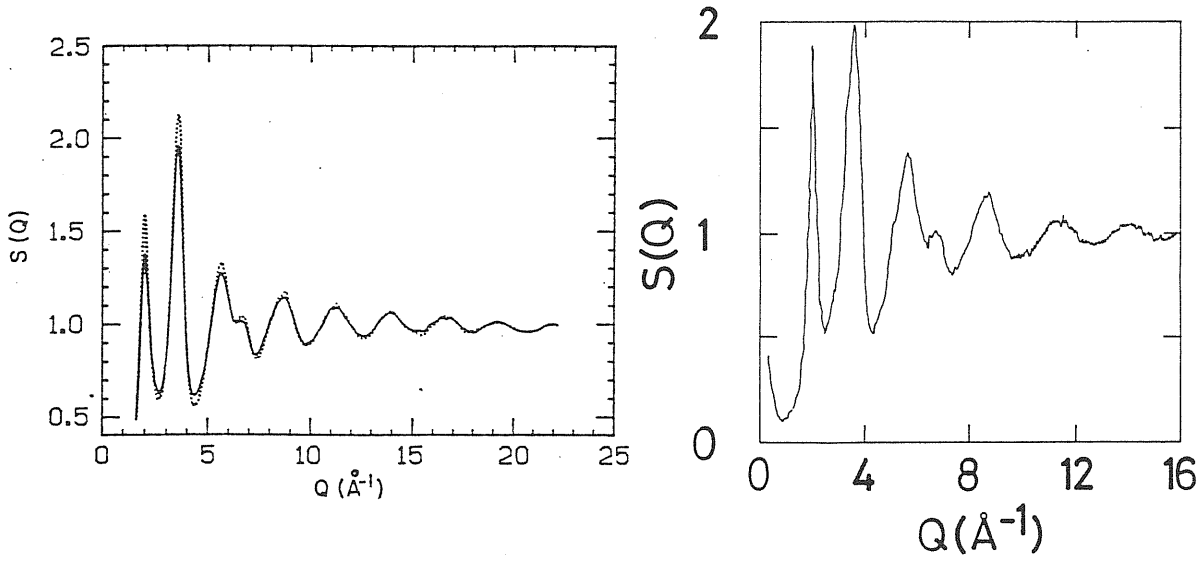

Fig.IV.4.1. Experimentally determined $S(k)$ of a-Si. Left panel: Neutron diffraction experiment of Fortner and Lannin (1989) (full line corresponds to as deposited and dotted line to annealed sample), Right panel: Neutron diffraction experiment of Kugler et al (1989).

To compare the real-space data is even more difficult because of a finite real-space resolution. The termination error involved in equation III.3.10 can be alleviated to a certain extent by multiplying the integrand in equation III.3.10 by a modification function $M(k)$, usually the one due to Lorch (1969)

$$M(k) = \frac{k_{max}}{\pi k} \sin\left(\frac{\pi k}{k_{max}}\right) \qquad (IV.4.1)$$

replacing a sharp discontinuity at k_{max} by a smoothly varying function. If the correlation function is taken to be

$$t(r) = 4\pi r \rho g(r) \qquad (IV.4.2)$$

the effect of all this is that from the experimental data the function (Etherington et al 1982)

$$\tilde{t}(r) = \int_0^\infty t(r')[P(r-r') - P(r+r')]\mathrm{d}r' \qquad (IV.4.3)$$

broadened with the peak function

$$P(r) = \frac{1}{\pi}\int_0^\infty M(k)\cos(rk)\mathrm{d}k \qquad (IV.4.4)$$

is extracted. The reason for using $t(r)$ rather than $g(r)$ is that it is in $t(r)$ and not $g(r)$ that the experimental broadening by $P(r)$ is symmetric and r independent (Etherington et al 1982). The real-space data are little affected, if due to sufficiently broad peaks in the real-space correlation functions, the oscillations in $S(k)$ have died away at $k = k_{max}$. Thus in covalent amorphous solids usually the first peak is strongly affected while the features at higher r are left relatively unchanged by the transformation in equation IV.4.3.

In Fig.IV.4.2 we show results obtained for the $S(k)$ and $g(r)$ and compare them with neutron scattering data (Fortner and Lannin 1989). The agreement with experiment can be considered as perfect. The reason why we compare the $g(r)$ and not $t(r)$ with experiment is that we found that $t(r)$ depends sensitively on the density ρ. Our model is free of voids and hence its density is higher than that of a real a-Si. The close agreement between the calculated and experimental $g(r)$ in the region of the second peak implies also a good agreement in the mean value of the bond-angles and their variation. The data reveal the disappearance of the third crystalline coordination shell. The area under the first peak of $g(r)$ (equation III.3.11) gives a local coordination $N^I = 4.04$. The distribution of local coordinations as calculated by setting the cutoff distance of the first minimum of $g(r)$, $r_m = 5.1 a.u.$, is in Tab.IV.4.1. We find a relatively high concentration of both threefold (T_3) and fivefold (T_5) atoms. Our finding is consistent with a recent suggestion that T_5 defects might exist and play an important role in real-life a-Si (Pantelides 1988). The high concentration of the coordination defects found may be a consequence of the system size and absence of any annealing treatment in our model. The structural defects will be more fully discussed in section IV.6.

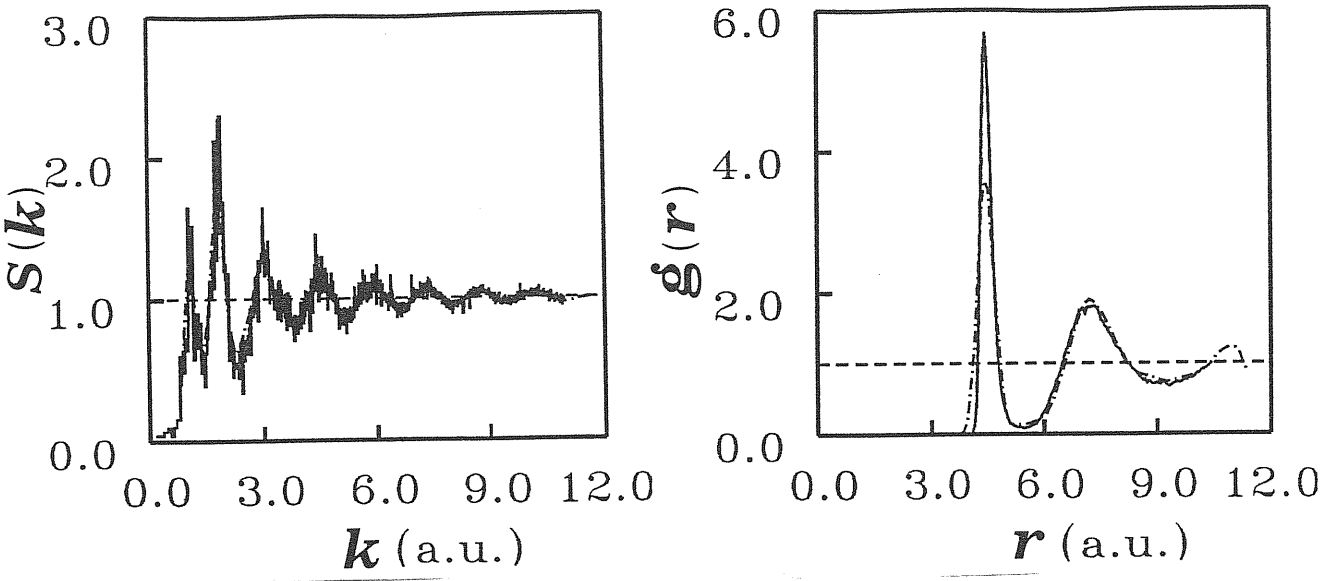

Fig.IV.4.2. Structural properties of a-Si. Left panel: Calculated static structure factor $S(k)$ of a-Si (full line) compared with neutron scattering data for the as deposited sample of Fortner and Lannin (1989) (dash-dotted line). Right panel: Calculated pair correlation function $g(r)$ of a-Si (full line) compared with data extracted from neutron scattering data for the as deposited sample of Fortner and Lannin (1989) (dash-dotted line).

Table IV.4.1. *Distribution of local coordinations in a-Si*

N ($r_m = 5.1 a.u.$)	$3(T_3)$	4	$5(T_5)$
% atoms	2.7	90.6	6.5

To assess the effect of finite experimental real-space resolution on the first peak of $g(r)$ we applied equations IV.4.1-4 with $k_{max} = 22\AA^{-1}$ (Fortner and Lannin 1988,1989) in the region of the first peak. The $g(r)$ was extracted from $\bar{t}(r)$ using equation IV.4.2. The result is reported in Fig.IV.4.3. In the same Fig. we report also the smoothed version of the calculated static structure factor $S(k)$. The results confirm an excellent agreement with the experimental data. An amorphous structure contains disorder in bond-lengths and bond-angles. The information on bond-length and its variation can be extracted from the first peak of the correlation function, while the information on bond-angles and their variation is contained in the second peak. We have fitted the first two peaks of

$$t(r) = 4\pi r \rho g(r) \qquad (IV.4.5)$$

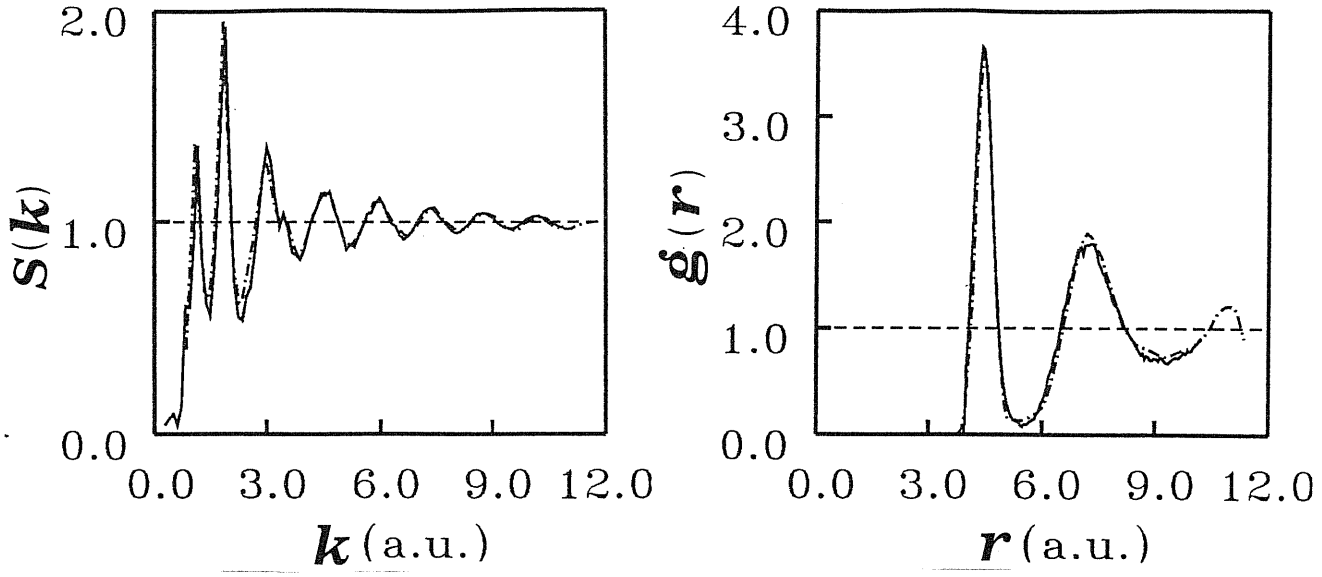

Fig.IV.4.3. Structural properties of a-Si. Left panel: the smoothed version of the calculated $S(k)$. Right panel: the calculated $g(r)$ with the first peak convoluted with the experimental resolution (full line). The dash-dotted lines show the neutron scattering data for the as deposited sample of Fortner and Lannin (1988,1989).

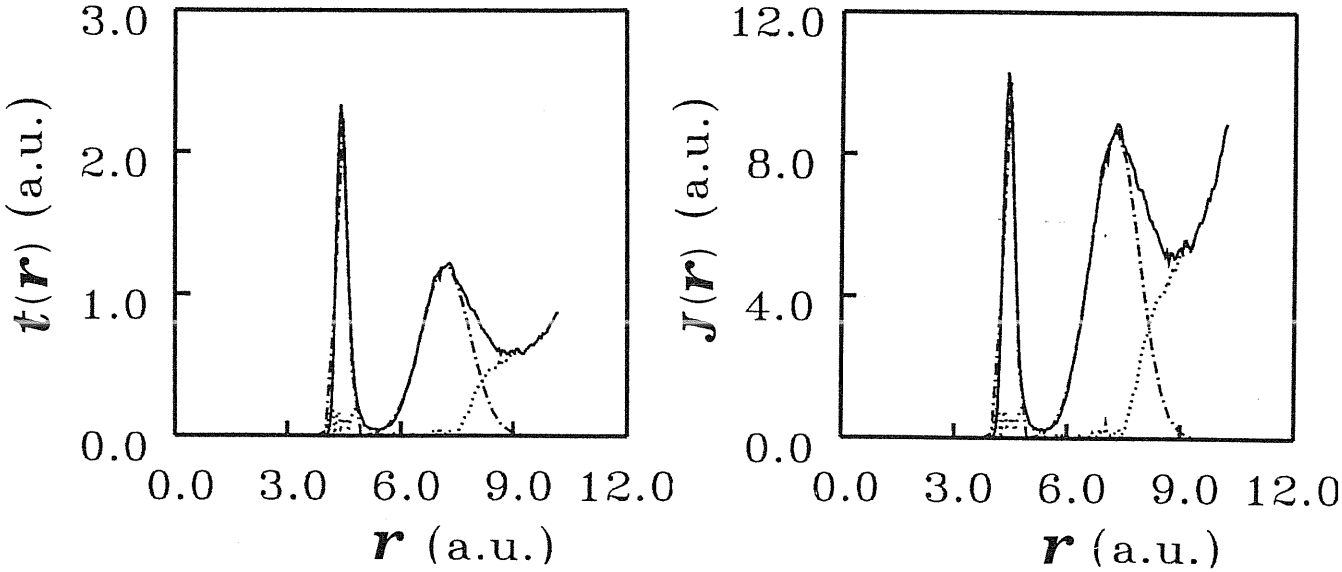

Fig.IV.4.4. The peak fits of the calculated correlation functions by Gaussians (dash-dotted line). The dotted line reports the residual. Left panel: $t(r)$, Right panel: $J(r)$.

and of the radial distribution function

$$J(r) = 4\pi r^2 \rho g(r) \qquad (IV.4.6)$$

by Gaussians. The second peak is only partially resolved and so in order to achieve a peak fit it was assumed that the second neighbour distribution is symmetric about

the maximum of the second peak (Etherington et al 1982). The result is shown in Fig.IV.4.4 and Tab.IV.4.2. Our bond-length variance σ_{r_1} (Table IV.4.2) is in very good agreement with recent X-ray absorption spectroscopy (XAS) measurements (Filipponi et al 1989). The triplet correlation function $g_3(\theta)$ is usually obtained from the pair-distribution function with the approximate relation (Lannin 1987)

$$g_3(\theta) = g(r_2) r_1 \cos\left(\frac{\theta}{2}\right) \qquad (IV.4.7)$$

assuming a relatively symmetric distribution of the second peak about the maximum. There is also the thermal contribution present in $g_3(\theta)$ which in the Gaussian approximation is just summed to the structural one (Etherington et al 1982)

$$\sigma^2 = \sigma_s^2 + \sigma_t^2. \qquad (IV.4.8)$$

We used the Gaussian fit of the second peak of $t(r)$ corrected for the thermal contribution (taken from the thermal width of the second peak of c-Ge) $\sigma_t = 0.197 a.u.$ (Etherington et al 1982). The result is shown in Fig.IV.4.5. and yields a variance $\sigma_\theta = 12.93°$ (Table IV.4.2).* The atoms that correspond to coordination defects usually build the tails of the distribution of bond-angles. Thus the above procedure is equivalent to cutting the tails of the distribution. The value so obtained is slightly larger than that extracted from neutron scattering data (Fortner and Lannin 1988,1989) or XAS data (Filipponi et al 1989) (c.f. Table IV.4.2).

Table IV.4.2. *Gaussian fit parameters of $t(r)$ and $J(r)$ of a-Si*

	r_1 $(a.u.)$	r_2 $(a.u.)$	θ (deg)	σ_{r_1} $(a.u.)$	σ_{r_2} $(a.u.)$	$\sigma_\theta^\dagger$ (deg)	N_1	N_2
calc. $t(r)$	4.437	7.185	108.127	0.148	0.643	12.93		
calc. $J(r)$	4.442	7.238	109.120	0.149	0.637		3.807	13.873
exp. $t(r)$	4.422*	7.256*		0.209*	0.602**	11.0**		
exp. $J(r)$			108.4**			10.8**		
exp.				0.143‡		9.6‡		

† thermal disorder subtracted

* Kugler et al 1989

** Fortner and Lannin 1989 (refers to as-deposited sample)

‡ Filipponi et al 1989

* Note that the coordination number N_1 obtained by Gaussian fit is smaller than that obtained from formula III.3.11. Gaussian fits are often used to determine the coordination number experimentally (Etherington et al 1982).

The rms bond-angle deviation has become almost a figure of merit for structural models. However, the comparison with experiment must be done with caution. The σ_θ parameter is a function of conditions of formation and may vary by more than 20% (Lannin 1987). Tests with other models (Wooten et al 1985) have shown that with systems of our size it is difficult to get σ_θ significantly $<\sim 13°$ (Wooten 1989). The angle variance also depends on the density of coordination defects and the way in which it is estimated. In Fig.IV.4.5 we show $g_3(\theta)$ calculated directly from the atomic coordinates taking $r_m = 5.1 a.u.$ This yields the value $\langle\theta\rangle = 108.15°$ and $\sigma_\theta = 16.289°$ without thermal correction. Hence, the rms bond-angle deviation must not be given undue weight.

The normalized dihedral-angle distribution $P(\theta)$ of our model is shown in Fig.IV.4.6. The definition used here gives for the perfect staggered configuration a 2 : 1 ratio of 60° : 180° angles and a 2 : 1 ratio of 60° : 0° angles for the eclipsed configuration. Even though the distribution of dihedral angles in Fig.IV.4.6 is broad the large value of the distribution near $\sim 180°$ indicates a nonrandom distribution with the prevalence of staggered configuration over the eclipsed one in accordance with the modeling studies of Temkin (1978). Our distribution should be interpreted carefully because the dihedral-angle distribution involves the third neighbours which are at the limits of present model. The study of Temkin has also suggested sensitivity of the third peak position of the pair- correlation function and the related 4.7Å feature in a-Ge to the dihedral-angle distribution. Experimentally, the constancy of the third peak in a-Si and the weak 4.6Å shoulder in the annealed sample suggest that evidence for substantial MRO is not strong (Fortner and Lannin 1988,1989).

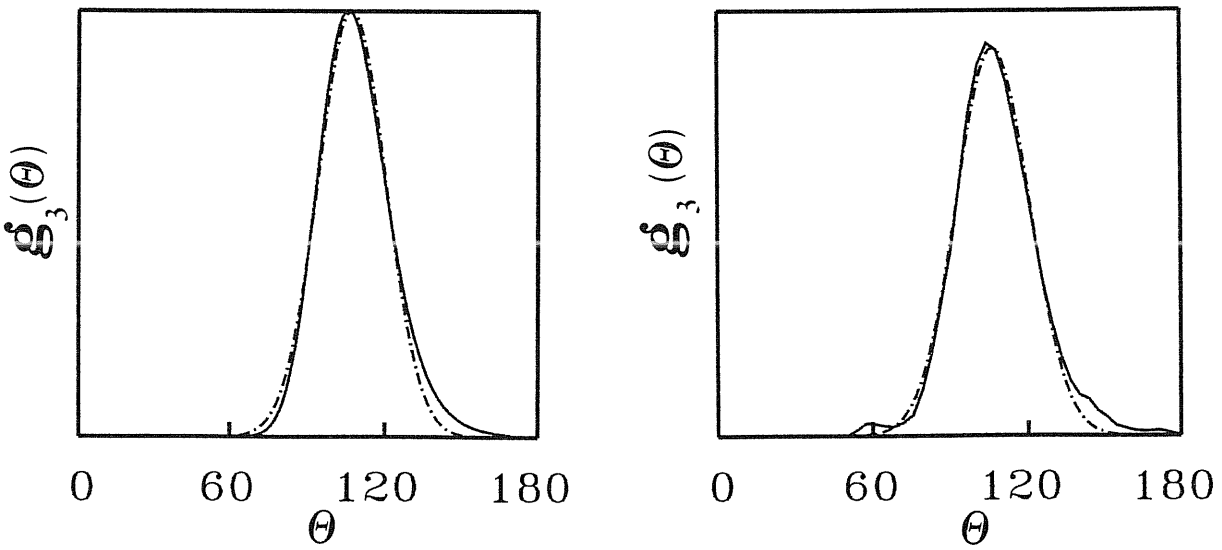

Fig.IV.4.5. The triplet correlation function of a-Si measured by the bond-angle distribution function $g_3(\theta)$. Left panel: Equation IV.4.7 used and thermal contribution subtracted. Right panel: Calculated directly from atomic coordinates. No thermal correction. The dash-dotted lines are Gaussian fits.

Finally, we shall discuss some of the vast number of existing structural models of a-Si (or a-Ge) and compare them with our model. The simplest models are *quasi-*

crystalline models (Etherington et al 1982, Elliot 1984) modeling the amorphous solid by a related polymorph, such as the normal diamond or Wurtzite structures or the Si III or Ge III (Joannopoulos and Cohen 1973) structures. Some of them incorporate distorted tetrahedral bonding and/or topological defects. Their common feature is that they yield too much structure in the pair-correlation function with peaks that are absent in the experimental data. The problem with this approach is that to achieve even a moderate agreement with scattering data, the crystallites must be made so small that they comprise only $\sim 50\%$ of the structure, the other half being an unspecified random tissue. Therefore these models are highly unsatisfactory.

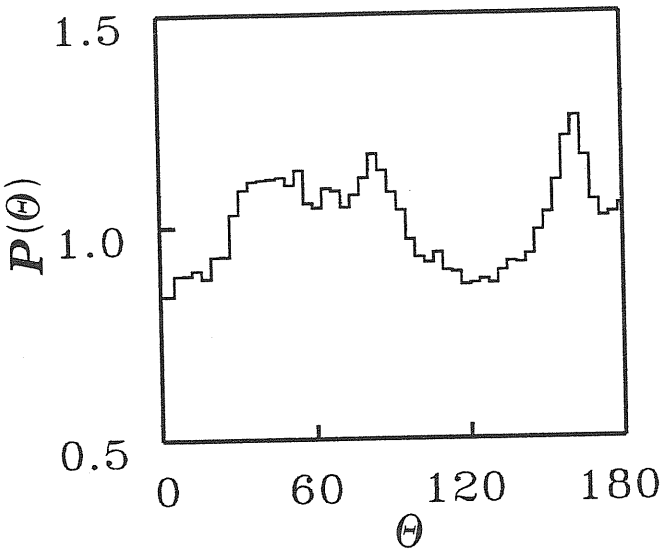

Fig.IV.4.6. Dihedral-angle distribution $P(\theta)$ in a-Si.

An idealized structure of covalently bonded amorphous solid may be modeled by *continuous random network model* (CRN) (Elliot 1984, Etherington et al 1982), where the fundamental tetrahedra (an atom with its four bonds) are connected together in the network, with their relative orientation being characterized by the dihedral-angle. CRN allow some degree of bond-angle distortion and more or less complete freedom of the dihedral-angle distribution. Also the topology includes odd-rings in addition to sixfold rings characteristic of the diamond structure. Some of these models consist of a ball-and-stick arrangement (Polk 1971, Polk and Boudreaux 1973, Connel and Temkin 1974, Henderson 1974), while others are computer generated (Henderson and Herman 1972, Duffy et al 1974). The CRN models usually reproduce the main features of the experimental correlation functions. The deficiency of the CRN models is that they usually do not yield any coordination defects and their dynamical and electronic properties are completely decoupled from structural modeling. Normally they don't have periodic boundaries, which are the most convenient and realistic way to terminate free surfaces.

Another rather realistic model from the CRN family is due to Wooten, Winer, and Weaire (WWW) (Wooten et al 1985, Wooten and Weaire 1984) which start from the diamond structure conformed to periodic boundary conditions. A series of

simple bond-switching operations is carried out which preserve tetrahedral bonding and introduce five- and sevenfold rings. The structure was finally relaxed to an energy minimum with both Keating (1966) and Weber (1977) interactions. The real-space correlation function shows no serious discrepancy with experiment in description of SRO. The static structure factor, however, exhibits a pronounced long-range residual diamond-structure order (Biswas et al 1987, Winer 1987). The WWW model is a purely structural one and doesn't incorporate any coordination defects.

There have been recent attempts to prepare a-Si (a-Ge) by molecular dynamics using empirical two- and three-body potentials either of the SW- (Ding and Andersen 1986, Broughton and Li 1987, Kluge et al 1987, Luedtke and Landman 1988) or the BH-type (Biswas et al 1987). The problem with the empirical potentials is that they cannot describe all the phases: crystal, liquid, and amorphous, with the same parametrization unless a highly empirical scaling of the three-body term is applied on cooling (Broughton and Li 1987, Luedtke and Landman 1988, Biswas et al 1987). If these difficulties are overcome they model reasonably well the SRO, incorporate the defect sites, and conform to periodic boundary conditions. The information on the electronic structure must be treated as a separated problem.

Our model is qualitatively similar to the original model of Car and Parrinello (1988a) but is prepared more carefully and hence is more accurate.

IV.5 Dynamical Properties of Amorphous Silicon

In the last section we discussed at length the static arrangement of atoms in a-Si. In this section we turn to the dynamical behaviour of such atoms and discuss the vibrational excitations of the atoms from their equilibrium positions.

The dynamical properties of an amorphous solid can be characterized by the vibrational density of states

$$Z(\omega) = \sum_j \delta(\omega - \omega_j). \qquad (IV.5.1)$$

This quantity is relatively easy to obtain in our simulation by taking the Fourier transform of the velocity autocorrelation function $Z(t)$ (equations III.5.3,III.5.9). The results are displayed in Fig.IV.5.1 and compared with recent inelastic neutron-scattering data for r.f. sputtered a-Si (Kamitakahara et al 1984, Kamitakahara et al 1987). A Gaussian appodization of $Z(t)$ was used in order to take account of the finite span of time records. In order to facilitate the comparison with experiments all the spectra in Fig.IV.5.1 have been normalized so as to give

$$\int_0^\infty Z(\omega)\mathrm{d}\omega = 1. \qquad (IV.5.2)$$

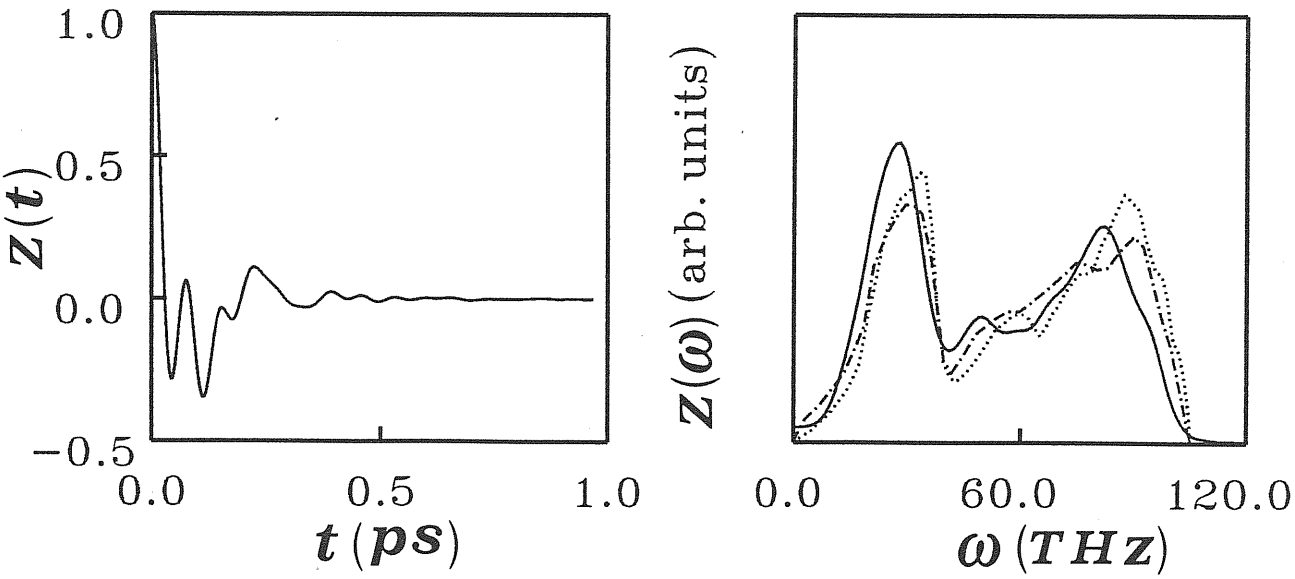

Fig.IV.5.1. Dynamical properties of a-Si. Left panel: Velocity autocorrelation function $Z(t)$. Right panel: Corresponding power spectrum $Z(\omega)$ (full line). Dash-dotted line reports the experimental data of Kamitakahara et al (1984) and the dotted line the data of Kamitakahara et al (1987).

The agreement between theory and experiment is very good, especially if one considers the difference between the two sets of experimental data and the absence

of any fitting parameter in the theory. One possible explanation for the difference in the experimental data might be the use of neutron wave vector Q of insufficient magnitude in the earlier experiment (Kamitakahara et al 1984). Only in the "incoherent approximation" where $Qa >> 1$ (with a being the average interatomic distance) the scattering data are proportional to the phonon density of states (Elliot 1984). In fact, our data are especially close to the later, more reliable, data (Kamitakahara et al 1987). The main difference is a small almost rigid shift by $\sim 6THz$ of the theoretical spectrum toward lower frequencies. We note that pseudopotential phonon calculations for c-Si with a $10Ry$ cutoff (Yin and Cohen 1982a) give phonon frequencies $\sim 3\%$ smaller than experiment. The $Z(\omega)$ for a-Si is quite similar to that of its crystalline counterpart, suggesting that it is the *short-range order* which essentially determines the vibrational properties. The van-Hove singularities are smeared out but otherwise the correspondence between the TA, LA, LO, and TO peaks in $Z(\omega)$ is very close. Kamitakahara et al (1984) have noted three main differences between $Z(\omega)$ of a- and c-Si. (i) the peak at the top edge of the TA band observed in c-Si is missing, (ii) the position of the LA feature occurs at higher frequency in the crystal, and (iii) the relative intensity of the TO peak (with respect to TA) is smaller compared to that of the crystal. We observe that, in accordance with (iii), the TO strength in our calculation is less than that of the TA peak, whereas all other models (Winer 1987, Winer and Bose 1988, Broughton and Li 1987, Luedtke and Landman 1988, Biswas et al 1988) except for that of Car and Parrinello (1988a) assign a larger strength to the TO peak. On the other hand, according to Lannin (1987), structurally more ordered samples are characterized by higher intensity of the TO peak with respect to the TA peak. This suggests that the TO/TA intensity ratio is a measure of the order implied by the $g_3(\theta)$ distribution, thus indicating more disorder in our model. Generally, a high density of low-frequency modes with respect to the crystalline case is a common feature of amorphous systems and can be seen, for instance, in low-T measurements of the specific heat (Mott and Davies 1979).

The dominance of the TO and TA peaks in a-Si can be inferred from the Weaire-Alben (1972) theorem as a result of the fourfold coordination and tetrahedral bonding present in a-Si and is usually reproduced by all structural models. The LA, LO peaks (LO peak as a shoulder superimposed on the broad TO peak), present in all experimental spectra, are usually missing from the phonon density of states calculated for poor structural models. The presence of these features in our model in remarkable agreement with experiments is an indirect indication for a realistic structural model.

Even though we have not studied the localization of the vibrational states, the presence of coordination defects is likely to enhance the disorder-induced localization at both high and low frequency band edges (Biswas et al 1988).

In conclusion, our calculated density of phonon states is in excellent agreement with recent inelastic neutron-scattering data. All important features are present in our spectra included the shift of strength from the TO to the TA peak in a-Si. The

slight overestimate of this tendency may be a consequence of some overstrain in our structural model.

IV.6 Coordination and Topological defects in Amorphous Silicon

We describe here coordination defects found in our simulation and their dynamics. An additional type of line defect associated with odd rings in the structure is also discussed.

To study the *coordination defects* we have assigned to the coordination shell all atoms with bond distances $r_b \leq r_m$ where $r_m = 5.1 a.u.$ corresponds to the first minimum position of $g(r)$. On average we find 2.7% of T_3 and 6.5% of T_5 defects. The presence of T_5's in our model is consistent with a recent suggestion that T_3 and T_5 are both natural conjugate defects in a-Si (Pantelides 1986, Pantelides 1988). We note that the number of coordination defects may change as a consequence of the relaxation processes present in our structure. In fact, a reduction of the number of T_5's was observed during the run. Further annealing of the data would be necessary to obtain a more conclusive answer regarding the number and possible dynamics of the defect sites. No defect on a rather large time-scale of our simulation ($\sim 3.2ps$) is an immobile, frozen in, defect. The division of the atoms into T_3, T_4, and T_5 is rather conventional and depends strongly on the cutoff distance imposed. The prevailing part of the defect sites are not truly three- or fivefold coordinated atoms but correspond rather to *weak bonds* (Car and Parrinello 1988a).

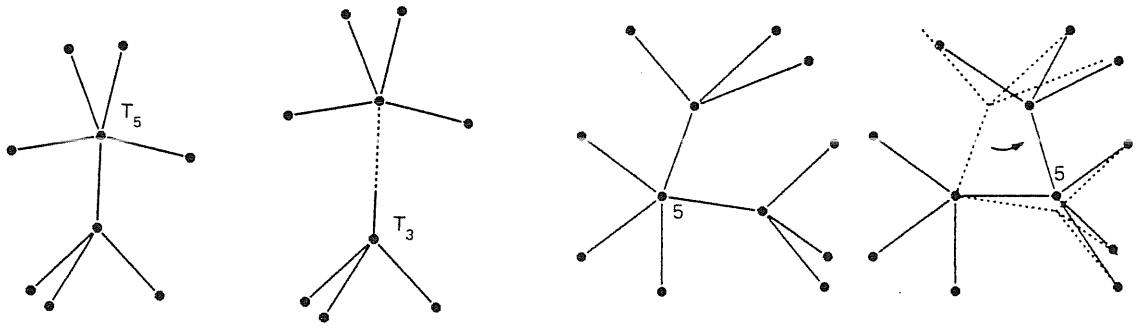

Fig.IV.6.1. Defect dynamics in a-Si. Left panel: Mutual interconversion of T_3 and T_5 defects. Right panel : Migration of T_5 sites by bond-switching mechanism. (According to Pantelides 1988)

We have observed several mechanisms of defect dynamics but the basic and most frequent mechanism found in our simulation is the mutual interconversion of T_3's and T_5's via small network distortions (Pantelides 1986, Car and Parrinello

1988a) (Fig.IV.6.1)

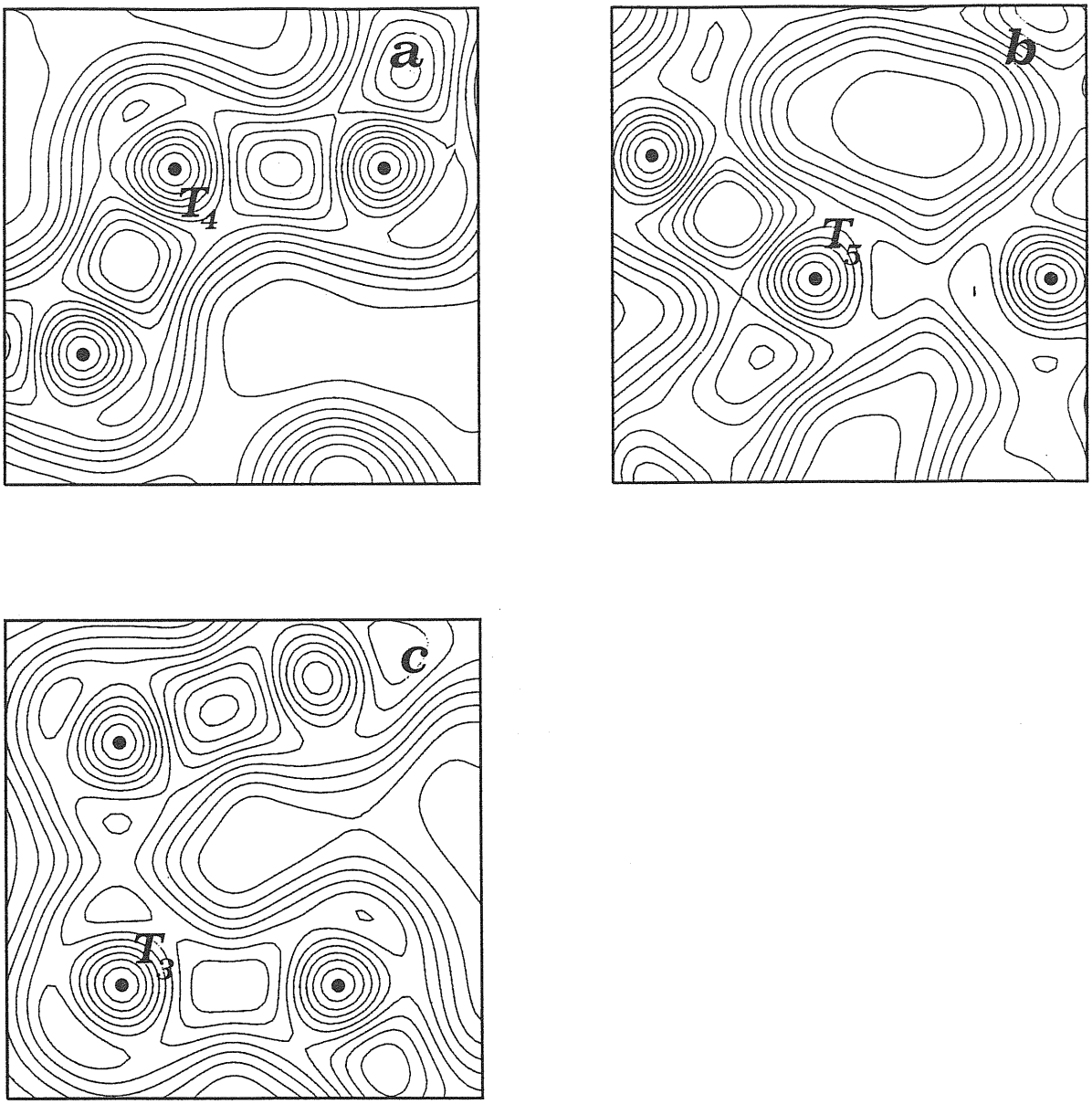

Fig.IV.6.2. Contour plots of valence electronic charge density in a-Si (for explanation see text). The dots indicate the positions of ions.

We have also studied the valence electronic charge density in the vicinity of defect sites. In Fig.IV.6.2a we report a central (fourfold coordinated) particle bonded to two neighbours at distances close to that of c-Si. The bonding picture in this case is very much like in perfect c-Si (Fig.III.4.1a). The central particle in Fig.IV.6.2b is a T_5 site. One of its bonds can clearly be recognized as a weak bond. On the other hand, the central atom in Fig.IV.6.2c is a T_3 which, however, has a weak bond to the atom in the upper left part of Fig.IV.6.2c ($r_b \sim 5.1 a.u.$). This analysis confirms

the validity of the concept of weak bonds in a-Si.

The defect dynamics will require a more detailed analysis, but already a preliminary study has revealed existence of T_3, T_5 sites migration by bond-switching mechanism (Fig.IV.6.1) (Pantelides 1987a, Pantelides 1987b, Pantelides 1988). This effect together with the $T_3 - T_5$ interconversion may play an important role in the Staebler-Wronski effect (1987b) or in peculiar low-T phenomena in hydrogenated a-Si (Pantelides 1987a). We have also observed clustering of the defect sites. To illustrate better this effect we have calculated the $g(r)$ of these sites. Only the configurations of $\sim 1ps$ were included, corresponding to the data before the first relaxation process set on. This result may be subject to changes upon further annealing of the data. The result is shown in Fig.IV.6.3. The pronounced first peak indicates that the coordination defects are clustered. The integral over the first peak gives a coordination number ~ 1.7. As we have explicitly checked, this coordination number is due to formation of chains of defect sites.

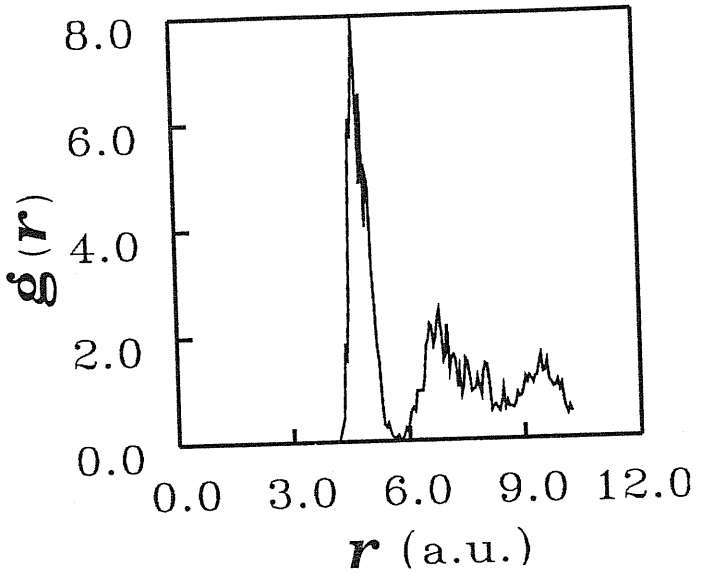

Fig.IV.6.3. $g(r)$ of the coordination defects in a-Si.

The weak-bond character of the coordination defects suggests also that the wave function associated with such defects should not be as localized as one expects for an ideal dangling bond state pointing toward a microvoid. This may be consistent with the localization properties of the D-center wave function (Stathis and Pantelides 1988). Clearly a more detailed study of the electronic properties of the defects generated in the simulation would be very interesting.

In a-Si there are additional structural elements- odd rings. The chemically bonded pairs of atoms (i.e. atoms whose bonding distance is in the first peak of $g(r)$) form closed rings in the structure. Unlike c-Si that consists only of six-fold rings, there is a large variety of ring sizes, both odd and even in a-Si. We have carried out a ring statistics characterization of our model based on shortest path (King 1967) analysis. The shortest path analysis takes in turn each atom in the structure as starting point and connects each couple of bonds attached to it

through the structure in the shortest possible path. This definition of ring statistics has the advantage of yielding a distribution for n-fold rings which is zero at high n. The results are in Fig.IV.6.4. The neighbour was defined by the same cutoff distance as in the analysis of coordination defects, i.e. $r_m = 5.1 a.u.$ The result is an average over 12 atomic configurations generated by MD. The analysis reveals a large portion of odd rings dominated by fivefold rings. In our model no atom lies in a local diamond-structure environment. Thus this model is a member of the purely amorphous class of structures.

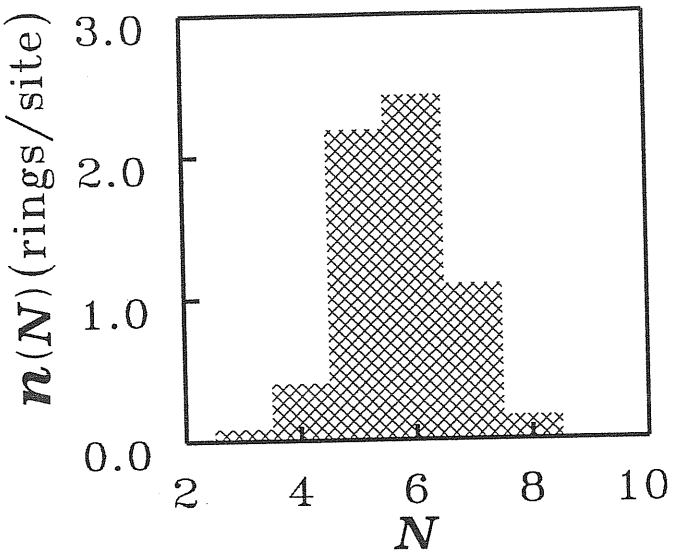

Fig.IV.6.4. Ring statistics $n(N)$ of a-Si (shortest path analysis).

The odd-membered rings can all be threaded through by continuous lines (called odd-, Rivier-, or disclination-lines), which avoid any even-membered ring and form closed loops in the network or terminate at surfaces (Rivier 1979). An odd-membered ring may be imagined to be produced by cutting a sixfold ring through the center, adding or removing a wedge of material and reconnecting the cuts; the edges of the cut have been rotated to make space for the wedge and so odd-membered rings surround the core of a disclination. Topological arguments also confirm that disclination lines are stable universal constituents of random structures. The chief conclusion of this analysis is that in three dimensions there is a one to one correspondence between the group Z_2 - the group isomorphic to the integers modulo 2 - and the physical states of the amorphous solids (Rivier 1987). There have been attempts to explain the anomalous low- and high-T properties, electronic and vibration states, elastic energy etc. of amorphous solids purely by disclinations (Rivier 1987). In the next section we shall briefly discuss the possible consequences of disclinations on the electronic density of states.

In conclusion, a large number of both T_3 and T_3 defects has been found in our model exhibiting a variety of possible dynamics mechanisms. In addition to the coordination defects there are topological defects in our model, dominated by fivefold rings.

IV.7 Electronic Properties of Amorphous Silicon

In this section we analyze the electronic properties of our model: the density of states, their localization, and the imaginary part of the dielectric function.

Similarly as in section III.6 we generated instantaneous adiabatic eigenstates $\{|i\rangle\}$ and eigenvalues $\{\varepsilon_i\}$ for 12 ionic configurations $\{\vec{R}_I\}$ generated by MD. The iterative MSD algorithm was used with fixed self-consistent potentials generated in course of the MD run. The single-particle *electronic density of* (K-S) *states*

$$N(E) = \sum_i \delta(E - \varepsilon_i) \qquad (IV.7.1)$$

is reported in Fig.IV.7.1. The δ-functions have been broadened into a histogram because of a finite sample size. In the same figure we show also the density of occupied states averaged over the entire MD trajectory. The comparison shows that the two curves are almost identical; hence the 12 configurations provide a sufficiently representative sample. The system has opened a gap at the Fermi level as a result of the atomic rearrangements upon cooling. Most likely the gap states in our amorphous structure are due to defect states introduced by the presence of weak bonds. The rather large density of gap states is a consequence of the large concentration of defects in our structure.

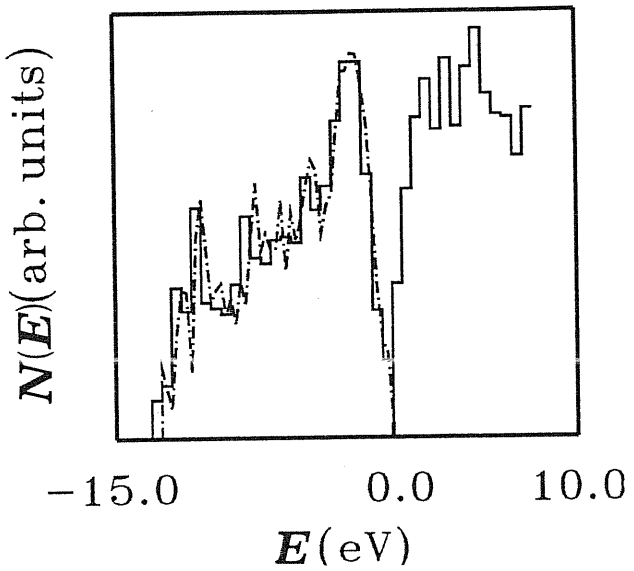

Fig.IV.7.1. Density of Kohn-Sham states $N(E)$ for a-Si. Full line: average over 12 ionic configurations. Dash-dotted line: average over the entire MD trajectory. The vertical line indicates the position of the Fermi energy.

The valence density of states of evaporated a-Si (and a-Ge) have been determined experimentally by X-ray photoemission spectroscopy (XPS) (Ley et al 1972). The results are shown in Fig.IV.7.2 for both crystalline and amorphous states. The gross features of c- and a-Si are similar. A striking aspect is that both have almost the same band width. Two significant differences between c-Si and a-Si are first that the two lower (s-like) peaks (II and III) merge into a single hump and second that

the topmost (p-like) peak (I) remains essentially unchanged but slightly skewed to higher energies. In the experiment the $N(E)$ is weighted by the photoemission cross section, hence the relative intensities of s-like and p-like peaks are affected. The merging of the s-peaks has been ascribed to the presence of odd-membered rings. This argument is strengthened by calculations on Si polymorphs (Joannopoulos and Cohen 1973) and CRN's with and without odd rings (Kelly 1980). Subsequent theoretical studies (Joannopoulos and Cohen 1976) concluded that no structural element other than odd rings is likely to add spectral weight between peaks II and III. Recently, however, there was some doubt about this conclusion and merging of peaks II and III was attributed to oxygen contamination of a-Si samples (Hayes et al 1985). The sharpening of the p-band has been studied using polymorphs (Joannopoulos and Cohen 1973) and analytic means (Singh 1981, Yonezawa and Cohen 1981). Joannopoulos originally attributed this effect to bond-angle disorder. In contrast, Singh attributed the sharpening to dihedral-angle disorder, what seems us more likely.

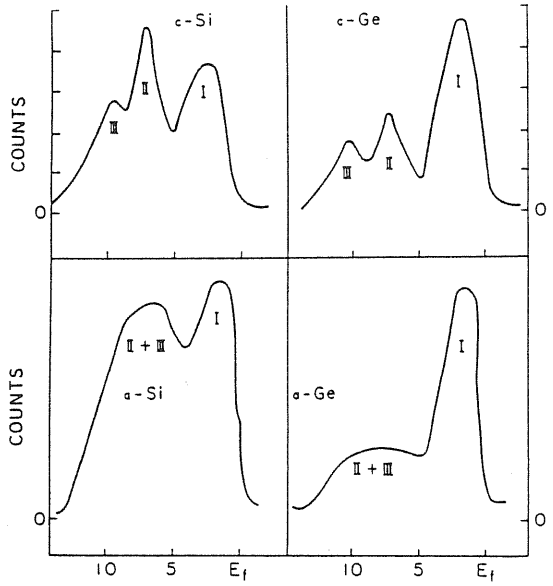

Fig.IV.7.2. Density of valence states in c- and a-Si (Ge) from the XPS measurement (Ley et al 1972).

Similarly as in the case of l-Si, strictly speaking the K-S eigenvalues are only Lagrange multipliers and the $\vec{k}$-point sampling may be here more stringent than in calculation of ionic forces. Despite the poor resolution in our calculation we observe in agreement with experiment: (i) a correct band width $\sim 12.7eV$ (Ley et al 1972, Pierce and Spicer 1972), (ii) no significant structure in the s-like peaks (Ley et al 1972), (iii) correct position of the p-like peak from the Fermi level ($\sim 1.9eV$) (Ley et al 1972, Pierce and Spicer 1972), (iv) no significant structure in the conduction band (Pierce and Spicer 1972). Our results agree qualitatively with the previous CP calculation (Car and Parrinello 1988a).

Now we turn to the nature of the electronic states, i.e. their spatial localization. This occurrence is more probable the greater the degree of disorder in the potentials experienced by the electrons, and so is more likely in the band tails, since these arise

in general from the most distorted sites (like weak bonds). The localization is not easy to study within our small model, because the localization length may become greater than the system size. Several criteria may be used to distinguish between localized and extended states (Elliot 1984, Thouless 1974). One way is to study the the *participation ratio*, i.e.

$$p(E) = \frac{\sum_i p_i \delta(E - \varepsilon_i)}{\sum_i \delta(E - \varepsilon_i)}$$
$$p_i = \frac{1}{\Omega} \frac{\left[\int_\Omega |\psi_i(\vec{r})|^2 d\vec{r}\right]^2}{\int_\Omega |\psi_i(\vec{r})|^4 \mathrm{d}\vec{r}}. \qquad (IV.7.2)$$

A localized state is characterized by a participation ratio tending to zero (which corresponds to a δ-function localization), whereas an extended state has a finite p. The participation ratio averaged over 12 configuration is depicted in Fig.IV.7.3. The gap states are characterized by a marked increase in the localization of the wave functions, the valence band states being more influenced than the conduction states. The Fermi level lies among a series of localized states. Experimental studies suggest that tailing of $N(E)$ is strongly affected by a given sample preparation (Pierce and Spicer 1972).

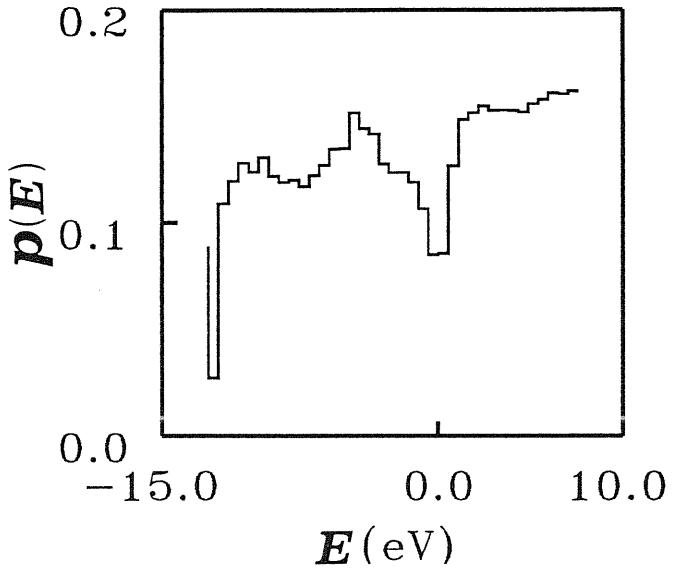

Fig.IV.7.3. Participation ratio $p(E)$ for electronic states in a-Si.

Finally, we discuss optical properties of a-Si. These are almost entirely determined by the imaginary part of the complex dielectric function

$$\varepsilon(\omega) = \varepsilon_1(\omega) + \varepsilon_2(\omega), \qquad (IV.7.3)$$

where $\varepsilon_2(\omega)$ is given in a one-electron approximation (Bassani and Pastori Parravicini 1975, Connell 1979) as

$$\varepsilon_2(\omega) = \frac{8\pi^2 e^2}{\Omega m^2} \langle \sum_i^{occ} \sum_j^{unocc} \frac{|M_{ij}|^2}{\omega_{ji}^2} \delta(\varepsilon_j - \varepsilon_i - \hbar\omega) \rangle, \qquad (IV.7.4)$$

where M_{ij} is the momentum matrix between states $|i\rangle$ and $|j\rangle$. In practice, the $\varepsilon_2(\omega)$ is often obtained by a Kramers-Kronig transformation of reflectivity data (Pierce and Spicer 1972).

The calculated $\varepsilon_2(\omega)$ for our model is compared with experimental data derived from measured reflectivity on evaporated a-Si (Pierce and Spicer 1972) in Fig.IV.7.4. Our data are averaged over 12 configurations. Except for small energies ($< 2eV$), the agreement is decent. At small energies our data are influenced by excitations into gap states. We assume here all the states up to the Fermi level to be doubly occupied. The experimental data in Fig.IV.7.4 correspond to a-Si where the presence of coordination defects and microvoids have been minimized. In less carefully prepared samples the optical-absorption edge may be shifted to lower energies (Pierce and Spicer).

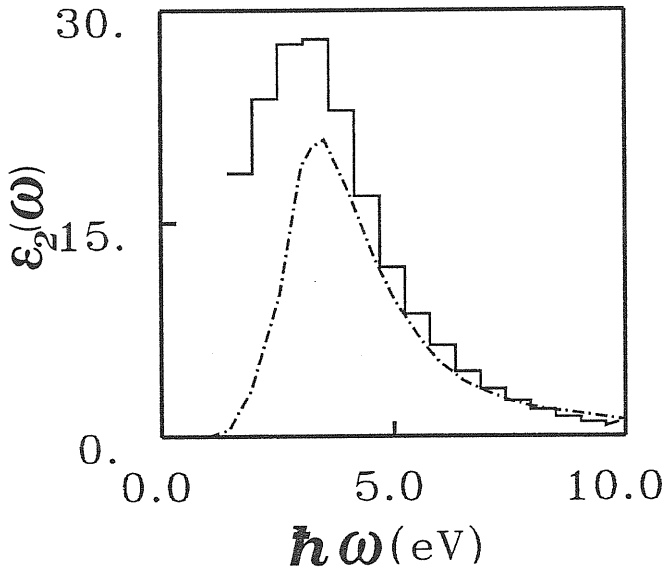

Fig.IV.7.4. Imaginary part of the complex dielectric function $\varepsilon_2(\omega)$ of a-Si. Full line: calculation. The curve was interrupted in the low energy region where our calculation is influenced by gap states. Experimental data of Pierce and Spicer (1972) are shown by dash-dotted line.

$\varepsilon_2(\omega)$ must satisfy the *plasma sum rule*

$$n = \frac{m}{2\pi^2 e^2} \int_0^{\omega_0} \omega \varepsilon_2(\omega) \mathrm{d}\omega \qquad (IV.7.5)$$

where n is the density of electrons contributing to the optical absorption up to an energy $\hbar\omega_0$. An important consistency check is obtained by integrating equation IV.7.5 over all possible transitions. This has been explicitly checked. In our calculation the RHS of equation IV.7.5 is typically $\sim 10\%$ smaller than the LHS. This error is due to the matrix elements M_{ij} that are in our calculations simply treated as if the potential were local (i.e. by taking $M_{ij} = \langle\psi_i| - i\nabla|\psi_j\rangle$). In a more elaborated calculation the nonlocality of the potential could be taken into account (Baroni and Resta 1986, Hybertsen and Louie 1987).

The optical spectra of a-Si are distinctly different from those of the crystal. The latter are sharply peaked at $4.4eV$, while the amorphous spectrum has a broad peak displaced toward lower energies (Pierce and Spicer 1972). The changes are due partly to the lack of $\vec{k}$ selection rule in a-Si (optical transitions without phonon assistance are vertical in $\vec{k}$). The $\vec{k}$ selection rule delays transitions in indirect gap crystals to higher energies. In amorphous semiconductors valence states can be excited to all conduction states. This has important practical implications. Both c- and a-Si are important solar cell materials. In c-Si the optical absorption is much lower than in a-Si in the region of $1-3eV$. The sum rule IV.7.5 requires the absorption in c-Si to be shifted to a higher energy region $(3-5eV)$. The $1-3eV$ region is just the region which contains most of the solar spectrum. This is a significant advantage of a-Si for large-scale applications.

In summary, a realistic electronic structure has been obtained for our a-Si which is in qualitative agreement with experimental data. The study of the participation ratio indicates a marked increase in the localization of the wave functions in the gap region.

V. Conclusions

In this thesis we have presented an extensive ab-initio molecular dynamics study of liquid and amorphous silicon. A reliable description of both phases at the state-of-the-art level was achieved. Until recently, such calculations were feasible only for crystals. In our study the interatomic potential was constructed from the electronic ground-state within the density functional framework in the local density approximation (LDA). This pushes these calculations at the limits of present-days computers and restricts the size of tractable systems. The small system size in our calculation is not necessarily a severe drawback since most properties of interest are determined essentially by short-range order. The computational intensity is justified by the absence of any fitting parameter in the theory and by the fact that all the results (structural, dynamical, and electronic) are a product of one single calculation. A numerical approach is generally required also in more traditional applications of statistical mechanical methods to real systems where, however, the results are biased by the choice of the model interatomic potential.

From the methodological point of view the most important results of this work are :

- Confirmation of the feasibility of the first-principles MD treatment of metallic systems

- Test of the validity of the BO and LDA approximations for l- and a-Si

- Test of the influence of precision and quality of the interatomic potentials on the MD

-Introduction and test of new robust and efficient methods for electronic structure calculation

Our simulation of l-Si is probably the first successful application of the ab-initio molecular dynamics to a metallic system. Problems arising from the nonadiabatic behaviour have been overcome. The description of the atomic structure is in excellent agreement with X-ray (Waseda and Suzuki 1975) and neutron (Gabathuler and Steeb 1979) scattering experiments. A careful analysis of bonding properties revealed a persistence in l-Si of some covalent bonding effects. Bond breaking and bond forming effects have been found important. Covalent bonding gives rise to a well identifiable feature in the power spectrum of the system dynamics. The calculated self-diffusion coefficient agrees well with indirect experimental estimates. The system shows metallic behaviour. The calculated a.c. electrical conductivity has a Drude-like falloff in close agreement with experimental data (Shvarev et al 1975).

Convergence tests have shown that the results are quite sensitive to variations in the energy cutoff. A cutoff of $12Ry$ was necessary to achieve convergence and produce a coordination in close agreement with experiments.

Upon cooling the system underwent profound structural changes; the coordination decreased from ~ 6.5 in the liquid to ~ 4 in the amorphous phase. The system developed a strong tetrahedral order and some degree of medium range order. The changes in atomic structure are accompanied by changes in electronic structure; the system developed an energy gap.

The structural characteristics of our model of a-Si agree well with recent diffraction data (Fortner and Lannin 1989). Also the bond lengths variance is close to experimental XAS (Filipponi et al 1989) findings. The only difference is a slightly larger bond angle variance in our model. This is likely a consequence of a small size of our model and a too fast cooling rate. Apart from an almost rigid shift to lower frequencies ($\sim 6THz$) the calculated vibrational spectrum exhibits all the features found experimentally (Kamitakahara et al 1987). There are both under- and over-coordination defects in our model. They have a character of weak bonds and exhibit dynamics that correlates well with recent theoretical models (Pantelides 1988). Our model is also topologically nontrivial. It contains a large portion of odd-membered rings, dominated by five-fold ones. Even though the poor resolution in the electronic structure calculation does not allow us to correlate the presence of topological defects with the shape of the electronic density of states, it does not show significant discrepancies with the XPS spectra (Ley et al 1972). The coordination defects introduce a relatively high density of gap states. Measurement of the participation ratio indicates an increase in the localization of wave functions belonging to gap states.

The bond angle variance and the intensity of the TO peak of the phonon density of states indicate the possibility of some overstrain in our structural model. There were also structural relaxations present at $T = 300K$ and the system was not yet well equilibrated. For these reasons it would be interesting to let the system go through an additional annealing cycle. Such a procedure is normally followed also in a real preparation of a-Si.

To complete fully the study of disordered Si phases one would like to anneal the a-Si data presented here and to study the electronic structure of defects present in the simulated structure. Another interesting point that deserves further study is the inherent structure of l-Si (Stillinger and Weber 1985, La Violette and Stillinger 1987). Preliminary calculation (Štich 1987) showed that our model may yield an inherent structure different from that originally found by Stillinger and Weber (1985) with an empirical potential.

Appendix 1. Empirical Interatomic Potentials

In chapter II.1 we discuss how the many-body energy surface $\Phi\big[\{\vec{R}_I\}\big]$ can be found from first-principles. An alternative approach consists in its suitable empirical parametrization. In empirical schemes the potential $\Phi\big[\{\vec{R}_I\}\big]$ is usually partitioned as

$$\Phi\big[\{\vec{R}_I\}\big] = \sum_{1\le I\le N} \phi^1(\vec{R}_I) + \sum_{1\le I\le J\le N} \phi^2(\vec{R}_I,\vec{R}_J) + \sum_{1\le I\le J\le K\le N} \phi^3(\vec{R}_I,\vec{R}_J,\vec{R}_K) + \ldots \tag{A.1.1}$$

where ϕ^n is an "n-body potential". In particular, the one body term corresponds to an external potential. The expansion A.1.1 is often truncated at the two-body term. This approach may be appropriate for simple closed-shell systems, like rare gasses or for simple metals. For covalent systems, more terms have to be included in order to describe the directional covalent bonds. Recently, various attempts have been made to model the many-body interactions for covalent systems by empirical potentials (Stillinger and Weber 1985, Biswas and Hamann 1985, Tersoff 1988) * These classical models were developed by fitting first-principles calculations and/or experimental data. We consider here the Stillinger-Weber (1985) (SW) potential, as a specific example. The SW potential includes two- and three-body terms which have the form ($R_{IJ} = |\vec{R}_I - \vec{R}_J|$)

$$\begin{aligned} \phi^2(R_{IJ}) &= A\big(BR_{IJ}^{-4} - 1\big)g_\gamma(R_{IJ}) \\ \phi^3(R_{IJ},R_{JK},R_{KI}) &= \phi_{IJK} + \phi_{JIK} + \phi_{IKJ} \\ \phi_{IJK} &= \lambda g_\gamma(R_{IJ})g_\gamma(R_{JK})\Big(\cos\theta_{IJK} + \tfrac{1}{3}\Big)^2. \end{aligned} \tag{A.1.2}$$

A, B, λ, γ are parameters, $g_\gamma(R) = \exp\big[\frac{\gamma}{R-a}\big]$ is a cutoff function that cutoffs at distances $R \ge a$, and θ_{IJK} is the angle between vectors $\vec{R}_{IJ}$ and $\vec{R}_{JK}$. The three-body term is zero at the ideal tetrahedral angle and positive otherwise. The system may develop a competition between the three-body term favoring tetrahedral coordination, which dominates at low temperature, and the two-body term which dominates at high T and prefers closer packing. In section III.3. we argue that the SW system at high T is qualitatively different from ours. It seems also a general conclusion that the SW potential (with one set of parameters) is unable to describe all Si phases: crystal, amorphous, and liquid (Ding and Andersen 1986, Broughton and Li 1987). This is not surprising, because the electronic structure that varies considerably going from one phase to another is taken into account only implicitly

* There is a different group of empirical potentials which formally correspond to Taylor expansion of the energy about the minimum. They may accurately describe small displacements, such as phonons and elastic deformations, but fail for large displacements. The Keating (1966) model is the most famous of them.

and in an averaged way. Although often very useful, the empirical potentials are not entirely satisfactory since (i) they miss the close connection between the electronic and atomic structure, (ii) the range of their validity is not known, and (iii) it is generally difficult to make detailed quantitative predictions for a particular material. There are other classical models tailored to Si (similar to SW in spirit) like Biswas-Hamann (1985) (BH) or Tersoff (1988) which may work better than SW in some special configurations, but leave the above general conclusions unchanged.

Appendix 2. Nonlocal Pseudopotentials

The total external potential can be expressed in terms of ionic pseudopotentials as

$$V^{ext}(\vec{r}) = \sum_I v_{ps}(\vec{r} - \vec{R}_I). \qquad (A.2.1)$$

The ionic pseudopotential is usually taken to be nonlocal and can be represented as

$$v_{ps}(\vec{r}) = \sum_{l=0}^{\infty} v_l(\vec{r})\hat{P}_l \qquad (A.2.2)$$

where $\hat{P}_l$ is the projector onto the l-th angular momentum. In our case $v_l(r)$ are norm-conserving pseudopotentials (Hamann et al 1979, Bachelet et al 1982). If we assume that $v_l = v_{l_{max}}$ for $l \geq l_{max}$ the infinite sum in equation A.2.2 can be written as

$$\begin{aligned} v_{ps}(\vec{r}) &= v_{l_{max}}(\vec{r}) + \sum_{l=0}^{l_{max}-1} \Delta v_l(\vec{r})\hat{P}_l \\ &= v_{loc} + v_{nonloc} \end{aligned} \qquad (A.2.3)$$

with $\Delta v_l(\vec{r}) = v_l(\vec{r}) - v_{l_{max}}(\vec{r}) = \Delta v_l(r)$. The total nonlocal potential is most conveniently written in momentum space as

$$\Delta V_{nonloc}(\vec{q}, \vec{q}\,') = \sum_I \sum_{l=0}^{l_{max}-1} \exp(-i\vec{q}.\vec{R}_I)\Delta v_l(\vec{q}, \vec{q}\,')\exp(i\vec{q}\,'.\vec{R}_I) \qquad (A.2.4)$$

where

$$\Delta v_l(\vec{q}, \vec{q}\,') = \frac{4\pi}{\Omega}(2l+1)P_l(\hat{q}\cdot\hat{q}\,')\int_0^{\infty} dr r^2 \Delta v_l(r) j_l(qr) j_l(q'r). \qquad (A.2.5)$$

In equation A.2.5 P_l and j_l are Legendre polynomials and spherical Bessel functions, respectively. $\hat{q}$ and $\hat{q}\,'$ are unit vectors in directions $\vec{q}$ and $\vec{q}\,'$ respectively, and Ω is the unit cell volume. A straightforward application of this operator to the wave function in Fourier space requires $O(M^2)$ operations. This can be reduced to $O(M)$ operations if Δv_l is separable in momentum space

$$\Delta v_l(\vec{q}, \vec{q}\,') = \sum_{s=1}^{S} W_s(\vec{q}) W_s(\vec{q}\,') \qquad S << M. \qquad (A.2.6)$$

This can be achieved in several ways (Štich et al 1989a, Allan and Teter 1987). Here we have used the separable nonlocal correction potential of the form suggested by Kleinman and Bylander(1982)

$$\Delta v_l(\vec{q},\vec{q}\,') = \frac{4\pi}{\Omega}(2l+1)P_l(\hat{q}\cdot\hat{q}\,')\times \frac{\int_0^\infty \mathrm{d}r r^2 \Delta v_l(r) j_l(qr)\phi_l(r) \int_0^\infty \mathrm{d}r r^2 \Delta v_l(r) j_l(q'r)\phi_l(r)}{\int_0^\infty \mathrm{d}r r^2 \phi_l^2 \Delta v_l(r)} \qquad (A.2.7)$$

where $\phi_l(r)$ are atomic radial pseudo-wave functions of the state used to generate the pseudopotential. The use of equation A.2.7 with $l_{max} = 1$ is a convenient and stable choice for Si. By construction the operator A.2.7 reduces to A.2.5 when applied to the reference state, so either choice of pseudopotential identically reproduces the all-electron properties of a reference atomic state. They both have the properties of transferability of norm-conserving pseudopotentials. Generally, however, they are different operators.

Appendix 3. Momentum Space Expansions

The methods introduced in chapter II were all based on the use of FFT techniques. The principal ingredient of these techniques is calculation of the unconstrained electronic forces

$$F_i^e(\vec{r}) = -\frac{\delta E}{\delta \psi_i^*(\vec{r})} = -H\psi_i(\vec{r}). \qquad (A.3.1)$$

Here we shall suppose that the Hamiltonian $H = -\frac{1}{2}\nabla^2 + V(\vec{r})$ in equation A.3.1 is purely local. The discussion of nonlocal operators was presented in Appendix 2. Inspection of equation A.3.1 shows that the electronic force $F_i^e(\vec{r})$ is a product of H and $\psi_i(\vec{r})$ and can be conveniently calculated through the use of FFT techniques. The action of the kinetic energy operator is easy to calculate in momentum space, while the action of the potential energy operator is easy to calculate in real space. Thus the product $V * \psi_i(\vec{r})$ is obtained by trivial multiplication on a uniform real space grid and the result is back transformed by an inverse Fourier transform to the momentum space. Under certain conditions these operations may constitute an exact algorithm.

Both $V(\vec{r})$ and $\psi_i(\vec{r})$ are periodic functions in coordinate space represented by their Fourier components $V(\vec{G})$ and $\psi_i(\vec{G})$ at the reciprocal lattice vectors $\vec{G}$. The expansion of ψ_i is truncated at $\vec{G}_{max}$ to include only M plane-waves, fixed by an kinetic energy cutoff $\frac{1}{2}|\vec{G}|^2 \leq E_{cut}$. The inspection of the convolution term $\sum_{\vec{G}'} V(\vec{G} - \vec{G}') * \psi_i(\vec{G}')$ shows that the expansion of V can be truncated at $2G_{max}$. The result of the convolution will also be truncated at G_{max}. In this case we obtain exactly the first M Fourier components of the convolution product $V * \psi$. Note, however, that it has been suggested recently that the assumption of a unique cutoff $\vec{G}_{max}$ for all expansions in plane-waves might also be adequate (Martins and Cohen 1988). For the systems treated in this thesis we found this approximation inappropriate. Stable and converged results were instead obtained by using momentum space cutoffs intermediate between the full expansion and that suggested by Martins and Cohen (1988). This has been used for calculations presented in chapter IV.

Appendix 4. Conjugate Gradient Minimization of the Energy Functional

Let us suppose that the function f to be minimized can be approximated by a multidimensional quadratic form around some point P taken as the origin of the coordinates

$$f(X) \approx c - \langle b \mid X \rangle + \tfrac{1}{2}\langle X \mid A \mid X \rangle \quad , \tag{A.4.1}$$

where

$$X \equiv (x_1, x_2, ..., x_L) \quad , \quad c \equiv f(P) \quad , \quad b \equiv -\nabla f|_P \quad , \quad A_{ij} \equiv \frac{\partial^2 f}{\partial x_i \partial x_j}|_P \tag{A.4.2}$$

with a symmetric positive definite $L \times L$ Hessian matrix A. An iterative minimization procedure is then defined by the sequence:

$$P^{(n+1)} = P^{(n)} + \lambda^{(n)} h^{(n)} \quad , \quad n = 0, 1, 2... \tag{A.4.3}$$

where $\lambda^{(n)}$ is a scalar and $h^{(n)}$ is a vector in multidimensional space. By using the information contained in the matrix of second derivatives A, a single operation is sufficient to minimize a perfectly quadratic function f. For large L it is impractical to deal with the large matrix A. In the conjugate gradient (CG) method (Press et al 1986) information on A is only used implicitly to define an optimal set of directions $h^{(n)}$ in the sequence of equations A.4.3, where the scalar $\lambda^{(n)}$ is obtained by a one-dimensional minimization along the line defined by $h^{(n)}$. The directions $h^{(n)}$ are given by

$$h^{(n)} = \begin{cases} g^{(n)}, & \text{n=0} \\ g^{(n)} + \gamma^{(n-1)} h^{(n-1)}, & \text{n=1,2,3...} \end{cases} \tag{A.4.4}$$

where

$$\begin{aligned} g^{(n)} &= -\nabla f(P^{(n)}) \\ \gamma^{(n)} &= \frac{\langle g^{(n+1)} \mid g^{(n+1)} \rangle}{\langle g^{(n)} \mid g^{(n)} \rangle} \quad . \end{aligned} \tag{A.4.5}$$

The directions $h^{(n)}$ are said to be conjugate. One can show (Press 1986) that for a quadratic function like the one in equation A.4.1, the following conjugacy property is satisfied

$$\langle h^{(n)} \mid A \mid h^{(m)} \rangle = 0 \quad \forall n \neq m. \tag{A.4.6}$$

This property guarantees that each step is actually an improvement over all the preceding ones, a property not shared by steepest descent (SD) based methods. The reason is that SD steps are often orthogonal or nearly orthogonal to one another.

It is natural to apply the CG procedure (equations A.4.3-5) to the electronic minimization problem. A difficulty arises in this respect because of the existence

of orthonormality constraints in the electronic problem. These originate forces of constraint that must be taken into account when the line minimizations are done. In order to deal with such constraints it is convenient to reformulate the electronic problem in terms of linearly independent but not orthonormal orbitals $\{\varphi_i\}$ (Štich et al 1989a). The orthonormal orbitals $\{\psi_i\}$ may be related to the $\{\varphi_i\}$ via

$$\psi_i = \sum_j S_{ij}^{-\frac{1}{2}} \varphi_j \quad , \tag{A.4.7}$$

where $S_{ij} = \langle \varphi_j \mid \varphi_i \rangle$ is the overlap matrix. The energy functional E can be written in terms of the $\{\varphi_i\}$ as

$$E = \sum_{ij}^{occ} S_{ij}^{-1} \langle \varphi_i \mid -\tfrac{1}{2}\nabla^2 \mid \varphi_j \rangle + \int \mathrm{d}\vec{r}\; V^{ext}(\vec{r})\; n(\vec{r}) +$$

$$\tfrac{1}{2} \int \mathrm{d}\vec{r}\mathrm{d}\vec{r}\,' \frac{n(\vec{r})\; n(\vec{r}\,')}{|\vec{r} - \vec{r}\,'|} + E^{xc}[n] + \tfrac{1}{2} \sum_{I \neq J} \frac{Z_I Z_J}{|\vec{R}_I - \vec{R}_J|}. \tag{A.4.8}$$

For initially orthonormal orbitals $\{\varphi_i\}$, one obtains the constrained electronic forces

$$\frac{\delta E}{\delta \varphi_i^*(\vec{r})} = H\varphi_i(\vec{r}) - \sum_m \langle \varphi_m \mid H \mid \varphi_i \rangle \varphi_m(\vec{r}). \tag{A.4.9}$$

It is convenient to reorthonormalize the $\{\varphi_i\}$ at any step. This will ensure that the S matrix remains nonsingular and allows the use of equation A.4.9. Equation A.4.9 defines the gradient $g^{(n)}$ from which one obtains the conjugate direction $h^{(n)}$ using equation A.4.4. A one-dimensional minimization of the functional E along $h^{(n)}$ allows to compute $\lambda^{(n)}$ and to accomplish the CG step defined in equation A.4.3. One possible way to carry out the one-dimensional minimization is to proceed as in nonself-consistent calculation and instead of E minimize $\tilde{E}$ given by (Štich et al 1989a)

$$\tilde{E}(\lambda^{(n)}) = \sum_{ij} \langle \varphi_i^{(n+1)} \mid \tilde{H} \mid \varphi_j^{(n+1)} \rangle S_{ij}^{-1\,(n+1)} \quad , \tag{A.4.10}$$

where $\varphi_i^{(n+1)} = \varphi_i^{(n)} + \lambda^{(n)} h_i^{(n)}$ and $\tilde{H} = \tilde{H}[\{\varphi_i^{(n)}\}]$; i.e. V^H and μ^{xc} are not varied as $\lambda^{(n)}$ is changed but are instead determined by the density corresponding to $\{\varphi_i^{(n)}\}$. Such an approach requires $\sim 2N_e M \log M + 4N_e^2 M$ operations for a local potential. An alternative approach consists in a series of parabolic approximations. This method was used in calculations presented here.

Appendix 5. Efficiency of Calculation of the BO Forces

As pointed out in section II, in order to calculate the BO or Hellman-Feynman ionic forces within DFT one has to minimize the energy functional $E[\{\psi_i\},\{\vec{R}_I\}]$ with respect to the "electronic degrees of freedom" $\{\psi_i\}$, i.e. the corresponding point on the BO surface $\Phi\big[\{\vec{R}_I\}\big]$ must be reached in some way for each ionic configuration $\{\vec{R}_I\}$

$$\Phi\big[\{\vec{R}_I\}\big] = \min_{\{\psi_i\}} E\big[\{\psi_i\},\{\vec{R}_I\}\big]. \qquad (A.5.1)$$

This objective can be reached essentially by two strategies. One way, which will be referred to as *adiabatic*, consists in solving the equations II.3.3a,b. In an MD with the system defined by the Lagrangian II.3.2 the system will keep the total energy of this dynamical system

$$E^{tot} = \sum_i \tfrac{1}{2}\mu \int d\vec{r}|\dot{\psi}_i(\vec{r})|^2 + \sum_I \tfrac{1}{2} M_I \dot{\vec{R}}_I^2 + E\big[\{\psi_i\},\{\vec{R}_I\}\big] \qquad (A.5.2)$$

constant. In the instantaneous electronic ground-state, when A.5.1 is valid, $\{\dot{\psi}_i = 0\}$ and effectively the total energy of the ionic subsystem

$$E^{I_{tot}} = \sum_I \tfrac{1}{2} M_I \dot{\vec{R}}_I^2 + \Phi\big[\{\vec{R}_I\}\big] \qquad (A.5.3)$$

is kept constant. Only when equation A.5.3. is a constant of motion, the ionic dynamics will be correct. It means that the electronic configuration must have always enough time to relax to the instantaneous ground-state of the simultaneously changing ionic configuration. This can be achieved by setting two time scales: a slow one for the ionic degrees of freedom and a fast one for the electrons. To set up such a regime requires μ to be small compared to M_I. A small μ in turn requires a small time integration step Δt in integration of the equations II.3.5a,b. This poses the question about whether the adiabatic dynamics is really the most efficient one.

An alternative way of calculation of the BO forces for the ionic dynamics, which will be referred to as *decoupled*, is based on a complete decoupling of the electronic and ionic dynamics by carrying out explicitly the minimization indicated in A.5.1 at any ionic step. Since there are very efficient minimization techniques, such as e.g. the CG method, to relax the electronic configuration, this alternative dynamics might be more efficient than the adiabatic one. In particular, the decoupled dynamics should relax the requirement of keeping the time step in the integration of the equations

$$M_I \ddot{\vec{R}}_I = -\frac{\partial \Phi\big[\{\vec{R}_I\}\big]}{\partial \vec{R}_I} \qquad (A.5.4)$$

small.

We have done rather extensive tests to compare how the above mentioned methods work in practice (Štich 1987). We have excited a phonon mode in the system consisting of eight Si atoms in the diamond lattice sites. The atoms were initially displaced from their equilibrium lattice positions in the direction of the eigenmode of the optical phonon at the Γ point of the supercell BZ. The system initially prepared in the electronic ground-state was then left to evolve under the action of the ionic forces calculated both within the adiabatic and decoupled dynamics. Here we give only the general conclusions. The details can be found elsewhere (Štich 1987). The general result of this test was that, within the adiabatic dynamics the ions performed periodic oscillations with correct frequencies (in the limits given by precision of that calculation). In the decoupled dynamics, instead, the phonon resulted to be damped what means that the forces on the ions were not calculated correctly. This tendency continued until an extremely high precision
($\sim$ ten significant figures) in the electronic minimization was required.

This rather surprising behavior has the origin in the dynamical optimization of the electronic degrees of freedom by MD (Štich 1987, Car and Parrinello 1989). The MD equation of motion for the electronic wave functions is

$$\mu\ddot{\psi}_i = F_i^{el}, \qquad (A.5.5)$$

stating the proportionality of the acceleration of the wave functions to the force acting on it. In the ground-state the wave functions do not move; the forces are zero. When the ions displace, the forces on the wave functions become nonzero and proportional to the ionic displacement. Thus the electronic wave functions will accelerate and catch up the delay until overtaking the ions when the forces begin to brake the motion of the wave functions. The electronic oscillations make the ionic forces to oscillate, thus stabilizing the calculation. In other words, the electronic and ionic dynamics are correlated. On the other hand in the decoupled dynamics the electronic wave functions obey first order equations of the SD type

$$\mu\dot{\psi}_i = F_i^{el} \qquad (A.5.6)$$

making the velocity of the wave function proportional to the forces on orbitals, leading to a systematic delay and error in the BO forces.

In conclusion, the use of the decoupled dynamics results in incorrect BO forces, unless an extremely high precision of the electronic minimization is required. The costly part of any first-principles MD is always the electronic structure calculation. This fact makes the adiabatic dynamics substantially more efficient than the decoupled dynamics.

Appendix 6. Convergence Study of the l-Si Simulation

We have carried out a convergence study of our l-Si calculation with respect to parameters quoted in section III.2, i.e. with respect to periodic boundary conditions, cell size, inclusion of p-nonlocality in the pseudopotential, and energy cutoff in the plane-wave expansion of the electronic wave functions.

The results were quite sensitive to variations in the energy cutoff. The results obtained with an energy cutoff of $6Ry$ and $8Ry$ are shown in Figs.A.6.1, A.6.2, respectively.

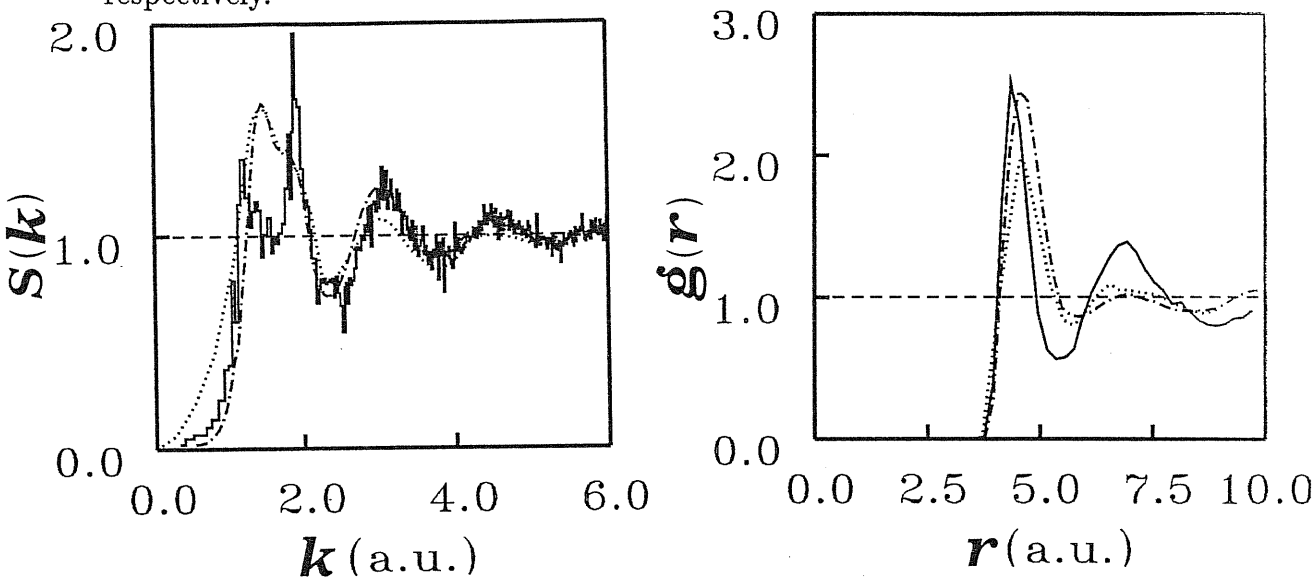

Fig.A.6.1. $S(k)$ and $g(r)$ of l-Si. Full line: MD simulation with an energy cutoff of $6Ry$. Here the cutoff in the expansion of the potential was taken equal to the cutoff for the wave functions (Martins and Cohen 1988, Appendix 3). The total time of the simulation was $\sim 0.6ps$. Dotted line: neutron diffraction experiment (Gabathuler and Steeb 1979), dash-dotted line: X-ray diffraction experiment (Waseda and Suzuki 1975).

Generally, a low energy cutoff reduced the tendency toward metallization and resulted in more structured system having lower average coordination. A closer inspection of the $6Ry$ l-Si structure reveals some similarity with the a-Si structure (section IV.4); this low cutoff structure may be close to the structure of a supercooled liquid. The latter conjecture is also in agreement with the reduced diffusion coefficient observed for this system. However, even this relatively poor model of l-Si does not change completely the underlying physics and shares many common features (like presence of some covalent bonds, bond-breaking (-forming) processes, form of $g_3(\theta)$, etc.) with the more accurate models. With the energy cutoff of $6Ry$ we reproduced, with the 64 atom SC cell, the structure already found in a preliminary calculation done with a 54 atom FCC cell and a similar cutoff (Car and Parrinello 1987). The observed relative independence of the structural properties

on the unit cell size and shape provides an indication that the calculation of the interatomic forces, which requires a BZ average, is essentially well converged with respect to $\vec{k}$-point sampling.

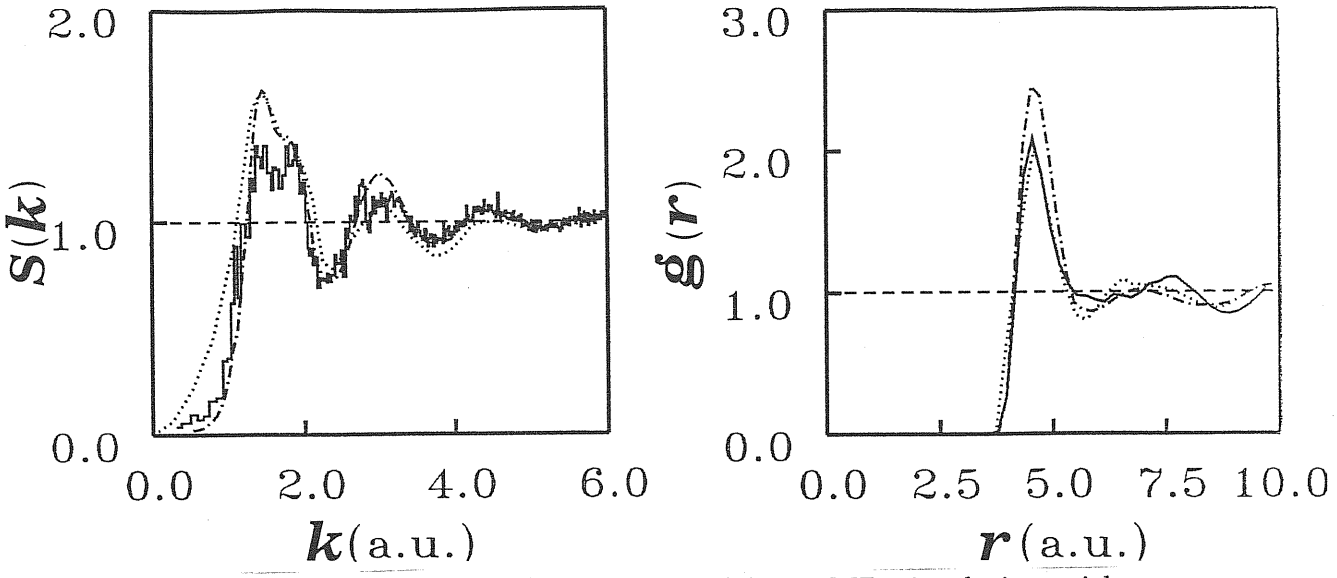

Fig.A.6.2. $S(k)$ and $g(r)$ of l-Si. Full line: MD simulation with an energy cutoff of $8Ry$. Here the cutoff in the expansion of the potential was taken equal to the cutoff for the wave functions (Martins and Cohen 1988, Appendix 3). The total time of the simulation was $\sim 1.2ps$. Dotted line: neutron diffraction experiment (Gabathuler and Steeb 1979), dash-dotted line: X-ray diffraction experiment (Waseda and Suzuki 1975).

We have also tested the effect of inclusion of the p-nonlocality in the pseudopotential. The result is reported in Fig.A.6.3. As can be seen the result does not exhibit strong dependence on the p-nonlocality in the potential. For this reason we carried out our study with the s-nonlocality only.

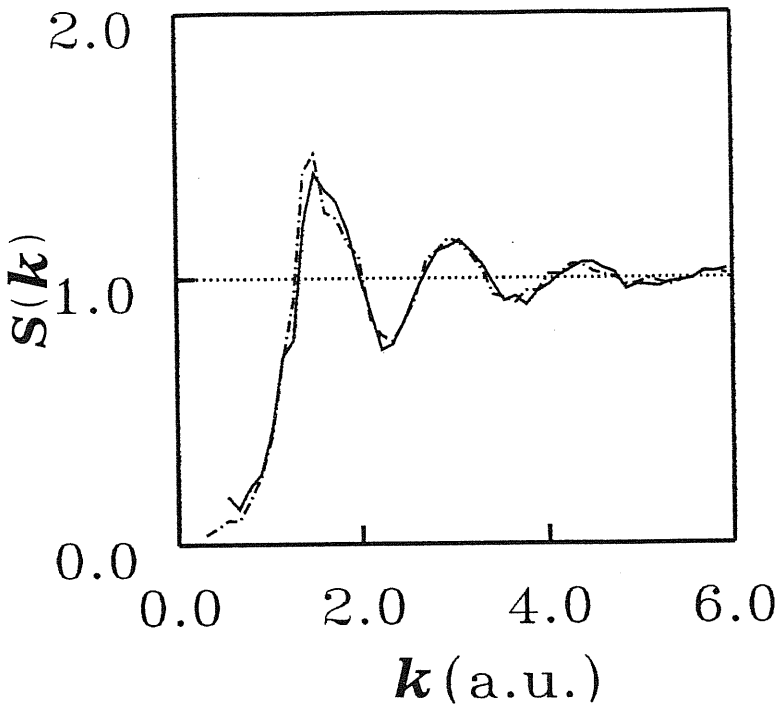

Fig.A.6.3. $S(k)$ of l-Si. Full line: result for s+p-nonlocality; Dash-dotted line: result for s-nonlocality. Both results correspond to an energy cutoff of $12Ry$ and the total time of simulation of $\sim 1.2ps$. To facilitate the comparison both curves have been smoothed.

References

Allan P.B. and Broughton J.Q. 1987, J.Phys.Chem **91**, 4964

Bachelet G.B., Hamann D.R., and Schüter M. 1982, Phys.Rev. **B26**, 4199

Baldereschi A. 1973, Phys.Rev. **B7**, 5212

Barna A., Barna P.B., Radnoczi G., Toth L., and Thomas P. 1977, Phys.Stat.Sol (a) **41**, 81

Baroni S. and Resta R. 1986, Phys.Rev. **B33**, 7017

Bassani F. and Pastori-Parravicini G. 1975, *Electronic States and Optical Transitions in Solids* (Oxford: Pergamon)

Binder K. (ed.) 1979,1984, *Monte-Carlo Methods in Statistical Mechanics*, Topics in Current Physics, vol. **7** and **36**, (Berlin: Springer)

Biswas R. and Hamann D.R. 1985, Phys.Rev.Lett **55**, 2001

Biswas R., Grest G.S., and Soukoulis C.M. 1987, Phys.Rev. **B36**, 7437

Biswas R., Bouchard A.M., Kamitakahara W.A., Grest G.S., and Soukoulis C.M. 1988, Phys.Rev.Lett. **60**, 2280

Biswas R., Kwon I., Bouchard A.M., Soukoulis C.M., and Grest G.S. 1989, Phys.Rev. **B39**, 5101

Broughton J.Q. and Li X.P. 1987, Phys.Rev. **B35**, 9120

Car R. and Parrinello M. 1985, Phys.Rev.Lett. **55**, 2471

Car R. and Parrinello M. 1987, in *Proc. 18th Int. Conf. Physics of Semiconductors*, O. Engstrom (ed.) (Singapore: World Scientific), p. 1165

Car R., Parrinello M., and Andreoni W. 1987, in *Proceedings of the First NEC Symposium of Fundamental Approaches to New Material Phases*, S. Sugano and S. Ohnishi (eds.) (Berlin: Springer)

Car R. and Parrinello M. 1988a, Phys.Rev.Lett. **60**, 204

Car R. and Parrinello M. 1988b, in *Simple Molecular Systems at Very High Density*,

(NATO ASI Series: Plenum)

Car and Parrinello 1989, to appear in J.Phys: Condensed Matter

Ceperley D.M. and Alder B.J. 1980, Phys.Rev.Lett. **45**, 566

Chadi D.J. and Cohen M.L. 1973, Phys.Rev. **B8**, 5747

Chang K.J. and Cohen M.L. 1985, Phys.Rev. **B31**, 7819

Cohen M.L., Heine V., and Weaire D. 1970, *Solid State Physics*, vol **24**, H.Ehrenreich, F. Seitz, and D. Turnbull (eds.), (New York: Academic)

Connel G.A.N. and Temkin R.J. 1974, Phys.Rev. **B9**, 5323

Connel G.A.N. 1979, in *Amorphous Semiconductors*, M.M. Brodsky (ed.), Topics in Applied Physics, vol. **36**, (Berlin: Springer)

Croxton C.A. 1974, *Liquid State Physics*, (Cambridge: University)

Davidson E.R. 1983, in *Methods in Computational Molecular Physics*, G.H.F. Diercksen and S. Wilson (eds.), vol **113** of *NATO Advanced Study Institute*, Series C, (New York: Plenum)

Ding K. and Andersen H.C. 1986, Phys.Rev. **B34**, 6987

Duffy M.G., Boudreaux D.S., and Polk D.E. 1974, J.Non-Cryst.Solids **15**,435

Economou E.N. 1983, *Green's Functions in Quantum Physics*, Springer Series in Solis State Sciences, vol. **7**, (Berlin: Springer)

Elliot S.R. 1984, *Physics of Amorphous Materials*, (London.New York: Longman)

Etherington G., Wright A.C., Wenzel J.T., Dove J.C., Clarke J.H., and Sinclair R.N. 1982, J.Non-Cryst.Solids **48**, 265

Faber T.E. 1972, *Introduction to the Theory of Liquid Metals*, (Cambridge: University)

Filipponi A.,DiCicco A., Benfatto M., and Natoli C.R. 1989, preprint

Filipponi A. 1989, private communication

Fortner J. and Lannin J.S. 1988, J.Non-Cryst.Solids **106**, 128

Fortner J. and Lannin J.S. 1989, Phys.Rev. **B39**, 5527

Gabathuler J.P. and Steeb S. 1979, Z.Naturforsch. **34a**, 1314

Galvin G.J., Thompson M.O., Mayer J.W., Peercy P.S., Hammond R.B., and Paulter N. 1983, Phys.Rev. **B27**, 1079

Glazov V.M., Chizhevskaya S.N., and Glagoleva N.N. 1969, *Liquid Semiconductors*, (New York: Plenum)

Gaspard J.P., Lambin Ph., Moutet C., and Vigneron J.P. 1984, Phil.Mag. **50**, 103

Gunnarson O. and Lundqvist B.I. 1976, Phys.Rev. **B13**, 4274

Hafner J. and Kahl G. 1984, J.Phys. **F14**, 2259

Hageman L.A. and Young D.M. 1981, in *Applied Iterative Methods*, Computer Science and Applied Mathematics, (New York: Academic), p. 138

Hague C.F., Sénémaud C., and Ostrowiecki H. 1980, J.Phys. **F10**, L267

Hamann D.R., Schlüter M., and Chiang C. 1979, Phys.Rev.Lett. **43**, 1494

Hansen J.P. and McDonald I.R. 1976, *Theory of Simple Liquuids*, (London.New York.San Francisco: Academic)

Hayes T.M., Allen J,W., Beeby J.L., and On S.J. 1985,
J.Non-Cryst.Solids **77 & 78** , 57

Heermann D.W. 1986, *Computer Simulation Methods in Theoretical Physics*,
(Berlin: Springer)

Henderson D. and Herman F. 1972, J.Non-Cryst.Solids **8-10**, 359

Henderson D. 1974, J.Non-Cryst.Solids **16**, 317

Hickey B.J., Morgan G.J., Weaire D., and Wooten F. 1985,
J.Non-Cryst.Solids **77 & 78**, 67

Hohenberg P. and Kohn W. 1964, Phys.Rev **136**, B864

Hoower W.G., Ladd A.J.C., and Moran B. 1982, Phys.Rev.Lett **48**, 1818

Hoower W.G. 1986, *Molecular Dynamics*, Lecture Notes in Physics,
(Berlin: Springer)

Hybertsen M.S. and Louie S.G. 1987, Phys.Rev. **B35**, 5585

Ichimaru S. and Utsumi K. 1981, Phys.Rev. **B24**, 7385

Joannopoulaos J.D.and Cohen M.L. 1973, Phys.Rev. **B7**, 2644

Joannopoulaos J.D.and Cohen M.L. 1976, in *Solid State Physics*, vol. **31**, H.Ehrenreich, F. Seitz, and D. Turnbull (eds.), (New York: Academic), pp.71-148

Kamitakahara W.A., Shanks H.R., McClelland J.F., Buchenau U., Gompf F., and Pintschovius L. 1984, Phys.Rev.Lett. **52**, 644

Kamitakahara W.A., Soukoulis C.M., Shanks H.R., Buchenau U., and Grest G.S. 1987, Phys.Rev. **B36**, 6539

Keating P.N. 1966, Phys.Rev. **145**, 637

Kelly M.J. 1980, in *Solid State Physics*, vol. **35**, H.Ehrenreich, F. Seitz, and D. Turnbull (eds.), (New York: Academic), p. 295

King S.V. 1967, Nature, 1112

Kirkpatrick S., Gelatt C.D., Vecchi Jr. and M.P. 1983, Science **220**, 671

Kleinman L. and Bylander D.M. 1982, Phys.Rev.Lett. **48**, 1425

Kluge M.D. Ray J.R., and Rahman A. 1987, Phys.Rev. **36**, 4234

Kohn W. and Sham L.J. 1965, Phys.Rev. **140**, A1133

Kugler S., Molnár G., Petö G., Zsoldos E., Rosta L., Menelle A., and Bellisent R. 1989, preprint

Landolt-Börnstein 1982, *Crystal and Solid State Physics*, vol **17a**, (Berlin: Springer)

Lannin J.S. 1987, J.Non-Cryst.Solids **97 & 98** , 39

Ley L., Kowalczyk S., Pollak R., and Shirly O.A. 1972, Phys.Rev.Lett. **29**, 1088

Lorch E.A. 1969, J.Phys. **C2**, 229

Luedtke W.D. and Landman U. 1988, Phys.Rev. **B37**, 4656

Lundqvist S. and March N.H. (eds.) 1983, *Theory of the Inhomogeneous Electron*

Gas, (New York: Plenum)

Martins J.L. and Cohen M.L. 1988, Phys.Rev. **B37**, 6134

Mermin N.D. 1965, Phys.Rev. **137**, A1441

Metropolis N., Rosenbluth A. and M., and Teller A. and E. 1953, J.Chem.Phys. **21**, 1087

Mott N.F. and Davies E.A. 1979, *Electronic Processes in Non-Crystalline Materials*, The International Series of Monomgraphs on Physics, (Oxford: Clarendon)

Nosé S. 1984a, Mol.Phys. **52**, 255

Nosé S. 1984b, J.Chem.Phys. **81**, 511

Orton B.R. 1975, Z.Naturf. (a), **30**, 1500

Pantelides S.T. 1986, Phys.Rev.Lett. **57**, 1505

Pantelides S.T. 1987a, Phys.Rev.Lett. **58**, 1344

Pantelides S.T. 1987a, Phys.Rev. **36**, 3479

Pantelides S.T. 1988, in *Amorphous Silicon and Related Materials*, H. Fritsche (ed.), (World Scientific), p. 541

Payne M.C., Joannopoulos J.D., Allan D.C., Teter M.P., and Vanderbilt D.M. 1986, Phys.Rev.Lett. **56**, 2656

Perdew J.P. and Zunger A. 1981, Phys.Rev. **B23**, 5048

Phillips J.C. 1973, *Bonds and Bands in Semiconductors*, (New York: Academic)

Pierce D.T. and Spicer W.E. 1972, Phys.Rev. **35**, 3017

Polk D.E. 1971, J.Non-Cryst.Solids **5**, 365

Polk D.E. and Boudreaux D.S. 1973, Phys.Rev.Lett. **31**, 92

Postol T.A., Falco C.M., Kampwirth R.T., Schuller I.K., and Yelon W.B. 1980, Phys.Rev.Lett. **45**, 648

Press W.M., Flannery B.P., Teukolsky S.A., and Vetterling W.T. 1986, *Numerical Receips*, (Cambridge: University)

Pulay P. 1969, Mol.Phys. **17**, 197

Rahman A. 1978, in *Correlation Functions and Quasi-Particle Interactions in Condensed Matter,* J.W. Halley (ed.) (New York: Plenum)

Rivier N. 1979, Phil.Mag. **A40**, 859

Rivier N. 1987, Adv.Phys. **34**, 95

Shih W.H. and Stroud P. 1984, Phys.Rev. **B31**, 3715

Shvarev K.M., Baum B.A., and Gel'd P.V. 1975, Sov.Phys.Solid.State **16**,2111

Singh J. 1981, Phys.Rev. **B23**, 4156

Slater J.C. 1974, *The Self-Consistent Field for Molecule and Solids,* vol. 4, (New York: McGraw-Hill)

Spaepen F. and Turnbull D. 1978, in *Proceedings of the Symposium on Laser- Solid Interactions and Laser Processing*, AIP Conf. Proc. No. 50, D.Ferris, H.J. Lemy, and J.M. Poate (eds.), (New York: AIP)

Srivastava G.P. and Weaire D. 1987, Adv.Phys. **36**, 463

Stathis J.H. and Pantelides S.T. 1988, Phys.Rev. **B37**, 6579

Štich I. 1987, *Magister Thesis*, ISAS Trieste, unpublished

Štich I., Car R., Parrinello M., and Baroni S. 1989a, Phys.Rev. **B39**, 4997

Štich I. 1989, to appear in Acta Phys.Slov

Štich I., Car R., and Parrinello 1989b, to appear in Phys.Rev.Lett

Štich I., Car R., and Parrinello M. 1989c, to be published

Stillinger F.H. and Weber T.A. 1985, Phys.Rev. **B31**,5262

Temkin R.J. 1978, J.Non-Cryst.Solids **28**, 23

Tersoff J. 1988, Phys.Rev. **B37**, 6991

Thompson M.O., Mayer J.W., Cullis A.G., Webber H.C., Chen N.G., Poate J.M., and Jacobson D.C. 1983, Phys.Rev.Lett. **50**, 896

Thouless D.J. 1974, Phys.Rep. **13**, 93

Verlet L. 1967, Phys.Rev. **159**, 98

La Violette R.A. and Stillinger F.H. 1987, Phys.Rev. **B35**, 5446

Wang C.Z., Chan C.T., and Ho K.M. 1989, Phys.Rev. **B39**, 8586

Waseda Y. and Suzuki K. 1975, Z.Physik **B20**, 339

Waseda Y. 1980, *The Structure of Non-Crystalline Materials; Liquids and Amorphous Solids*, (New York: McGraw-Hill)

Weaire D. and Alben R. 1972, Phys.Rev.Lett. **29**, 1505

Weber W. 1977, Phys.Rev. **B15**, 4789

Wigner E. 1937, Phys.Rev. **46**, 1002

Winer K. 1987, Phys.Rev. **B35**, 2366

Winer K. and Bose S.K. 1988, Phys.Rev. **B38**, 12683

Wooten F. and Weaire D. 1984, J.Non-Cryst.Solids **64**, 325

Wooten F. Winer K., and Weaire D. 1985, Phys.Rev.Lett. **54**, 1392

Wooten F. 1989, private communication

Yin M.T. and Cohen M.L. 1982a, Phys.Rev. **B26**, 3259

Yin M.T. and Cohen M.L. 1982b, Phys.Rev. **B26**, 5668

Yonezawa F. and Cohen M.H. 1981, in *Fundamental Physics of Amorphos Semiconductors*, F Yonezawa (ed.), Springer Series in Solid State Physics, vol **25**, (Berlin: Springer), pp. 119-144

Zallen R. 1983, *The Physics of Amorphous Solids*,)
(New York.Chichester.Brisbane.Toronto.Singapore: J.Wiley& Sons)

Acknowledgements

It is a pleasure to acknowledge gratefully the fruitful collaboration with my supervisors profs. R. Car and M. Parrinello, their continuous interest in this project and their encouragement during this work, that significantly contributed to my better understanding of this field.

I am also indebted to Drs. G. Chiarotti, G. Pastore, F. Ercolessi , and to all my colleges in SISSA for many illuminating discussions and for a good working atmosphere they created.

I also acknowledge a generous allocation of computer time and facilities in the computer center CINECA in Bologna which made the realization of this project possible.

Last but not least i am grateful for the hospitality of SISSA as the place where this work has been done.